TÉCNICO LISBOA

UNIVERSIDADE DE LISBOA

INSTITUTO SUPERIOR TÉCNICO

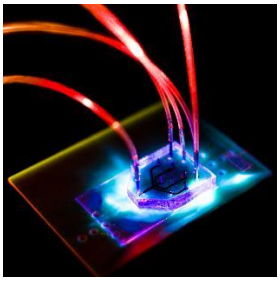

Screening of multimodal ligands for the capture and polishing of antibody streams:

A microfluidic approach for rapid optimization of chromatographic operating conditions

Inês Fernandes Pinto

Supervisor: Doctor Ana Margarida Nunes da Mata Pires de Azevedo
Co-Supervisors: Doctor João Pedro Estrela Rodrigues Conde
Doctor Maria Raquel Múrias dos Santos Aires Barros

Thesis approved in public session to obtain the PhD Degree in

Biotechnology and Biosciences

Jury final classification: Pass with Distinction and Honour

2018

TÉCNICO LISBOA

UNIVERSIDADE DE LISBOA

INSTITUTO SUPERIOR TÉCNICO

Screening of multimodal ligands for the capture and polishing of antibody streams:

A microfluidic approach for rapid optimization of chromatographic operating conditions

Inês Fernandes Pinto

Supervisor: Doctor Ana Margarida Nunes da Mata Pires de Azevedo
Co-Supervisors: Doctor João Pedro Estrela Rodrigues Conde
Doctor Maria Raquel Múrias dos Santos Aires Barros

Thesis approved in public session to obtain the PhD Degree in

Biotechnology and Biosciences

Jury final classification: Pass with Distinction and Honour

Jury

Chairperson: Doctor Duarte Miguel de França Teixeira dos Prazeres, Instituto Superior Técnico da Universidade de Lisboa

Members of the Committee:

Doctor Steven M. Cramer, School of Engineering, Rensselaer Polytechnic Institute, USA

Doctor Duarte Miguel de França Teixeira dos Prazeres, Instituto Superior Técnico da Universidade de Lisboa

Doctor Sofia de Medina Aires Martins, INESC Microsistemas e Nanotecnologias, Lisboa

Doctor Marília Clemente Velez Mateus, Instituto Superior Técnico da Universidade de Lisboa

Doctor Ana Margarida Nunes da Mata Pires de Azevedo, Instituto Superior Técnico da Universidade de Lisboa

Funding Institutions:

Fundação para a Ciência e Tecnologia (FCT) – PhD Grant SFRH/BD/96442/2013

2018

Dedicated to my uncle Augusto

"Guarda um cantinho da tua nuvem
Para um dia eu lá morar"

“However difficult life may seem,
there is always something you can do and succeed at”

Stephen Hawking

"If I have seen further it is by standing on the shoulders of giants."

Isaac Newton

Acknowledgements

The journey of a PhD is a life-changing and overwhelming period that means much more than academic achievements. The last four years were undoubtedly the most important of my life so far, as they shaped me as a researcher, a student, a colleague and a human being. However, all the personal and professional realizations would not be possible without the contribution of an extraordinary group of people that celebrated my successes, lifted me up in hard times and never allowed me to give up no matter how dark the future seemed.

Firstly, I would like to express my sincere gratitude to my advisor Professor Ana Azevedo for the honor of being her first (official) PhD student. I am grateful for the example she has provided not only as a scientist and teacher, but also a resilient and persevering person. I am also extremely grateful to my co-advisor Professor João Pedro Conde for having me in his research group in INESC-MN, without even planning it in the first place. The first months I spend in his group were truly enlightening and game-changing in my PhD project and I was lucky enough to be able to start working almost full-time in INESC-MN. I deeply appreciate all his contributions of time, ideas and opportunities of conferences to make my PhD a stimulating and productive experience.

I am also thankful to Professor Raquel Aires Barros, for her help and availability considering her busy schedule, and to Doctor Virginia Chu, for her dedication and insightful ideas, despite not being my formal advisor.

As I worked in two research groups there are a number of people to whom I owe an acknowledgment. From the Bioseparations Laboratory, I would like to thank Sara Rosa for kindly providing the cell culture supernatants that I used in numerous experiments. Also, a profound acknowledgement goes to André Nascimento and Isabel Campos Pinto for all the joyful moments shared inside and outside the lab and for the friendship that remains even at distance. From the INESC-MN side, I am grateful to Denis Santos for his dedication to the sensor measurements and for the endless hours we spent in the dark optics room. I am also thankful to Rui Pinto for his support in the electrode fabrication

and electrokinetic measurements. His creativity and knowledge were highly inspiring for me. A special acknowledgment to Catarina Caneira, Eduardo Brás, Ricardo Fradique, Catarina Bombaça and Tatiana Arriaga for the times we worked together in the BioLab and for the nice conversations that relieved the stressful moments. Finally, a big thank you to Rafael Lopes, for being the most resilient and funny summer student ever, in spite of the challenging measurements and discouraging results.

This paragraph is dedicated to Narayanan Srinivasan, for being one of the most important persons life has put in my way. I am extremely grateful for the opportunity of working alongside him, even if only for a few months. More than that, I am grateful for having met such an altruist and special person, who became a truly close friend that lifted up my spirit throughout this journey. He has taught me more than I would imagine about science and life and has proved me true friendship knows no boundaries of any kind.

Finally I would like to thank my parents, for their endless love and encouragement during the multiple personal and professional challenges I faced in the last years. They raised me to put all my dedication and efforts in my pursuits while honoring my values and, for those lessons, I am truly grateful. Last but not the least, I am thankful to my husband-to-be Ruben Soares, for being an extraordinary companion both inside and outside the lab, for fostering my creativity and helping me to improve myself every day. He taught me that few things in life are possible without the right dose of work, wisdom and persistency. I taught him that faith sometimes helps as well. With him I found the perfect balance in my life and my gratitude is beyond what can be put down in words.

Resumo

A selecção e optimização de ligandos cromatográficos para a purificação de biofármacos constitui um desafio considerável para os profissionais de biotecnologia. No caso particular dos anticorpos monoclonais (mAbs), ligandos sintéticos incluindo vários tipos de interacções (multimodais) podem proporcionar vantagens processuais e económicas comparativamente a ligandos de afinidade baseados em proteínas. No entanto, a optimização das condições operatórias destes ligandos multimodais requer o desenvolvimento de plataformas de rastreio de alto rendimento que sejam simples, eficazes e de baixo custo.

Nesta tese é apresentada uma nova estratégia baseada em microfluídica para realizar uma selecção rápida de condições operatórias no contexto da purificação de mAbs a partir de sobrenadantes de cultura celular usando cromatografia. Foram desenvolvidos dispositivos progressivamente integrados, visando (i) a optimização simultânea de múltiplos ligandos cromatográficos; (ii) a detecção multiplexada de diferentes moléculas-alvo em solução; (iii) a inserção automática e sequencial de líquido no dispositivo; e (iv) o acoplamento de fotossensores miniaturizados para a leitura do sinal directamente no dispositivo. Os estudos de optimização em microfluídica foram realizados com moléculas (IgG, BSA) marcadas com um fluoróforo em soluções-tampão ou em sobrenadantes de cultura celular, permitindo obter a tendência de parâmetros importantes (pureza, rendimento) em conformidade com ensaios realizados à escala laboratorial convencional. As principais vantagens proporcionadas pelos dispositivos miniaturizados e as suas diferenças intrínsecas relativamente à operação cromatográfica tradicional são também exploradas e discutidas nesta tese.

Este trabalho fornece importantes contribuições para o desenvolvimento e melhoramento de plataformas de optimização que visam auxiliar nas fases iniciais do desenvolvimento de processos cromatográficos. Para além disso, embora o foco tenha sido colocado na purificação de mAbs, esta abordagem pode ser aplicada a outras biomoléculas de alto valor comercial, sendo provável que tenha um elevado impacto na purificação de proteínas em geral.

Palavras-chave: Cromatografia multimodal, Anticorpos monoclonais, Microfluídica, Optimização, Fotodíodos

Abstract

The selection and optimization of chromatography ligands for the purification of biopharmaceuticals is a demanding challenge for biotechnologists. In the particular case of monoclonal antibodies (mAbs), synthetic ligands comprising multiple types of interactions (multimodal) can provide process and economic advantages compared to protein-based affinity ligands. However, optimizing the operating window of these multimodal ligands requires the development of simple, effective and affordable high-throughput screening platforms.

In this thesis, a novel microfluidics-based strategy to perform rapid screening of chromatography operating conditions in the context of the purification of mAbs from cell culture supernatants is presented. Increasingly integrated devices were developed, aiming at (i) performing a simultaneous optimization of multiple chromatography ligands; (ii) addressing a multiplexed detection of different target molecules in solution; (iii) integrating automated and sequential liquid flow in the device; and (iv) coupling miniaturized photosensors for on-chip signal read-out. Microfluidic optimization studies were performed using fluorescently labeled molecules (IgG, BSA) in plain buffer solutions or spiked in real cell culture supernatants, enabling the trending of important parameters (purity and recovery yield) in accordance to conventional laboratory scale assays. The main advantages provided by the miniaturized devices and their intrinsic differences relative to a traditional chromatographic operation are also explored and discussed.

This work provides important contributions towards the development of improved high-throughput screening platforms for early-stage process development of chromatographic separations. In addition, although a focus was given to antibody purification, the approach can be applied to other high-value biomolecules and is likely to have a high impact on protein purification in general.

Keywords: Multimodal chromatography; Monoclonal antibodies; Microfluidics; Optimization; Photodiodes

Table of Contents

List of Figures

List of Tables

List of Abbreviations

AEX – Anion Exchange

ATCC – American Type Culture Collection

BC – Binding Capacity

BF – Bright Field

BGG – Bovine Gamma Globulin

BSA – Bovine Serum Albumin

CAD – Computer Aided Design

CCD – Charge-coupled Device

CEX – Cation Exchange

CHO – Chinese Hamster Ovary

CM – Carboxymethyl

CV – Column Volume

DEAE – Diethylaminoethyl

DHFR – Dihydrofolate Reductase

DI – Deionized

DNA – Deoxyribonucleic Acid

DWL – Direct Write Lithography

EMA – European Medicines Agency

EQE – External Quantum Efficiency

FBS – Fetal Bovine Serum

FDA – Food and Drug Administration

GFP – Green Fluorescent Protein

GPIB – General Purpose Interface Bus

HCIC – Hydrophobic Charge Induction Chromatography

HCP – Host Cell Proteins

HEA – Hexyl Amine

HIC – Hydrophobic Interaction Chromatography

HPLC – High Pressure Liquid Chromatography

HSA – Human Serum Albumin

HTPD – High-throughput Process Development

IEF – Isoelectric Focusing

IEX – Ion Exchange

IgG – Immunoglobulin G

IL – Interleukin

IPA – Isopropyl Alcohol

ITO – Indium Tin Oxide

IVIG – Intravenous Immunoglobulin

LED – Light Emitting Diode

LHS – Liquid Handling Station

mAb – Monoclonal Antibody

MBI – 2-mercapto-5-benzimidazole Sulfonic Acid

MCSGP – Multicolumn Countercurrent Solvent Gradient Purification

MEP – 4-mercaptoethylpyridine

MLSL – Multilayer Soft-Lithography

MMC – Multimodal Chromatography / Mixed-mode Chromatography

MuLV – Murine Leukemia Virus

MVM – Minute Virus of Mice

MW – Molecular Weight

MWCO – Molecular Weight Cut-Off

NHS – N-Hydroxysuccinimide

PBS – Phosphate Buffered Saline

PCB – Printed Circuit Board

PCR – Polymerase Chain Reaction

PDMS – Polydimethylsiloxane

PECVD – Plasma Enhanced Chemical Vapor Deposition

PEG – Polyethylene Glycol

PF – Purification Factor

PGMEA – Propylene Glycol Monomethyl Ether Acetate

PPA – Propyl Amine

PSEA – Pyridinylsulfanylethylamine

PSPA – Pyridinylsulfanylpropylamine

RSD – Relative Standard Deviation

SD – Standard Deviation

SDS-PAGE – Sodium Dodecyl Sulfate Polyacrylamide Gel Electrophoresis

SEC – Size Exclusion Chromatography

UV – Ultraviolet

UVO – Ultraviolet-Ozone

VLP – Virus-like Particle

"A journey of a thousand miles begins with a single step."

Lao Tzu

Chapter 1
Introduction

The separation of biological compounds by chromatography is a well-established technique that plays an important role in sectors such as medical and healthcare, chemical industry, environmental industry and even in food safety applications. The biopharmaceutical industry, in particular, uses chromatographic separations as a standard means of achieving robust and efficient purification processes, in order to comply with the strict purity requirements enforced by regulatory agencies [1]. Monoclonal antibodies (mAbs) are currently the most prominent class of compounds in the pharmaceutical pipeline, holding great promise as new therapeutic agents in the treatment of several diseases including cancer, neurological and auto-immune disorders. According to data from 2016, six out of ten best-selling drugs were either mAbs or mAb-derived molecules, with sales reaching over U.S. $80 billion [2]. In fact, treatments using mAb-based drugs have an average monthly cost per patient of U.S. $8,000 - $12,000 (*e.g.* for cancer treatment) [3]. These high prices are in part associated with the complex and expensive purification processes of mAb products, which typically rely on affinity chromatographic steps using protein-based ligands. The drawbacks of these bioaffinity ligands (*e.g.* protein A, G or L) have been widely discussed [4-7] and are namely due to their intrinsic economical and performance limitations. In this context, novel synthetic ligands have been receiving increasing attention as cost-effective alternatives to be integrated in the downstream processing of mAbs or other high-value molecules [8, 9].

As an increasing number of novel chromatography ligands are being made available, the use of high-throughput screening platforms becomes essential during the early stage process development, when time and reagents are scarce resources. Most of the approaches to perform a high-throughput optimization of operating conditions are based on the use of microtiter plates [10-14], miniature columns [15-17] or micro-tips [18], operated in robotic liquid handling stations. However, these approaches (i) rely on a significant consumption of molecules and buffers (mg- and mL- range); (ii) require long incubation times (several minutes to hours) per step; (iii) depend on the use of expensive

equipment to achieve parallelization and automation; and (iv) often lack the continuous flow operation intrinsic to conventional chromatography.

In an attempt to further miniaturize liquid chromatography and circumvent some of the limitations of current approaches, the use of microfluidics has been reported for the purification of small quantities of proteins [19], determination of adsorption isotherms and breakthrough curves [20, 21], and rapid screening of chromatography operating conditions [22].

Objectives of the work

This thesis aims at addressing the challenging recovery of monoclonal antibodies by developing innovative and cost-effective purification processes based on chromatography ligands alternative to protein A. In particular, multimodal ligands were evaluated with respect to the capture and polishing of an anti-interleukin 8 (IL-8) mAb in model solutions and directly from complex cell culture supernatants. Interleukin-8 (IL8) is a key mediator associated with inflammation and it is also implicated in other medical conditions, such as certain types of cancer and in the pathology of cystic fibrosis [23, 24]. Multimodal ligands comprise multiple interaction groups, such as hydrophobic, electrostatic and hydrogen bonding, which can potentially make them ideal competitors to protein A affinity chromatography. Their application, however, depends on a deep understanding of the behavior of the ligands, which is very often a difficult and demanding task, requiring extensive empirical optimization studies. In this context, an innovative screening platform was developed using a miniaturized approach based on microfluidics.

The work here presented reports the design and development of *in-house* fabricated microfluidic devices for the rapid screening of chromatographic operating conditions using multimodal ligands, by monitoring adsorption/elution events in real-time, at bead-level. Optimization studies were performed by immobilizing chromatography beads in a microchannel and flowing solutions containing fluorophore-labeled proteins, namely mAbs and BSA.

Specific objectives of this thesis comprise:

1) Assessment of the ability of multimodal ligands to selective capture mAbs directly from culture media;

2) Optimization of binding and elution conditions of mAbs towards improved yields and purities;

3) Development of progressively integrated microfluidic devices that enable (i) the simultaneous optimization of multiple chromatography ligands; (ii) the multiplexed detection of different target molecules; (iii) the integration of sequential liquid flow in the device; and (iv) the coupling of on-chip signal monitoring;

4) Validation of purification processes optimized in miniaturized assays using conventional lab-scale chromatographic assays.

This thesis provides important contributions towards the development of integrated high-throughput screening microfluidic platforms amenable to be scaled-out for early-stage process development in a biopharmaceutical setting. Although this work was focused on antibody separation, the approach here reported can easily be applied to different high-value biomolecules, adding significant knowledge to the current state-of-the-art towards the improvement of protein purification in general.

Thesis outline

This thesis is organized in **eight** chapters, five of which containing the description of experimental methods and the main results achieved in this work. The footnotes in the title of the chapter refer to publications in scientific journals resulting therefrom. The results obtained in the context of collaborative works are also properly referenced. Each chapter begins with a brief introduction of the state-of-the-art corresponding to the content of the chapter and is concluded with a summary of the main achievements and outlooks, aiming also at introducing the subsequent chapter.

Chapter 1 presents the overall motivation and main objectives of this work, as well as the organization of the thesis.

Chapter 2 discusses the state-of-the-art on the purification of monoclonal antibodies, namely the current standards employed in the industrial downstream processing of these molecules and an overview of emerging chromatographic options, namely multimodal chromatography. The relevance of high-throughput screening for the development of chromatographic processes is also presented and the most relevant strategies employed in

this context are overviewed, namely (i) microtiter plates, (ii) micropipette tips and (iii) miniature columns. Furthermore, the combination of microfluidics and chromatographic separations is also reviewed in this chapter by exploring some of the few reports available in the literature. The last section of chapter 2 establishes the transition into the novel concept reported in this thesis, since applications in the context of the optimization of chromatographic separations using integrated microfluidic devices are largely unexplored.

Chapter 3 presents the detailed microfabrication processes of the devices used in the chromatographic optimization studies presented in the subsequent chapters. The design and functionalities included in the microfluidic structures were aimed towards an automated device. The fabrication processes of integrated pneumatic valves and miniaturized a-Si:H photodiodes used in the optical detection of the on-chip chromatographic separations are also presented.

Chapter 4 introduces the first optimization studies performed in a novel microfluidic device comprising a nanoliter column. A multimodal ligand was thoroughly studied in terms of adsorption and elution of a fluorophore-labeled monoclonal antibody spiked in several buffers. The results motivated subsequent optimization studies using more complex sample solutions and improved microfluidic structures.

Chapter 5 presents the development of a multi-chamber device to perform the simultaneous screening of three different chromatography resins. In addition, a quantitative analytical method was developed and optimized to allow the simultaneous detection of IgG and BSA mixed in solution via fluorescence measurements. The throughput of the miniaturized assays was significantly improved, and the concept of multiplexing was presented for the first time in terms of multiplicity of chromatography resins and target molecules analyzed in a single experiment.

Chapter 6 reports achievements towards an integrated and automated microfluidic device, capable of being operated in a high-throughput manner for early-stage optimization of chromatographic operating conditions. The experiments were performed using a cell culture supernatant spiked with a fluorophore-labeled monoclonal antibody, the liquid insertion in the device was controlled by integrated pneumatic valves and the fluorescence signal was measured in real time at bead-level using miniaturized a-Si:H photodiodes coupled to the microfluidic device.

Chapter 7 includes preliminary studies involving the label-free monitoring of chromatographic separations using miniaturized a-Si:H photodiodes. Binding of native BSA and IgG molecules to chromatographic beads inside a microchannel was successfully accomplished by measuring the transmittance of UV (280 nm) light through (i) a column packed with beads and (ii) a channel downstream of the column. This type of measurements match those used in conventional chromatography assays, in which binding/elution of molecules is performed under native conditions (*i.e.* without a previous labeling procedure) and the UV sensor is placed at the outlet stream of the chromatography column.

Finally, *chapter 8* summarizes the achievements and main conclusions of this thesis and presents an outlook for further developments and possible applications of bead-based microfluidic systems in different areas.

"Nothing in life is to be feared, it is only to be understood.
Now is the time to understand more, so that we may fear less."

Marie Curie

Chapter 2
Purification of Monoclonal Antibodies: Overview and Miniaturization Strategies

This chapter covers the concepts and state-of-the-art of the two major areas of investigation that bridged this work – chromatography and microfluidics. A literature review of conventional and emerging chromatographic technologies for the purification of monoclonal antibodies is firstly presented[§]. Then, the application of microfluidics to perform a rapid optimization of chromatographic conditions and support process development in this context is also covered. Important theoretical concepts are introduced whenever necessary.

2.1. Antibody purification: a historical perspective

The dawn of antibody purification, particularly IgG, started with the plasma fractionation technique, in which ethanol was used to precipitate proteins at their isoelectric points. This relatively simple method was first applied to the extraction of albumin from blood plasma [25], and years later found an homologous application in the purification of IgG for the first intravenous immunoglobulin (IVIG) formulation [26]. The large production scale of intravenous IgG combined with the low manufacturing cost provided by the plasma fractionation process [27], raised the debate about borrowing this method for the purification of recombinant monoclonal antibodies (mAbs). However new trends started to be framed in a completely different direction, with chromatographic operations playing a major role in addressing the purification of these compounds.

Back in the 1990s, early processes for mAb purification included multiple steps organized in a complex manner, which reflected the lack of process-wise knowledge and the need

This chapter contains sections reproduced from the following review article:

[§]I.F. Pinto, M.R. Aires-Barros, A.M. Azevedo, 2015 "Multimodal chromatography: debottlenecking the downstream processing of monoclonal antibodies" *Pharm Bioprocess* **3**(3) 263-279.

for improved separation media. The employed process included multiple filtration media for harvest, the combination of a wide range of different chromatographic steps for protein separation (including protein A, protein G, ion exchange, size exclusion and hydrophobic interaction chromatography), the implementation of ultrafiltration and diafiltration at different points of the process, and the use of methods involving solvents or detergents to accomplish viral inactivation [27].

At the time, since the upstream cell culture titers were very low, there was no need to have resins tailored for high binding capacities and the focus was centered on the ability to rapidly process large volumes of feedstock [27]. A change in paradigm took place when increased expression levels and higher cell densities started to be reached upstream [28-30], and also when mAb products evolved from pure murine to fully human protein sequences [31], which required the design of alternative and more versatile processes. Currently, almost all marketed mAbs are produced by mammalian cell culture using either chinese hamster ovary (CHO) or mouse myeloma cells. Advances in molecular biology and protein engineering have led to remarkable improvements in cell culture productivities, with antibody titres now routinely exceeding 10 g/L for the CHO expression system [27].

The stringent requirements enforced by the regulatory agencies (FDA, EMA) fostered the use of chemically-defined components in the production of the biopharmaceutical products, which led to an increasing adoption of serum-free media in upstream processes. In the downstream processes, these requirements led, for example, to the development of recombinant protein A ligands to replace the native bacterial protein ligand [32]. The engineering of protein A ligands was also motivated by the need of having improved stability to pH and cleaning solutions, using milder elution pH and achieving higher dynamic binding capacities [33, 34]. The investigation and knowledge gathered over the years, allowed to improve the chromatographic matrices in terms of binding capacity, rigidity, and tolerance to higher flow rates, which increased the robustness of the chromatographic steps and simplified their integration and organization in a standardized platform format [35].

2.2. Downstream processing of monoclonal antibodies

The introduction of biopharmaceutical products in clinical trials must cope with different challenges, being process development one of the limiting steps. The explosion in the number of mAbs entering clinical trials has created the need for employing a rather standardized approach for process development to reduce the time and resources required for this task. It is known that a high degree of homology exists among mAbs, however even slight variations in complementarity-determining regions and framework sequences may represent a specific purification challenge, making unfeasible the processing of different mAb products without changes to the operating conditions. Despite these variations, the advantages of employing a generic process with minimal optimization for the different mAb candidates are undeniable and, in fact, this platform strategy has been adopted by most companies working on the purification of mAbs. The platform approach (**Figure 2.1**) is based on a common sequence of unit operations that were developed and integrated to allow the maximum speed to clinic, which constitutes one of the major competitive advantages for biotechnology companies.

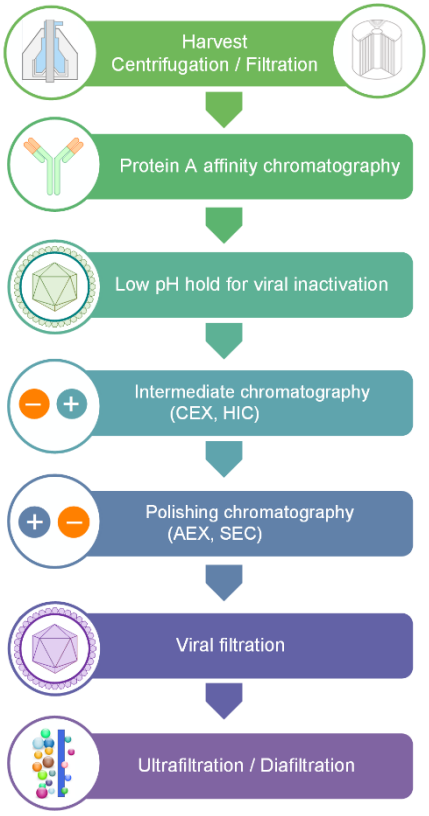

Figure 2.1 – Sequence of unit operations comprising the platform approach employed in the downstream processing of mAbs. CEX - Cation exchange chromatography; HIC - Hydrophobic interaction chromatography; AEX - Anion exchange chromatography; SEC - Size exclusion chromatography.

The first step of the downstream processing is the initial removal of cells and cell debris from the culture broth using **centrifugation**, followed by **depth filtration** to clarify the cell culture supernatant that contains the antibody product. The high cell densities that are now typically achieved increased the burden on this primary recovery, which can be significantly challenging at manufacturing scale and may account for up to 12% of the downstream processing costs [36].

After harvest, **protein A affinity chromatography** has been adopted as the capture step of choice by most manufacturers, due to the high selectivity towards mAbs and the extremely high purity that is achieved by directly loading the cell culture supernatants [37]. This affinity capture step relies on the specific interaction of the antibody Fc region with the immobilized protein A, a cell wall protein of Staphylococcus aureus **(Figure 2.2).** This chromatographic step is also effective in removing host cell proteins (HCP), host DNA, process-related impurities, and potential adventitious viral contaminants, while providing a volume reduction of the mAb product [38]. So, the excellent performance parameters that this capture step delivers, reduce the burden on the subsequent polishing steps, which are still required to ensure that the product complies with the quality requirements.

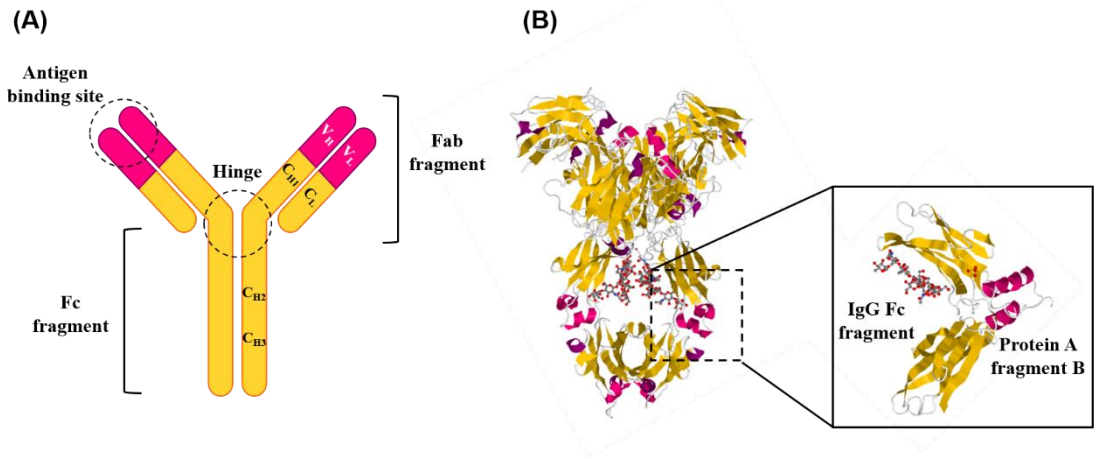

Figure 2.2 – Schematic structure of a human immunoglobulin G (IgG) monoclonal antibody. **(A)** Y-shaped structure showing the four polypeptide chains (two heavy chains – V_H, C_{H1}, C_{H2}, C_{H3} – and two light chains – V_L, C_L). Variable (V) and constant (C) domains are represented in pink and yellow, respectively. **(B)** Ribbon 3D representation of a human IgG with β-sheets and α-helices represented in yellow and pink, respectively. Zoom in illustrates the binding region of protein A fragment B (pink) to the IgG Fc fragment. The carbohydrate moiety composing the Fc fragment is also represented. Structure data files (1HZH **[39]** and 1FC2 **[40]**) were downloaded from the Protein Data Bank website (http://www.rcsb.org/pdb) **[41]**.

Despite all the advantages, a series of limitations can also be pointed out to protein A, being the most significant related to the high cost of the resin, which can account for over 50% of the entire downstream processing costs [26]. In addition to the economic-related constraints, protein A also suffers from leaching problems due to the action of proteases, which may cause the co-elution of ligand fragments along with the target antibody, and from a poor stability to the harsh pH elution and the sanitization conditions [38]. To address this problem, there is an increasing effort from the manufacture companies in improving the stability of the protein A ligand (*e.g.* GE Healthcare developed a recombinant protein A ligand – MabSelect SuRe^{TM} – that can withstand 0.1–0.5 M NaOH during cleaning and sanitization protocols). The loading capacity of the protein A resin is often a rate-limiting step [37] to cope with the high mAb titers coming from the upstream feedstocks [42].

The low pH applied during mAb elution from protein A is typically used for **viral inactivation,** since most of the mAbs can be briefly maintained under low pH conditions without detrimental effects. The viruses present in the purification process can be of endogenous origin, arising from the mammalian cells used in the production of mAbs, or can be adventitiously introduced by occasional infection of the cells during processing. In any case, the kinetics of virus inactivation should be carefully considered [26], in order to define the appropriate time hold for an effective pH incubation step.

The subsequent **chromatographic polishing steps** are aimed at reducing host cell protein levels, host DNA, high molecular weight aggregates and leached protein A that may remain after the capture step [37]. At least two orthogonal chromatographic steps are typically employed, most commonly anion exchange or cation exchange chromatography, although hydrophobic interaction chromatography can also be used [26, 37]. The sequence chosen for the polishing steps is dependent on the nature of the product and the trace impurities to remove, in order to ensure that the final solution is in accordance with the particular formulation to be used [43, 44].

For **viral clearance** purposes, a filtration step is the most suitable choice to ensure the log reductions imposed by safety requirements, since this is a robust operation that is relatively independent on the process parameters, and there is a wide variety of virus filters available for the biotechnology industry [37]. In addition to viral filtration, most chromatographic methods also have some degree of viral clearance. Total viral clearance of the purification process is then calculated by the addition of the log reduction values

of all orthogonal purification steps. The completion of the downstream purification process occurs after buffer exchanging the product into the formulation buffer, which is typically accomplished with an **ultrafiltration step** in diafiltration mode. This final step is of capital importance, since its optimization allows to handle high therapeutic doses in a limited formulation volume.

The need for cost-effective processes seems to start outpacing protein A as an industry standard, despite all its inherent advantages, and has triggered the demand for alternative strategies for mAbs purification [45, 46]. However, these should be capable of successfully replace the affinity capture step and fit in a platform format. The alternatives range from non-chromatographic techniques, namely aqueous two-phase separation, membrane filtration, precipitation or crystallization, to chromatographic steps based on non-biological ligands, such as traditional single-mode interaction chromatography or emergent modalities as multimodal chromatography.

2.3. Multimodal chromatography

Multimodal or mixed-mode chromatography (MMC) can be defined as a chromatographic method employing multiple types of interaction between a stationary phase and a mobile phase, in which the different solutes are present. The binding modes that are more frequently employed in multimodal ligands comprise ion exchange, hydrogen bonding, and hydrophobic interaction groups [47], although others may be included for specific purposes, and the magnitude of each individual interaction can be manipulated accordingly.

Selectivities and specificities that differ from those of traditional single-mode ligands endow multimodal chromatography with a high versatility to deal with challenging purification problems compared to its single-mode counterparts. However, considering the multitude of interactions that can be simultaneously promoted within a multimodal ligand and all the factors that govern the different selectivities, the optimization of operating conditions is an extremely complex process, in which several studies are required. Purification studies using these ligands can start with a design of experiments (DoE) [11, 48], to determine the conditions that will allow to take full advantage of the multimodal potential. Monte Carlo simulations can also be of great importance in improving the process performance [49]. In all these cases, process development relies

on effective high-throughput screening platforms to rapidly predict the useful range of operating conditions, before making a transition to laboratory or preparative scales.

Multimodal chromatography has been receiving considerable attention over the last 15 years (2003 – 2017), with more than 100 publications (including research articles, reviews, patents and proceeding) per year since 2008 in ISI-index journals. According to **Figure 2.3-A** there has been a steady increase in the number of publications covering general chromatographic procedures (analytical and preparative) that exploit ligands with multimodal properties for different applications. **Figure 2.3-B** shows the number of publications covering chromatographic procedures specifically focused on the purification of antibody-based molecules, marked by two paper-boom events in 2008 and 2013. These events may be explained by (i) an increase in the availability of automated liquid handling platforms to perform high-throughput optimization of novel ligands and (ii) a growing interest in making multimodal ligands commercially available, facilitating their potential application in the purification of emergent antibody-derived molecules with biopharmaceutical interest, such as antibody fragments, for which a standardized purification platform is not yet available. As an example, in 2017 almost 30% of the publications were related to the purification of bispecific antibodies or antibody fragments.

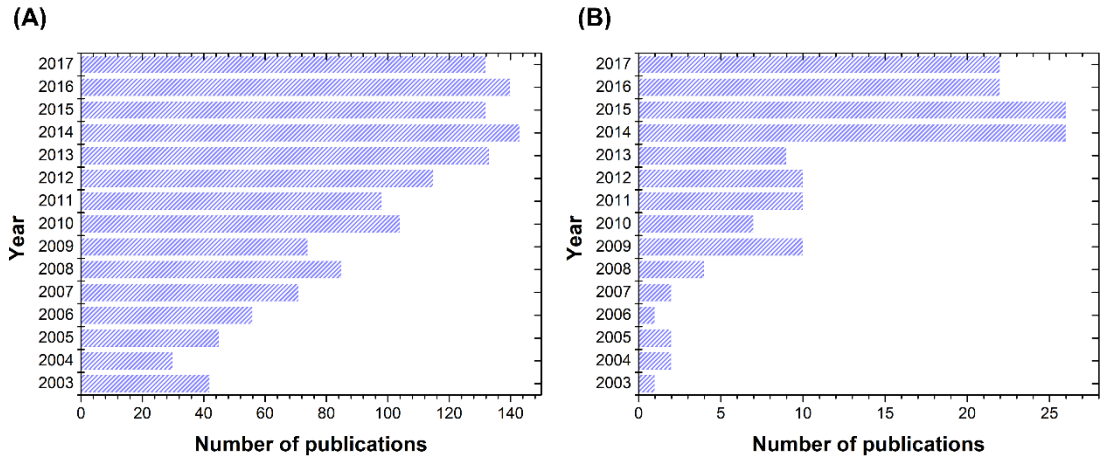

Figure 2.3 - Number of publications addressing multimodal chromatography over the last 15 years. **(A)** Publications covering chromatographic procedures in general using ligands with multimodal properties. The search keywords were as follows: ((multimodal AND chromatography) OR (mixed-mode AND chromatography)). **(B)** Publications covering chromatographic procedures using multimodal ligands specifically applied to the purification of antibody-based molecules. The search keywords were as follows: ((multimodal AND chromatography) OR (mixed-mode AND chromatography)) AND (antibodies OR antibody OR IgG). The data was retrieved from ISI Web of Science on 17th June 2018.

2.3.1. Design of ligands and selection of functional groups

The preparation of multimodal chromatography resins can be accomplished using different approaches. Typically, the ligand carries two or more interactions connected via a chemical scaffold, and additional functionalities can be introduced upon further modifications on the scaffold. However, a simpler approach can also be used, in which the different functionalities are equally, randomly and independently distributed on the chromatographic support. In this last approach, two ligands are effectively present in the resin but in such close proximity that the interaction with the same molecule occurs in a complete different manner as if only one of the ligands was present [50]. Thus, instead of having the different functionalities on the same scaffold, these can be provided on separate ligands, which need to be sufficiently close to bind the target in a multimodal fashion. These two different ways of creating multimodal ligands are schematically shown in **Figure 2.4**.

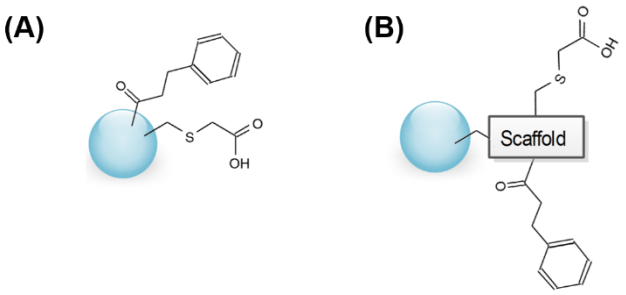

Figure 2.4 – Multimodal ligand rational design. **(A)** Different interaction groups can be randomly placed on the chromatographic support (*e.g.* bead). **(B)** Different moieties can be attached to the chromatographic support via connection with a chemical scaffold. Additional groups can be introduced upon further chemical modification on the scaffold.

In multimodal ligands, the hydrophobic moiety is normally given by an aliphatic or aromatic group, while the ionic moiety can comprise both weak and strong ion exchanger groups, such as amino, carboxyl and sulfonic groups [51]. It should be highlighted that weak and strong do not refer to binding strength, but rather to the charge behavior at certain pH values. Strong ion exchangers are charged at any practical pH (2.0-10.0), whereas the charge of weak ion exchangers depends on the pH value. Weak cation exchangers (*e.g.* carboxyl groups) carry a negative charge at pH values greater than ~5.0, while weak anion exchangers (*e.g.* diethylaminoethyl - DEAE) are positively charged at pH values lower than ~9.0 [52].

In the architecture of a multimodal ligand, there is normally a primary functionality that governs the interaction with target molecules, while additional functional groups in the ligand promote synergistic effects under certain operating conditions and depending on their location relatively to the primary functionality [53].

Heterocyclic groups represent good hydrophobic patches, which due to their hydrophobicity and dissociation properties, allow adsorption to be performed at moderate or high ionic strengths [54-56]. In the case of ionic moieties, knowing the degree of dissociation of the ionic groups (pKa) is important to predict the behavior of the ligand during the purification step, particularly to achieve efficient elution upon decreasing the working pH below the isoelectric point of the protein and the pKa of the ligand, for example.

In addition to these moieties, hydrogen bonding groups are also reported to have influence on the performance of multimodal ligands, through the possibility of hydrogen donation or acceptance, although their impact is frequently subsidiary for selectivity purposes [57]. Thiophilic interactions can also be exploited for integration in multimodal ligands and are in fact particularly advantageous in the purification of immunoglobulins (IgGs), since these biological molecules have a known affinity towards sulfur-containing ligands [58]. The thiophilic functionality is frequently introduced by means of a reactive site for ligand coupling, where the mercapto groups contribute with sulfur atoms for binding [54].

Regarding the supporting materials for multimodal chromatography, these frequently comprise polysaccharide beads made of agarose or cellulose [57, 59], which are biocompatible for protein purification purposes and, at the same time, are stable and relatively inexpensive. In analogy to affinity chromatography, a spacer arm should also be introduced in multimodal chromatography, to ensure adequate accessibility of the proteins to the ligand, and depending on the groups used for the effect, it may occur that the spacer arm contributes itself for protein binding, as reported by Burton and co-workers [60].

2.3.2. Overview of multimodal ligands

Since the establishment of multimodal chromatography as a promising choice for the downstream processing of biological products, there has been an increasing interest in developing and synthesizing novel ligands for this purpose. In the context of the

purification of mAbs, focus has been put on creating ligands that are able to work under conditions milder than those used in protein A chromatography. Furthermore, efforts are also being made in order to broaden the selectivity of these ligands towards different classes of immunoglobulins or antibody-like molecules (*e.g.* minibodies, antibody fragments), since in these cases protein A lacks the required specificity [61]. Some multimodal ligands that have been routinely reported in the literature for the purification of mAbs or mAb-related molecules are summarized in **Table 2.1.**

An important family of multimodal ligands is the hydrocarbyl amine family, which includes the hexyl amine (HEA HyperCel™), the propyl amine (PPA HyperCel™), and the 2-aminomethylpyridine ligands. The chemistry of these ligands offers hydrophobic and electrostatic interactions and the site for ligand immobilization is provided by an amine group, which constitutes the patch for electrostatic interactions. The binding of proteins occurs at physiological conditions through a combination of electrostatic and hydrophobic interactions (either aliphatic or aromatic). The elution is normally achieved through a charge repulsion mechanism, by decreasing the pH of the elution buffer below the protein isoelectric point and the ligand pKa, which causes both protein and ligand to become positively charged. This constitutes the basic principle of hydrophobic charge induction chromatography (HCIC), firstly reported by Burton and Harding [62].

Another family of ligands important to consider is the Capto™ family, which includes the N-benzyl-N-methyl ethanolamine (Capto™ adhere) and the 2-benzamido-4-mercaptobutanoic acid (Capto™ MMC), two of the most widely reported multimodal ligands. The development of these ligands derive from the finding that the introduction of hydrogen bonding groups in the proximity of the charged groups would provide high breakthrough capacities at high ionic strength conditions [50, 63]. Capto™ adhere is a strong anion exchanger with additional possibility of hydrophobic interactions in the phenyl group, and a hydroxyl group for hydrogen bonding. On the other hand, Capto™ MMC is a weak cation exchanger with a phenyl group as hydrophobic moiety, an amide group for hydrogen bonding, and a thioether group for thiophilic interaction. These ligands are frequently referred to as “salt-tolerant” resins [64], due to their ability to maintain high dynamic binding capacities in a range of ionic strengths from moderate to high (*e.g.* 15 $mS.cm^{-1}$). This characteristic is particularly important for performing the purification of biological products directly from the cell culture supernatants, which normally have a conductivity higher than 5 $mS.cm^{-1}$.

Table 2.1 – Novel ligands synthesized to be employed in multimodal chromatography. The chemical nomenclature, pKa and molecular structure of the ligands are indicated. The commercial name of some of the ligands is indicated in brackets. §Pall Life Sciences, §§GE Healthcare.

	Name	pKa	Structure
Positively charged ligands	4-mercaptoethylpyridine (MEP HyperCel™§)	4.85	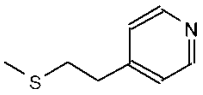
	Phenylpropylamine (PPA HyperCel™§)	6.0 - 7.0	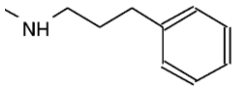
	Hexylamine (HEA HyperCel™§)	≈ 10	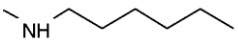
	2-Aminomethylpyridine [62]	$pKa_1 = 2.2$ $pKa_2 = 8.5$	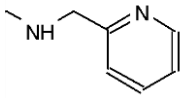
	Aminophenylpropanediol [62]	9.0	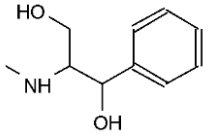
	2-(pyridin-2'-ylsulfanyl)ethanamine [65]	-	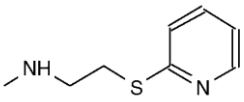
	3-(pyridin-2'-ylsulfanyl)propanamine [65]	-	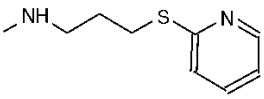
	N-benzyl-N-methyl ethanolamine (Capto™ adhere§§)	-	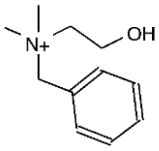
Negatively charged ligands	2-mercapto-5-benzimidazole sulfonic acid (MBI HyperCel™§)	-	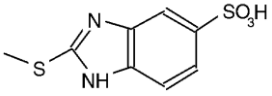
	2-benzamido-4-mercaptobutanoic acid (Capto™ MMC§§)	3.3	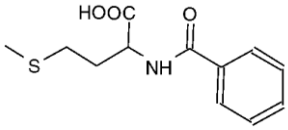

The mechanism of protein elution in these two ligands is complex, as it usually requires an increase in both salt concentration and pH value [64], in opposition to the elution by charge repulsion that is simply driven by changes in the pH value. Several studies have been performed in an attempt to reach optimal elution conditions, including the use of

controlled pH gradients [66] and the evaluation of different mobile phase modifiers [9, 67-71], such as arginine hydrochloride, ethylene glycol or urea.

The group of Hearn *et al.* [65, 72] reports a novel class of multimodal ligands, based on the synthesis of N-heterocyclic ligands comprising variations in the type and extent of a common pyridyl ring substitution. These ligands were explored for protein purification purposes, particularly antibodies, and are based on a heterocyclic ring (typically a pyridyl ring) from which pend, for example, alkylthiol, alkylamine or hydroxylalkyl nucleophilic groups. The pending arm enables an efficient immobilization of the ligand on the support material, while providing a spacer arm liable to be modified to alter the hydrophobicity of the ligand. These compounds are characterized by improved aromaticity/ hydrophobicity and dissociation properties, which lead to important performance advantages comparing to their aliphatic or aromatic counterparts [73].

Additional ligand diversity can be introduced by incorporating extra substituents into the heterocyclic ring, and by including analogues with one or more additional aromatic ring structures [65]. One of the most known and used member of the heterocyclic compounds family is the mercapto-ethyl-pyridine (MEP HyperCel™). MEP exhibits a binding mechanism that includes a mild hydrophobic effect, an electrostatic effect caused by the charge on the heterocyclic ring, and also a thiophilic effect on the sulfur group [74]. In a physiological pH environment, the binding occurs through the uncharged pyridine ring, in a way similar to the traditional HIC resins, and desorption is achieved according to the principles of HCIC [62]. However, these new generation ligands do not suffer from the main limitations of conventional HIC resins operated in bind-elute mode, which include (i) relatively low binding capacities and (ii) elution pools still containing fair amounts of salt, as sufficient binding of proteins in HIC can only be achieved with extremely high salt concentrations (*e.g.* 1-1.5 M Na_2SO_4, 1-2 M NaCl) [73]. It is also important to note that the additional affinity towards immunoglobulins, in principle provided by the sulfur atom, demonstrated by MEP HyperCel™, makes it a good candidate to replace protein A while not relying on extremely acidic pH values for elution of the proteins [75, 76].

2.3.3. Application in the purification of monoclonal antibodies

Multimodal chromatography has been applied to the separation of a wide variety of compounds, such as oligonucleotides [77, 78], nucleic acids [79] including plasmid DNA

[80], oligosaccharides [81], peptides, phosphopeptides and glycoproteins [82, 83], human growth factor [84], and monoclonal antibodies [85, 86].

The introduction of this type of chromatography into a purification workflow requires some aspects to be considered, namely the determination of the functionalities that the ligand should present, the optimal conditions that should be applied, the most suitable mode of operation (*flowthrough* or *bind-elute*), and the viability of an eventual scale-up. In addition, for a multimodal step to be industrially implemented in the purification of monoclonal antibodies, the type and extent of the interactions ligand-antibody and ligand-impurities should be completely understood, and the multimodal ligand must be thoroughly characterized in terms of toxicity and tendency to leaching [47].

Capture applications

The tailored selectivities combined with the cost-effectiveness and resistance to sanitization procedures of multimodal ligands have led to virtually all being evaluated as potential alternatives to protein A in the capture step. According to the supplier, the protein A resin MabSelect SuRe (~\$16,000/L_{resin}) is approximately 5 times more expensive than the multimodal resin Capto™ MMC (~\$3,100/L_{resin}) and 3.5 times more expensive than the multimodal resin Capto™ adhere (~\$4,500/L_{resin}).

In this section, the application of multimodal chromatography as a first capture step in the purification of mAbs or mAbs-based molecules is discussed, as well as the main conditions applied to achieve appropriate performances, and the impact of the particularities of each ligand in the purification design.

As previously mentioned, the antibody-selective MEP Hypercel™ resin has been extensively studied as an eventual alternative to protein A, as it provides similar binding capacities at approximately 25% of the cost, without suffering from ligand contamination or instability. In a study performed by Schwartz *et al.* [87], the isolation of a mAb from a protein-free cell culture supernatant was accomplished with purity values ≥ 95% and yields ranging from ~83% to 98%. Moreover, the MEP ligand proved to be effective in reducing the levels of a model virus (MVM – minute virus of mice), and also the DNA content, with a large fraction of DNA being removed during adsorption and washing steps. The MEP ligand was preferably operated at a pH near neutrality and at physiological ionic strength, while desorption was easily achieved by changing the pH,

rather than by variations in the buffer ionic strength [88]. Promising results were also reported by Guerrier *et al.* [89], in which MEP was used to directly capture antibodies from (i) mouse ascites fluid and (ii) a cell culture supernatant containing 5% fetal bovine serum (FBS). The purity values reached 83% and 60%, respectively, the latter being further improved (>98%) by a second step comprising hydroxyapatite chromatography. The elution pH used with MEP, although acidic (pH ~4.0), is much milder than that typically employed with protein A chromatography (pH 2-3), which reduces the probability of product inactivation or aggregate formation [90]. In this case, a difference in only one pH unit can be relevant, especially for antibody molecules that are extremely prone to inactivation under acidic conditions.

The elution at less acidic conditions is one of the most attractive characteristics transversal to multimodal ligands, including those in HEA Hypercel™ and the PPA Hypercel™ resins [91]. Toueille *et al.* [48] explored the properties of the HEA Hypercel™ ligand, which performed better in terms of clearance of protein aggregates than protein A. In the case of Pezzini *et al.* [11], a systematic screening of operating conditions was used to investigate how variations in some parameters (pH, conductivity, load concentration) would affect the performance of different multimodal ligands. Amongst the resins tested, PPA HyperCel™ was the one demonstrating the highest efficiency in removing HCPs and the highest percentage of mAb recovery. In this study, the authors showed that despite having some similarities, the ligands tested also have specific particularities that should be taken into account in the optimization of the purification process. For example, the optimal conditions for the washing step were significantly variable in terms of conductivity (7 – 23 $mS.cm^{-1}$), but close in terms of pH (5.5 – 6.5). Regarding the elution, a pH ranging from 3.8 to 4.0 allowed electrostatic repulsion between the positive ligand and the positive protein surface, at low conductivity (3 $mS.cm^{-1}$) to reduce the hydrophobic interaction. Different ligands also behaved differently with respect to the elimination of host cell proteins, as demonstrated by mass spectrometry analysis. Nonetheless, all the resins evaluated performed very adequately for a capture step, after optimal conditions had been previously obtained based on a model.

Synthetic ligands comprising heterocycles have also been described for the capture of monoclonal antibodies. In the case of the 2-mercapto-5-benzimidazole sulfonic acid (MBI HyperCel™), a negatively charged group was introduced in the ligand to repel acidic protein impurities that would be negatively charged at the pH used for adsorption.

On the other hand, the pH conditions can also be adjusted so that the sulfonic group contribute to IgG binding via electrostatic interactions, providing additional alternatives for the binding mechanism [92]. In the work of Girot *et al.* [93], the MBI ligand was successfully evaluated for the capture and separation of antibodies from different feedstocks, including a cell culture supernatant supplemented with FBS. To deal with the presence of albumin, the binding pH was adjusted to slightly acidic (5.2 – 5.5) conditions, to achieve complete binding of IgG while avoiding the co-adsorption of albumin. The binding mechanism was found to result from a combination of electrostatic and hydrophobic interactions, although the presence of a sulfur atom in the ligand may be considered for enhanced interaction.

Capto™ MMC, a negatively charged hydrophobic multimodal ligand, was patented for the capture of mAbs directly from cell culture supernatants [94, 95]. Joucla and co-workers [96] have conducted a comparative study involving this promising multimodal ligand and a conventional cation exchanger (Capto™ S) with respect to the capture of an antibody secreted by CHO cells. The binding conditions were optimized in a microplate assay using a pure human immunoglobulin. It was observed that increasing the buffer conductivity (up to 8 $mS.cm^{-1}$) showed not to significantly impact the antibody retention by the multimodal resin, while using the traditional cation exchanger the retention was expectedly reduced. The rationale for this behavior in the multimodal ligand is that a decrease in the electrostatic interaction is counterbalanced by an increase in the hydrophobic interaction, which translates into a salt-tolerant binding.

Kaleas *et al.* [97] performed a process comparison involving Capto™ MMC and protein A affinity chromatography as the initial capture step for the purification of two mAbs directly from harvested cell culture feedstocks. As the elution tends to be a critical task, four different elution strategies were evaluated in the multimodal adsorbent, comprising a pH-gradient, a sodium chloride gradient with and without urea, and an L-arginine HCl gradient. Overall, the mAb desorption seemed to be mainly achieved by disruption of the ionic interaction, although the disruption of other eventual interactions may enhance the elution. The performance obtained in terms of antibody yield was comparable for all the elution strategies employed and for the different feedstocks loaded on both multimodal and protein A resins, with values ranging from 90 to 100%. According to the authors, the major drawback reported for Capto™ MMC was the low level of HCPs clearance, which

could probably be enhanced by further optimization of the elution or by introduction of a wash step to selectively remove these proteins.

The increasing interest in using multimodal ligands with different selectivities has motivated the synthesis of multimodal ligands *à la carte* [65, 98, 99] to specifically capture monoclonal antibodies. The pyridine-based multimodal ligands reported in the work of Mountford *et al.* [72] were evaluated in both static and dynamic binding studies using pure mAb samples, with recoveries of 90% or higher being typically achieved. The PSEA (pyridinylsulfanylethylamine) and PSPA (pyridinylsulfanylpropylamine) classes of ligands, which differ in the length of the spacer arm between the exocyclic sulfur and the terminal primary amine (see **Table 2.1**), were further evaluated in the purification of mAbs from crude cell culture supernatants, and while the former showed a better selectivity, the latter revealed higher capacity for protein binding.

Charged/hydrophobic multimodal ligands with strong cation exchange functionalities appear as feasible options to be used as a capture step, unlike their anion exchanger counterparts, which strongly interact with phospholipids and DNA, thus reducing the capacity for purifying IgG in a bind-elute mode. For this reason, positively charged multimodal ligands do not directly represent an alternative to protein A and have been mostly evaluated as intermediate or polishing steps.

Polishing applications

In the downstream processing of monoclonal antibodies, the protein A affinity chromatography is normally followed by two additional polishing steps to fulfill the final product specifications imposed by regulatory agencies, in terms of host cell protein, DNA, virus and aggregate contents. The ineffective removal of these compounds during purification can be detrimental for the safety of the therapeutic formulation, since multiple side effects can be unpredictably triggered. The chromatography operations that are typically employed as polishing steps can involve cation and anion exchange resins, hydrophobic interaction resins, and ceramic hydroxyapatite adsorbents.

Considering the potential of multimodal ligands, attempts are currently being made to remove one of the intermediary/polishing steps that are currently used in the downstream processing of monoclonal antibodies. Manufacturing costs to produce mAb-based drugs would be highly reduced if the purification process could combine a highly selective first

capture step (protein A-based or not) and only one multimodal anion exchange chromatography polishing step, for example.

Capto™ adhere was specifically designed for the polishing of mAbs following protein A chromatography, and it is the most widely reported ligand for this purpose. The application of this multimodal ligand has been however limited by poor understanding of its behavior and attributes. Nevertheless, several research studies have been performed to evaluate its performance in flowthrough mode, particularly for aggregate removal, at a commercial manufacturing scale [100]. Overall, Capto™ adhere is reported to perform better than conventional anion exchange resins, exhibiting higher binding capacity for aggregates, while individual mAb molecules flow through the resin without being retained. Chen *et al.* [101] described the advantage of loading the neutralized elution fraction from protein A directly on Capto™ adhere to achieve a reduction of dimer aggregates. Similar finding was reported by Gao *et al.* [99], who were able to reach a purity of 97.4% in terms of aggregate removal using Capto™ adhere, based on the rationale that mAb dimers would bind more strongly to the multimodal ligand than the monomeric forms. The authors discuss that the hydrophobicity of mAb molecules increases with the degree of aggregation and that aggregates have more local negative regions compared to the monomeric forms. Thus, the combination of hydrophobic and electrostatic interactions and the existence of more binding sites provided by the aggregates would favor the interaction with the functional groups of the positively-charged multimodal ligand, compared to a conventional single-mode ligand.

In another study, Eriksson *et al.* [102] proposed a purification step to follow protein A also based on Capto™ adhere multimodal anion exchanger. The conditions were optimized using DoE for the operation in flowthrough mode. The authors have observed that not only the amount of dimers/aggregates was considerably reduced (<0.1%), but it was also possible to retain key contaminants, including host cell proteins, DNA, leached protein A and viruses. Regarding viral clearance, two model viruses (MVM – minute virus of mice – and MuLV – murine leukemia virus) were successfully removed using conditions of both high and low ionic strengths, which would not be expected to occur in a conventional anion exchanger.

Although Capto™ adhere is usually operated in flowthrough mode, there are some examples in which the operation in bind-elute mode was advantageous as a polishing step.

Voitl and co-workers [103] explored the possibility of using Capto™ adhere to separate an antibody (pI = 8.3-8.6) from lysozyme (pI = 11.35), by binding the antibody at neutral pH, while the weakly bound impurity flowed through the resin. Depending on the isoelectric point of the mAb and the impurity protein, this may not be achieved in a pure anion exchanger, making an apparently simple separation between two different proteins an extremely challenging task. Other studies mention developed processes comprising a polishing step with Capto™ adhere in bind-elute mode to consistently obtain a product within the specifications limits in terms of HCP content, which failed when operated in flowthrough mode [104].

In summary, the application of multimodal ligands for the polishing of mAbs can be promising for shortening the number of steps required to achieve the final specifications of the product. Although the primary mode of interaction relies typically on anion exchange groups, additional groups included in the multimodal ligand allow the operation in either flowthrough or bind-elute modes, depending on the intended purpose.

Table 2.2 summarizes purification conditions and the corresponding performance parameters reported in the literature for multimodal ligands employed in the capture or polishing of mAbs from different feedstocks.

As the window of operation is greatly enlarged with the multitude of interactions provided by multimodal ligands, rapid optimization of chromatographic conditions is likely to be required on a case-to-case basis for an effective process development. The next section presents an overview of high-throughput screening methodologies that have been used for early-stage optimization of chromatographic processes.

Table 2.2 – Benchmarking of purification conditions and performance parameters obtained in the purification of monoclonal antibodies using multimodal chromatography ligands. A: Adsorption; W: Wash; E: Elution; PF: Purification factor; PBS: Phosphate buffered saline; HCPs: Host cell proteins; MCSGP – Multicolumn countercurrent solvent gradient purification.

Ligand	Feedstock	Purification Conditions	Performance Parameters	Ref
MEP HyperCel™	Cell culture supernatant containing FBS	A: 25 mM phosphate + 25 mM NaCl, pH 7.2 W: A + 25 mM sodium caprylate E: 50 mM acetate, pH 4.0	Yield = 76% Purity = 69% PF = 40	[89]
	Protein-free cell culture supernatant	A: 50 mM Tris-HCl, pH 8.0 E: 50 mM acetate, pH 4.0	Yield ~ 83% - 98% Purity ≥ 95%	[87]
HEA HyperCel™	Cell culture supernatant	A: PBS W: 5 mM sodium phosphate, pH 7.4 E: 50 mM sodium acetate, pH 5.5	Yield = 92% HCPs = 730 ppm Aggregates < 0.5%	[48]
PPA HyperCel™	CHO cell culture supernatant	A: pH 7.3; 13 $mS.cm^{-1}$ W: pH 5.5; 23 $mS.cm^{-1}$ E: pH 3.8; 3 $mS.cm^{-1}$	Yield = 93% HCPs = 430 ppm	[11]
MBI HyperCel™	Cell culture supernatant containing FBS	A: 50 mM acetate + 0.14 M NaCl, pH 5.2 E: 50 mM carbonate + 0.14 NaCl, pH 9.0-9.5	Yield: no antibodies were found in the flowthrough fraction Purity > 90%	[93]
Capto™ MMC	CHO cell culture supernatant	A: 0.1 M sodium citrate, pH 5.0 E: 0.1 M sodium phosphate, pH 7.5	Yield = 92% – 93% Purity = 95 – 96%	[96]
	CHO cell culture supernatant	A: Variable to match the pH of the feedstock E1: pH gradient from 7.0 to 10.0 E2: salt gradient from 0 to 0.3 M NaCl, pH 7.0 E3: 2 M urea + gradient of 0.3 M NaCl, pH 7.0 E4: L-arginine HCl gradient from 0 to 0.3 M, pH 7.0	Yield = 90% - 91% Monomer = 96.8% - 98.5% HCPs = 500 – 2600 ng/mg	[97]
2-PSEA	Pure mAb sample	A: 600 mM sodium sulfate + 25 mM Tris, pH 9.0 E: 25 mM HEPES, pH 7.0	Yield = 85% - 96%	[72]
2-PSPA	Pure mAb sample	A: 600 mM sodium sulfate + 25 mM Tris, pH 9.0 E: 25 mM HEPES, pH 7.0	Yield = 84% - 91%	[72]
Capto™ adhere	Elution pool from protein A capture	A: 50 mM phosphate, pH 7.5 E: 50 mM citrate, pH 2.6	Yield = 80.1% HCPs = 14.5 ppm Aggregates = 2.6%	[99]
	Elution pool from a MCSGP capture	A: 10 mM phosphate, pH 8.0 E: 10 mM phosphate + 10 mM citrate, pH 4.0	Purity > 99.7% HCPs < 3 ppm	[104]

2.4. High-throughput screening for the development of chromatographic processes

The design and optimization of chromatographic processes constitute a supporting pillar of the biopharmaceutical industry. The increasing number of drug candidates demands a short timeline from process development to launching the product, since pharma companies can lose several million U.S. dollars for each day a potential blockbuster drug fails to be released to the market [105].

Trial and error strategies based on univariate optimization methods are no longer sufficient to address current industrial needs. An increase in sample throughput and a multivariate analysis of different process parameters becomes necessary, which requires **miniaturization**, **parallelization** and **automation**. Thus, the challenge lies in developing effective high-throughput screening platforms that can work with reduced sample materials and deliver results within a short time frame.

One of the first techniques attempting a high-throughput screening in chromatography for isolation of biological products was reported by Mazza *et al.* [106] and did not yet rely on an automated setup. This technique aimed at screening 33 displacer molecules for protein displacement in ion-exchange chromatography (**Figure 2.5**). Two different ion exchange resins were evaluated with respect to the displacement of either lysozyme or cytochrome C. The process was initiated by equilibrating the stationary phase with 36 mL of protein solution and the incubation times to attain complete equilibrium ranged from 5 and 7 hours, depending on the resin. The stationary phase with the protein bound under equilibrium conditions was then distributed in 25 μL aliquots and the 33 displacers were evaluated and ranked in terms of percentage of protein displaced.

Although a certain degree of parallelization could be attained using this strategy, the process was laborious and time-consuming, as the analytics involved in determining the amount of protein displaced in each case required equilibrium conditions to be reached (incubation times of several hours). In addition, the starting material also required a significant amount of protein to analyze, which is often a limitation in early-stage process development.

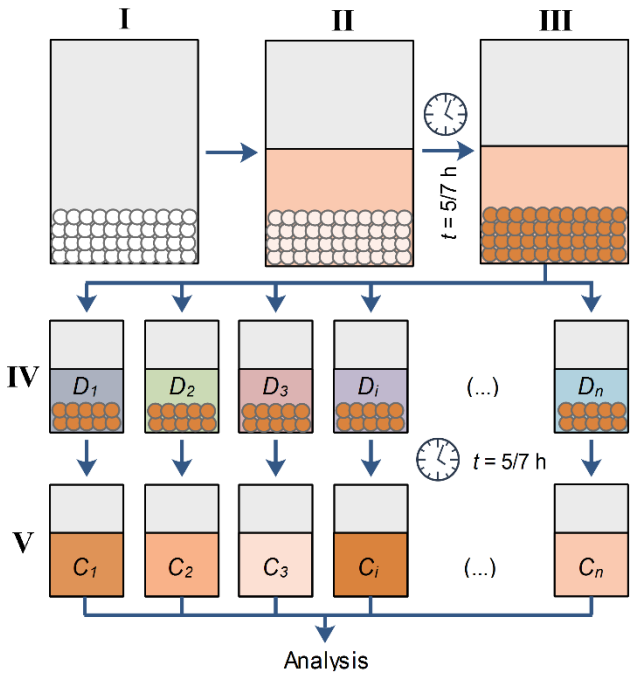

Figure 2.5 – Schematic representation of the high-throughput screening technique for displacer screening. **I** – Equilibration of stationary phase in buffer; **II** – Load of protein solution; **III** – Stationary phase equilibrated in protein solution; **IV** – Equilibrated stationary phase distributed into aliquots to enable parallel screening of different displacers (*D*); **V –** Amount of protein displaced (*C*) in each batch determined using an appropriate analytical technique. Adapted from Mazza *et al.* [106].

As robotic platforms and automated liquid handling stations became widely available, both in industry and academic laboratories, novel strategies for performing a high-throughput screening of chromatographic processes emerged. The current miniaturized techniques for the development of chromatographic processes are often considerably different from laboratory-scale fixed-bed chromatography, both in format and intrinsic operation. In this context, the most commonly used HTPD-compatible formats for initial screening of chromatography resins or process conditions are based on (i) microtiter plates, (ii) micropipette tips and (iii) miniature columns. These are subsequently discussed in detail.

2.4.1. Microtiter plates

The use of 96-well microtiter plates allows a high degree of experimental parallelization and is amenable for integration with automated liquid handling stations. However, optimization studies in this format differ significantly from a standard chromatographic operation in terms of hydrodynamics, as the different steps are performed in a batch mode instead of a continuous liquid flow through the stationary phase. Consequently, considering that a chromatography column can be regarded as cascade of equilibrium

stages (multiple theoretical plates) where a separation occurs, a single well represents only a single stage in such a cascade (one theoretical plate). Nevertheless, the steps performed in a microtiter plate are the same as those in a conventional chromatographic separation, comprising (i) equilibration of the resin; (ii) sample loading; (iii) wash of non-specifically bound molecules; and (iv) elution.

The schematics of the batch operation using microtiter plates is shown in **Figure 2.6**. This approach can be used to (i) perform equilibrium isotherm studies under different operating conditions or (ii) optimize the performance of a particular separation.

The isotherm studies aim at correlating the concentration of a target molecule in solution (C_e) with the corresponding concentration in the stationary phase (q_e) at equilibrium conditions. The concentration (C_e) can be determined by analyzing the liquid supernatant after reaching equilibrium, while q_e can be indirectly calculated by knowing C_e and the initial concentration of the target molecule (C_i) or by eluting the target molecule and determining the concentration in the eluate (C_{el}). The different concentrations can be related by **Equation 2.1**, where V_i and V_r correspond to the initial volume and volume of resin in the well, respectively.

$$C_i \times V_i = q_e \times V_r + C_e \times V_i \qquad \textbf{Equation 2.1}$$

To obtain a complete set of isotherm data points, the equilibrium concentration should be varied over a range of interest, in order to fit the points to a Langmuir isotherm equation (**Equation 2.2**), where q_m is the maximum capacity of the stationary phase and K_d is the dissociation constant.

$$q_e = \frac{q_m \times C_e}{K_d + C_e} \qquad \textbf{Equation 2.2}$$

In the case of using the microtiter plates for the screening of different operating conditions, it becomes relevant to evaluate the performance of the separation by calculating the recovery yield (Y_{rec}) according to **Equation 2.3**. It is important to highlight that during the different steps some of the target protein may be lost in the flowthrough ($C_e \times V_f$) or in the wash step ($C_w \times V_w$), before elution is accomplished.

$$Y_{rec} = \frac{C_{el} \times V_{el}}{C_i \times V_i} \times 100 \qquad \textbf{Equation 2.3}$$

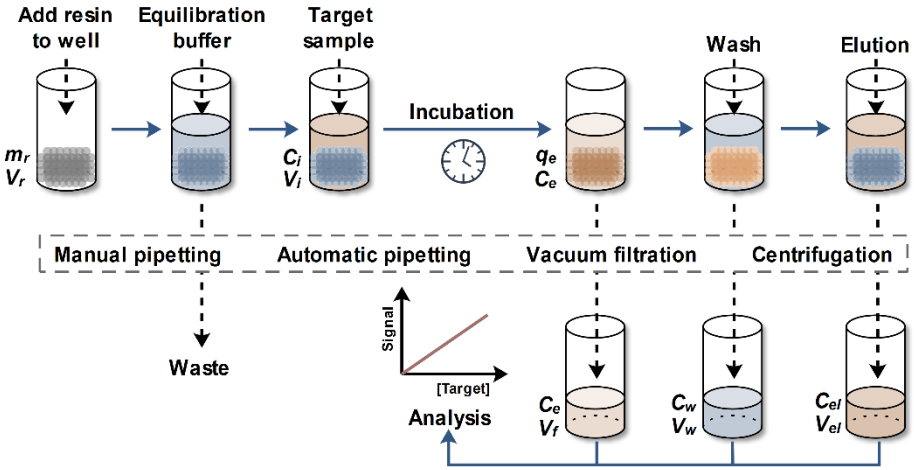

Figure 2.6 – Schematics of the batch operation using microtiter plates for isotherm studies or high-throughput screening of chromatographic conditions. Liquid manipulation in the different steps can be achieved manually or by integration with an automated liquid handling station. m_r – mass of stationary phase (resin); V_r – volume of stationary phase (resin); C_i – initial concentration of target molecule; V_i – initial volume of molecule solution; q_e – concentration of target molecule in the stationary phase at equilibrium; C_e – concentration of target molecule in solution at equilibrium; V_f – volume of flowthrough solution; C_w – concentration of target molecule in the wash; V_w – volume of wash solution; C_{el} – concentration of target molecule in the eluate; V_{el} – volume of eluate solution.

Several works report the use of 96-well plates to devise purification strategies with different chromatography resins [13, 48, 107]. Pezzini *et al.* [11] investigated four multimodal resins for the direct capture of an antibody from a CHO cell culture supernatant and characterized the contaminating host cell proteins (HCPs). Although the use of a 96-well plate format allowed the simultaneous exploration of many conditions, the biological material was firstly incubated for 60 min and multiple washing steps (5 min each) were employed before elution. These lengthy incubation steps limit the number of conditions that can be evaluated within a short time frame, therefore, mathematical modelling allowed the authors to predict the behavior of the resins at any conditions inside the tested range. Chu *et al.* [10] employed a similar approach to optimize the separation of human serum albumin (HSA) using membrane-bottomed 96-well microtiter filter plates operated in a vacuum manifold apparatus.

It is important to consider that there are several factors influencing the performance of the high-throughput technique based on 96-well plates, namely (i) the reproducibility of the aliquoted resin volume, (ii) the contact time of the solution and resin during mixing, and (iii) the volume of liquid carried through the resin after the liquid phase is removed by centrifugation or vacuum filtration. Along these lines, Coffman *et al.* [12] performed a study centered on the manipulation of a miniaturized batch-binding system for protein

purification and quantification of error and non-idealities associated with such system. As a conclusion, the authors highlight that the results of the miniaturized platform are not necessarily identical to those obtained in conventional chromatography columns, however they enable the trending of important parameters (purity and recovery yield) and are sufficient to assist in the development of chromatographic processes.

2.4.2. Micropipette tips

Miniaturization of chromatography in a micropipette tip format consists in immobilizing the chromatography resin at the bottom of a pipette tip (volume of resin can range from 10 – 160 μL). Unlike the operation in a chromatographic column, the sample and different buffers are pipetted bi-directionally (back and forth) through the stationary phase during each dispense-aspiration cycle (**Figure 2.7**). Therefore, each aspiration operation corresponds to a single stage of equilibrium, similarly to the batch operation using microtiter plates. However, in the case of micropipette tips there is a dynamic flow of the solutions through the chromatographic bed, which improves the efficiency of mass transfer and decreases processing time (no convective mixing is required).

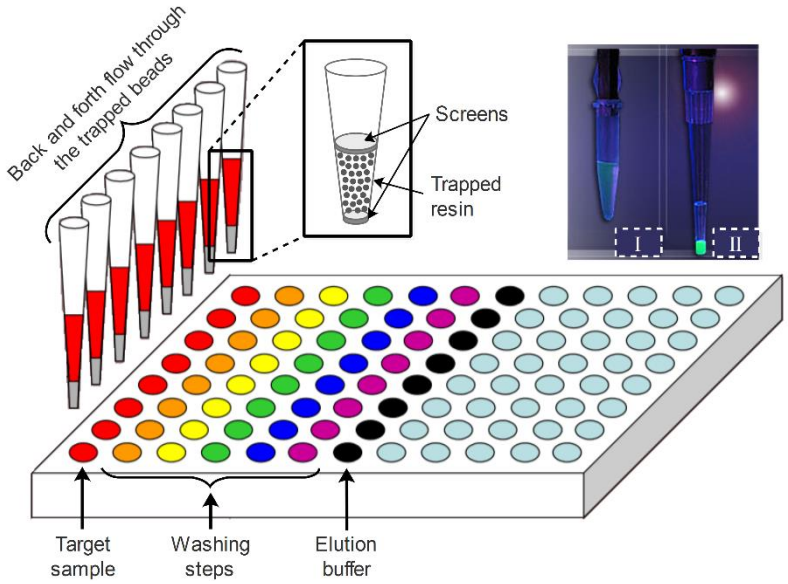

Figure 2.7 – Schematic diagram of the micropipette tip format. The chromatography resin is encased at the end of the pipette tip and capture, wash and elution steps are performed in parallel for up to 12 samples simultaneously from a 96-well microtiter plate. The photograph inset shows the affinity purification of a fluorescently-labeled antibody sample using protein A beads trapped in the micropipette tip: I – Low concentration Alexa488-labeled antibody showing low fluorescence intensity; II – Protein A micropipette tip column after processing the antibody sample. The Alexa488-labeled antibody was successfully captured and the sample was purified by washing the column. Adapted from PhyNexus webpage.

It is important to highlight that the bed height of the micropipette tip is slightly tapered, which means that the linear velocity of the liquid will change through the chromatographic bed. For this reason, the optimization of linear velocity and residence time is crucial in the development of a micropipette tip-based purification process, as reported by Wenger *et al.* [108]. The authors were able to successfully scale-down 1000-fold the purification of virus-like particles (VLPs) from a yeast cell lysate by operating micropipette tips (40 – 80 μL resin) in a robotic workstation equipped with a microtiter-plate gripping arm and an eight-channel pipetting arm with disposable tip adapters (**Figure 2.7**). The linear velocities used in the assays were optimized to be within the range of typical laboratory column operations, however reduced residence times were obtained due to the short bed height inside the tip. The strategy adopted by the authors to increase the residence time was to perform multiple aspiration-dispense cycles, which allowed the binding of ≥87% of the VLPs. The throughput of the experiments was improved by 10-fold and, overall, the results obtained in the miniaturized platform were concordant with the lab-scale method in terms of VLP recovery and purity.

Chhatre *et al.* [18] reported additional parameters that need to be optimized in the robotic operation of chromatography micropipette tips, which mostly rely on iterative and trial and error proceedings. One is the distance of the tips to the bottom of the wells plates, to ensure that the resin remains covered with liquid at full aspiration and avoid the risk of aspirating air during the operation. The other is the delay time between aspiration-dispense cycles, to account for the resistance to fluid flow imposed by the packed bed inside the tip, particularly when pipetting viscous solutions.

In a comparative study of three high-throughput screening formats (96-well filter plates, micropipette tips and miniature columns) by Feliciano *et al.* [15], the quality and process performance attributes of mAb monomer purity, host cell protein levels and yield were evaluated for a protein A capture step. From all the formats, the micropipette tips underperformed in terms of recovery yield (~5% lower than other formats) and reproducibility (2.5% RSD *vs* 0.5-1.5% RSD for other formats). Nonetheless, this study reinforces the idea that miniaturized formats are useful to support optimization of chromatographic processes by enabling the identification of significant parameters and experimental trends.

2.4.3. Miniature columns

The miniaturization of chromatographic operations has proved difficult to establish on automated liquid handling stations mainly due to the need for a continuous, positive pressure-driven flow through the column. The latter fails to be provided by miniaturized formats as microtiter plates and micropipettes tips, but can successfully be achieved when using miniature columns, which mimic more closely a conventional packed-bed format. Still, the packing densities are not comparable to the ones used in industrial process settings, since the diameter of these columns is only one to two orders of magnitude higher than the diameter of the most relevant large scale beads (*e.g.* 90 μm).

Miniature columns can be provided in a 96-array format organized in a series of blocks, each containing 8 columns arranged side-by-side, which are compatible with both manual operation (standard pipettes or centrifuges) or with robotic platforms. The work of Wiendahl *et al.* [109] reports the use of 200 μL Media Scout RoboColumns™ (Repligen) operated in a robotic liquid handling station to study dynamic chromatographic operations, such as frontal analysis (breakthrough) and elution experiments. The miniature columns consisted of a conical duct coupling the pipetting needle of the robotic workstation to the inlet of the column, sealed by an O-ring. The resin was compressed from the top of the column, by using the conical duct as a pressing stamp. This setup allowed a reproducible packing of the resin, a tight but flexible linkage between the pipetting needle and the miniature column, as well as the possibility of a constant positive pressure-driven flow through the column (**Figure 2.8-A**). Fraction collection was performed directly beneath the miniature column using 96-well plates, and the smallest fraction size amenable to be collected was determined to be ~25 μL (approximately the size of the droplets leaving the columns, representing 12.5% of the resin volume). This volume represents a limitation in terms of analytical quantification, since a sufficient liquid height inside the wells is required for an appropriate signal read out in a spectrophotometer. The difficulty of measuring with accuracy the volume of the collected fractions is another limitation of this method. An overview of the experiments performed by the authors is shown in **Figure 2.8-B** for breakthrough and elution studies. Major challenges were related to well-to-well deviations caused by variations in the number of droplets collected per fraction and the difficulty in performing a linear gradient for the elution. Since each column is connect to a single pump via the pipetting needle, a linear gradient has to be mimicked by a series of small steps, as illustrated in **Figure 2.8-B**.

Nevertheless, the methodology to collect fractions during the chromatographic operation and the application of a quasi-linear gradient allowed to obtain consistent results between the miniaturized and lab-scale approaches.

While this screening format is still unlikely to provide a baseline separation of molecules, its application has been successful in rapidly providing information on promising chromatographic systems to test at lab or pilot scale processes [16, 17].

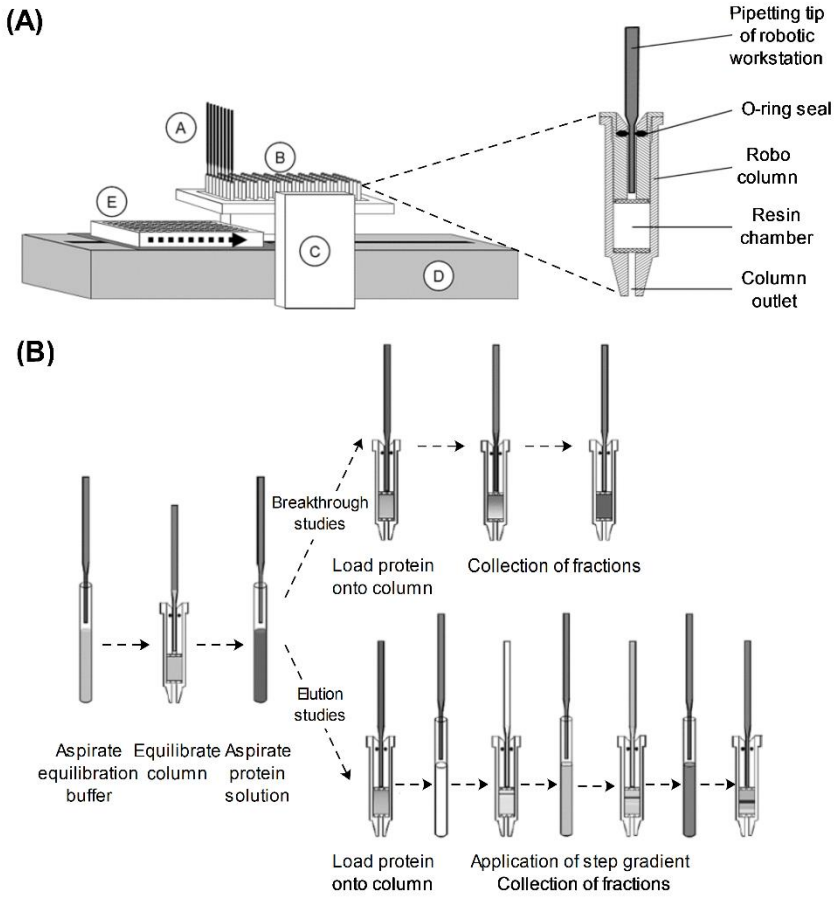

Figure 2.8 – Automation of parallel chromatography on a liquid handling station (LHS). **(A)** Components on a Tecan Evo Freedom 200 LHS: A – pipetting tip of the LHS; B – 96-column array; C – column array carrier; D – Te-link module; E – microtiter plate in collect position. **(B)** Schematic overview of chromatography experiments performed using the LHS. Adapted from Wiendahl *et al.* [109].

2.5. Chromatographic separations using microfluidics

Liquid chromatography is one of the most extensively studied method for analytical and preparative application in the separation of biological compounds, so there is a particularly high demand for its miniaturization [110]. In fact, over the last 18 years there has been a significant increase in the number of publications combining chromatographic

operations and microfluidic devices (**Figure 2.9**). It is interesting to note that this increasing trend started in 2000 alongside the introduction of new technologies in microfluidic chip fabrication, namely the soft-lithography technique for polydimethylsiloxane (PDMS) replica molding [111].

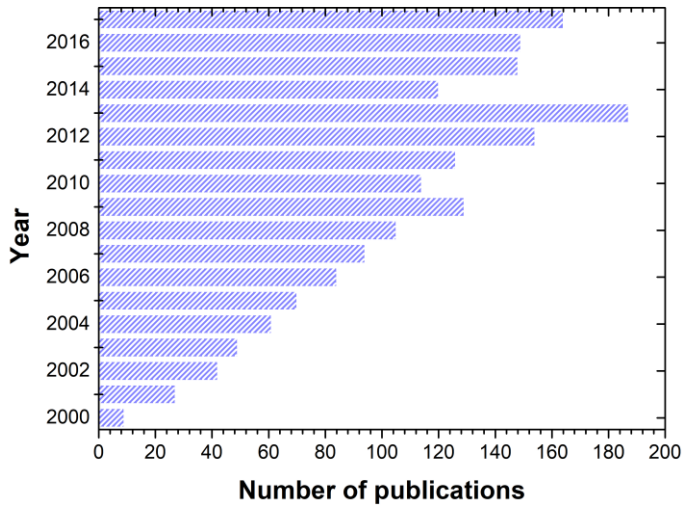

Figure 2.9 – Number of publications covering chromatographic applications in microfluidic devices over the last 18 years. The search keywords were as follows: ((chromatography) AND (microfluidics OR microfluidic)). The data was retrieved from ISI Web of Science on 17th June 2018.

Microfluidic devices offer the possibility of constructing chromatographic columns containing different types of stationary phases, such as functionalization of the channel walls, *in situ* generation of monoliths or particle-based packings. The latter, in particular, presents several challenges, namely in terms of (i) strategies for particle retention in the microfluidic channel, (ii) preparation of reproducible and compact microcolumns, and (iii) strong dependence of back pressure during operation.

In order to achieve comparable versatility to their column-based counterparts, microfluidic devices for chromatographic separations are being integrated with flow control functionalities [112] (*e.g.* valves and pumps) and various types of miniaturized sensors for on-chip signal monitoring [113, 114].

2.5.1. Concept and critical variables

The flow in microfluidic channels is typically characterized by a laminar regime ($Re << 1$), meaning that mixing only occurs through molecular diffusion [115]. In the particular case of chromatographic separations, this characteristic can be a limitation if one considers the integration of a gradient generator [116] for performing an elution in gradient mode or for testing different buffer compositions in high-throughput screening

applications. In a microchannel with packed beads, an increase in the Reynolds number is expected, as the liquid velocity through the beads will increase by a factor of approximately 2-fold, assuming a bed void fraction of 0.55 [117]. Nevertheless, the laminar regime conditions are maintained.

Considering a typical rectangular microchannel, with 100 μm width and 20 μm height, a surface-to-volume ratio of ~10^5 m^2/m^3 is obtained. In this scenario, the maximum degree of interaction of the molecules in solution with the surface of the channel can be evaluated by the Péclet number (Pe), which measures the ratio of convective to diffusive forces according to **Equation 2.4**, where U is the characteristic flow velocity, L is the characteristic channel dimension, and D is the diffusion coefficient. In this case, considering a flow rate of 0.5 μL/min ($U \sim 10^{-3}$ m/s), the characteristic Péclet number is about 10^5 for a typical antibody ($D \sim 10^{-12}$ m^2/s [118]). This means that the molecules at the center of the microchannel have a very limited interaction with the channel walls.

$$Pe = UL/D$$ **Equation 2.4**

Therefore, in microchannels there is a compromise between a high rate of molecular capture and a high efficiency of capture. This implies that if a rapid supply of molecules is required (high flow rates), a larger fraction of molecules (>90%) will be lost [119]. In the case of on-chip chromatography, the insertion of nanoporous microbeads in a microchannel leads to a pronounced enhancement of the surface-to-volume ratio by a factor of 50 [120] considering for example 4% cross-linked agarose beads. The short analyte transport length, reduced to the distance between adjacent beads and bead pore sizes, results in a simultaneous enhancement in both the rate and efficiency of capture of biomolecules [121, 122].

One of the main performance parameters of a chromatographic separation system is the number of theoretical plates, N, that can be accommodated by a column of a certain length, L, and resolved by an appropriate detection scheme. The number of theoretical plates can be determined by **Equation 2.5**, where H is the column plate height.

$$N = L/H$$ **Equation 2.5**

The plate height is also related to peak broadening of a sample eluted from the column, as expressed by the Van Deemter equation (**Equation 2.6**), where A, B and C are variables associated to various characteristics of the column and u is the mobile phase linear velocity through the column. In the case of conventional packed columns, A is influenced

by the packing quality, B is a function of longitudinal diffusion in the column and C accounts for the resistance to mass transfer in both the stationary and mobile phases [123]. Band dispersion in microfluidic chromatography columns can be improved using beads with increasingly reduced and monodisperse dimensions (∅ = 2–5 μm), to avoid irregularities between spherical particles and the presence of large stagnant spaces.

$$H = A + \frac{B}{u} + Cu \qquad \textbf{Equation 2.6}$$

Therefore, according to **Equation 2.5**, it becomes clear that scaling down the column length (L) results in a decreased number of theoretical plates (N) assuming a constant plate height (H), which adversely impacts the performance of the separation [123]. This is particularly relevant if an analytical application is pursued. On the other hand, such decrease may not be significant if the device is intended to be used for the optimization of chromatographic parameters and separation performances (bead-level analysis).

Modelling approaches applied to microfluidic chromatographic systems can be used to describe and further understand binding of biological molecules to the chromatographic resins at bead-level. The analytical methods currently used at macroscale fail at capturing the concentration variations of the biomolecules through the column, which are dominant in microscale systems. In this context, the work of Gerontas *et al.* [117] reports a model to describe the hydrodynamics, mass transfer and adsorption/desorption kinetics of chromatographic processes at bead-level. The main concept is shown in **Figure 2.10-A**, in which chromatography beads were trapped inside a microfluidic channel by fabricating two channels at different heights and fluorescently labeled lysozyme was used as a model protein to study the breakthrough profile through the column. Important assumptions reported by the authors include (i) the mass transfer within the beads being controlled by diffusion and (ii) the target protein not significantly binding to the walls of the microfluidic column [117].

As chromatography beads are normally inhomogeneous in terms of size distribution, it is difficult to obtain a regular packing inside the microchannel, which causes bed void fractions above 0.5 to be frequently obtained in these systems. The simulation results of Gerontas *et al.* [117] show that the higher void fraction occurs in the vicinity of the walls of the channel, as spherical beads cannot be properly accommodated close to the walls, which causes a higher level of protein concentration in these areas. This can be seen in **Figure 2.10-B** (cross-sectional view of the channel), where deep red areas (high

concentration of lysozyme) are located near the walls of the channel and deep blue areas (low concentration of lysozyme) are located inside the beads.

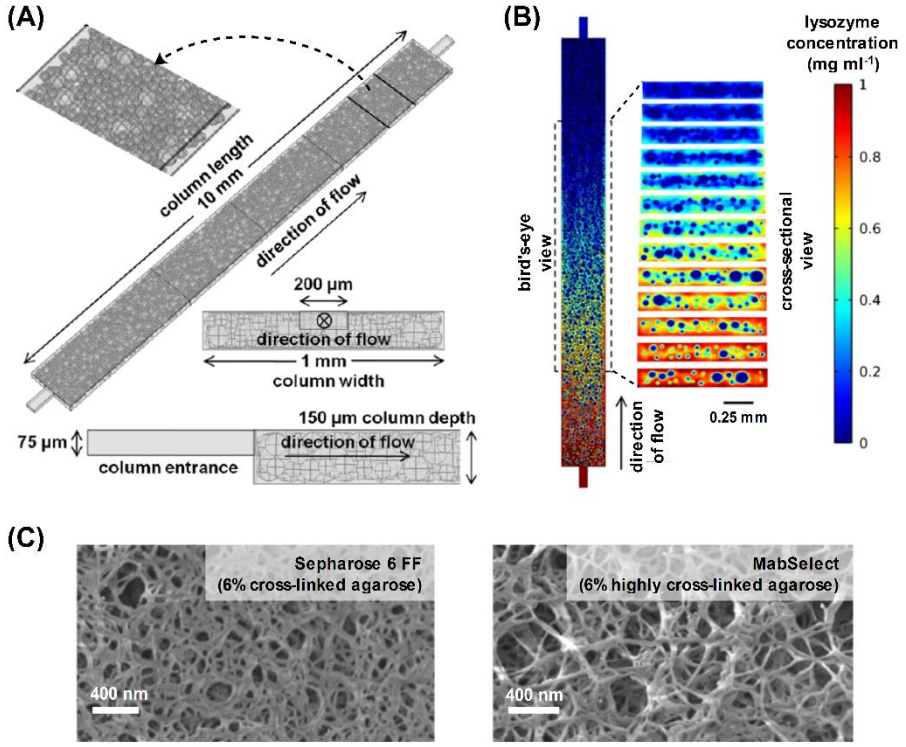

Figure 2.10 – Example of chromatography modelling to describe protein adsorption at bead level using a microfluidic channel with packed beads. **(A)** Three-dimensional schematic view of the microfluidic column. According to the simulations performed by the authors [117], the number of beads in the microfluidic column is ~4700 and their diameter is normally distributed between 40 and 100 µm (average bead diameter: 70 µm). The bed void fraction was estimated to be 0.55. **(B)** Lysozyme concentration profiles at the liquid phase of the column 250 s after loading (protein initial concentration 1 mg.mL^{-1}). The left-hand side image gives a bird's-eye view of the lysozyme concentration profile on a plane oriented parallel to the direction of the flow. The right-hand side image provides lysozyme concentration cross-sectional profiles, oriented perpendicularly to the direction of the flow. Adapted from Gerontas *et al.* [117]. **(C)** Scanning electron microscopy images of chromatography resins showing Sepharose 6FF (6% cross-linked agarose) and MabSelect (protein A ligand, 6% highly cross-linked agarose). Micrographs were taken post-critical point drying. Adapted from Nweke *et al.* [124].

In terms of fluid flow across the column, the liquid velocity inside the pores is approximately zero (dead-end pores), and the hydraulic resistance through the pores is much higher than in the bulk of the interparticle space. Thus, the transport of biomolecules in solution through the pores of the beads occurs uniquely by diffusion mechanisms, creating a transient gradient of protein concentration from the surface to the inner space of the beads [125]. Depending on the percentage of agarose and extent of the cross-linking process, different magnitudes of pore sizes can be achieved. The micrographs in **Figure 2.10-C** show examples of commercially available

chromatography beads [124] where pores of approximately 100 nm can be visualized, 1000-fold smaller than the typical height of a microfluidic channel.

2.5.2. Applications in the context of biomolecule purification

Microfluidic-based approaches are well suited as a miniaturized and automated technology for preparing small quantities of pure molecules on demand, which has been increasingly explored for personalized health-care diagnostics and point-of-use production treatments [19]. In addition, the development of miniaturized processes consuming small amounts of sample and offering a continuous liquid flow through a chromatographic column is necessary for optimizing chromatographic separations in early stages of process development [20, 21, 126].

The work of Shapiro *et al.* [20, 126] reports the development of a glass microchip for quantifying protein breakthrough using standard preparative chromatography beads (**Figure 2.11-A**). The system allows the visualization of binding/elution events within a packed chromatography bed (W = 0.15 mm; L = 10 mm; H = 1 mm) using fluorescence microscopy. The device was operated at *"true"* flow rate conditions (*i.e.* comparable to those typically used at bench scale) and the results in terms of breakthrough and elution studies showed good quantitative agreement between the microfluidic column and 2-mL and 30-mL conventional columns. Along the same lines, Rho *et al.* [21] developed a valve-integrated microfluidic device for determining the adsorption characteristics of a molecule (~6 μg per experiment) to commercial beads. The device could automate the process of (i) trapping the beads, (ii) loading the beads and reagent solutions into a reaction chamber, (iii) mixing the solutions, (iv) circulating the beads in the solution and (v) determining the concentration of the target molecules bound to the particles.

The versatility of microfluidic devices enables creative approaches for addressing specific purification challenges, as demonstrated by Millet *et al.* [19] in a device that combines different chromatography modules for point-of-care protein purifications (**Figure 2.11-B**). The architecture of each module consisted of a single inlet with branched channels to uniformly distribute the liquid when entering the chromatographic column (W = 7 mm; L = 1.2 cm; H = 130 μm) (**Figure 2.11-B i**) and the beads were retained inside the column by a line of rectangular barriers placed in the direction of flow path at both ends of the column (**Figure 2.11-B ii**). The performance of the chromatographic module was evaluated by monitoring the fluorescence emission of eGFP during loading, saturation

and elution (**Figure 2.11-B iii-v**). Although the fabrication of the device was relatively complex, it was possible to customize different sequences of chromatography operations by manually interconnecting the microfluidic modules using cast-in-place 3D fluidic bridges (**Figure 2.11-B vi-vii**). This approach eliminates the need for fabricating new devices for different fluidic configurations, however, it introduces a significant dead volume in the fluidic path compared to a structure with built-in microfluidic connections.

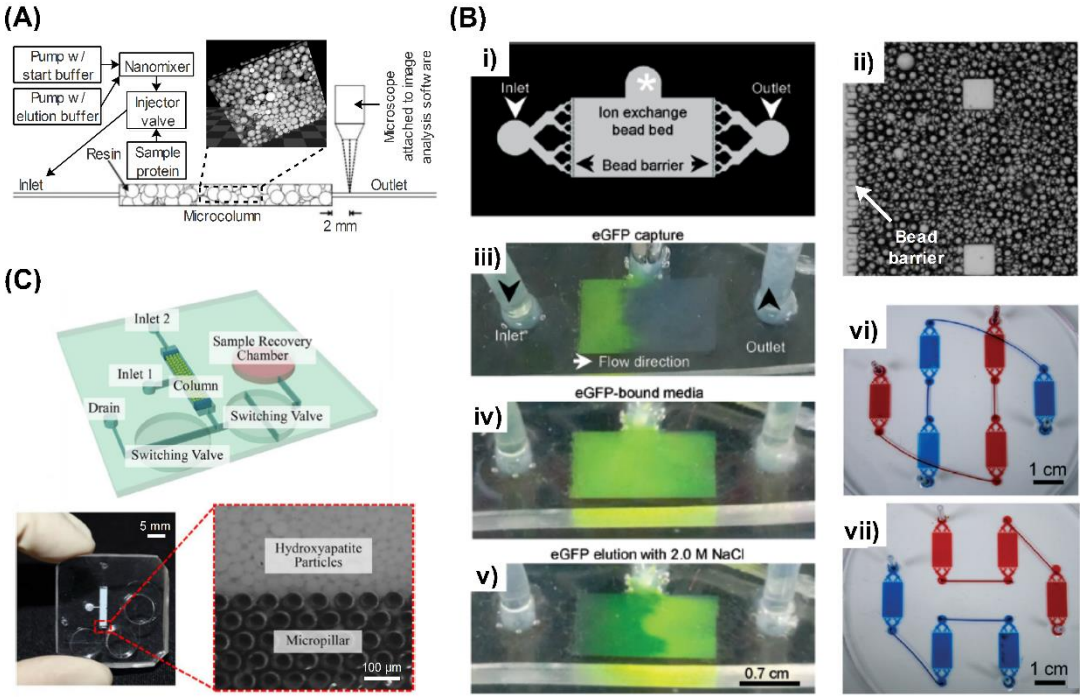

Figure 2.11 – Examples of chromatographic separations combined with microfluidics. **(A)** Schematic diagram of an experimental setup used for microfluidic elution chromatography. Start buffer and elution buffer were pumped through a nanomixer into the microfluidic column containing Q Sepharose FF beads. Fluorescently labeled proteins were injected into the microfluidic column and measured downstream of the column using a fluorescence microscope. Adapted from Shapiro *et al.* [20, 126]. **(B)** Modular microfluidics for point-of-care protein purifications. **(i)** Modular design for ion exchange chromatography (11 µL bed volume). **(ii)** Beads were retained in the separation chamber using a line of rectangular microporous barriers in the flow path at both ends of the column. **(iii-v)** Capture, column saturation and elution of e-GFP using a microfluidic chamber packed with DEAE Sepharose. **(vi-vii)** Module customization with fluid paths through 3D fluidic bridges. Red or blue dyes were injected into the two independent paths. Adapted from Millet *et al.* [19]. **(C)** Microfluidic chip for purification and enrichment of virus using hydroxyapatite chromatography. Selective elution of impurities (proteins) and viruses was accomplished using two different elution buffers. Reproduced from Niimi *et al.* [127].

For a different application, Niimi *et al.* [127] reported a microfluidic chip for virus purification and enrichment by hydroxyapatite chromatography, aiming at detecting an early-stage virus infection at the point-of-care. The authors propose a novel and simple valve mechanism that allow valve switching by hand (**Figure 2.11-C**), which is an attractive feature for a portable device that can be used by non-specialized personnel. The results showed that viruses were successfully isolated from a suspension containing FBS

proteins as model impurities, and good enrichment efficiencies were obtained upon optimization of the design of the microcolumn (W = 1 mm; L = 20 mm; H = 100 μm).

2.5.3. Integration of miniaturized valves and photodetectors

The use of conventional microfluidic systems often relies on bulky off-chip equipment, such as pumps, centrifuges and microscopes for flow driving, sample preparation and monitoring, respectively, which limit their implementation in clinical, laboratory or field environments. Recent developments in microfabrication technologies have been allowing to obtain *'self-contained'* microfluidic systems, which are able to perform multiple functions, including driving and control of fluid flow, sample preparation, purification, concentration and detection of targets, and quantitative real-time analysis of results [128].

For chromatographic applications, the possibilities offered by microfluidic devices in terms of integration allow to create autonomous systems that can closely resemble the operation in traditional chromatography equipment. Miniaturized valves are the most often reported component integrated in chromatographic microfluidic devices, as metering and sequential addition of reagents is fundamental for chromatographic separations. The introduction of multilayer soft-lithography techniques [112] allowed to exploit the elastomeric properties of PDMS to create pumps and valves of different types within a single device. The classical push-up shut-off configuration of a valve consists of two PDMS layers – a top fluidic layer and a bottom control layer. By pressurizing the control layer, the PDMS membrane between the two layers deflects upwards and completely blocks the cross-sectional area of a rounded fluidic channel, effectively preventing liquid from flowing [112]. Inspired by this mechanism, Rho *et al.* [129] developed a novel v-type valve for cell and particle manipulation in microfluidic devices. The v-type valve was designed to trap particles of predetermined sizes without completely blocking the fluid flow in the channel (**Figure 2.12-A i**). By optimizing the pressure applied in the control channel, the authors were able to trap spherical particles with 7 μm and 15 μm and cells with a larger diameter (**Figure 2.12-A ii**). Furthermore, the same strategy was used to pack/unpack chromatography columns inside a microchannel by simply actuating/deactivating the valve (**Figure 2.12-A iii**).

In a continuous trend of complexity, Huft *et al.* [130, 131] combined parallel separation columns with on-chip pumping to achieve a fully integrated system for on-chip chromatography. The device was able to autonomously perform (i) sample loading, (ii)

gradient generation, (iii) molecule separation, (iv) fluorescence detection and (v) sample recovery (**Figure 2.12-B**), by using long valves for control and pressure alleviation of tightly packed channels.

The clear majority of the chromatographic microfluidic systems reported in the literature are based on fluorescence measurements to monitor the adsorption/elution of the target molecules, which involves a prior modification of the molecules with an appropriate fluorophore. The reduced optical path length of microfluidic channels makes it difficult to use alternative optical detectors (*e.g.* UV), thus explaining the widespread use of fluorescence microscopy. Furthermore, there is the possibility of integrating miniaturized photosensors with the device, which eliminates the need for a bulky equipment as a microscope to perform the fluorescence measurement, allowing to have portable stand-alone devices. The integration of miniaturized photosensors with microfluidic devices has been reported [113, 114, 132-134] for fluorescent, chemiluminescent and colorimetric detection of biomolecules, although their application to on-chip chromatography in particular has not yet been explored.

There is currently a large variety of fluorescent labels that can be used to tag the molecules of interest. However, for chromatographic separations, it is important to ensure that these labels are small to avoid conformational changes upon label attachment and steric hindrance during adsorption. In addition, it is important that the labels maintain their quantum efficiencies under a wide range of pH and conductivity conditions, since the chromatographic operations typically involve a large diversity of buffer solutions. Nonetheless, it has been reported that some labels affect the physicochemical properties of labeled proteins, such as charge and size [135], and that the way fluorescently-labeled proteins interact with chromatography resins while adsorbing can significantly change, even though the structure of the protein may remain undisturbed [136]. All the limitations that may arise from the use of fluorescence to monitor chromatography events, motivate the investigation of alternative label-free detection methods amenable to be integrated in miniaturized chromatography devices, such as improved strategies to electrokinetic detection [137, 138]. UV and impedimetric measurements, which are the standard methods for monitoring chromatography at conventional scale, have so far not been demonstrated in microchannels with packed chromatography beads.

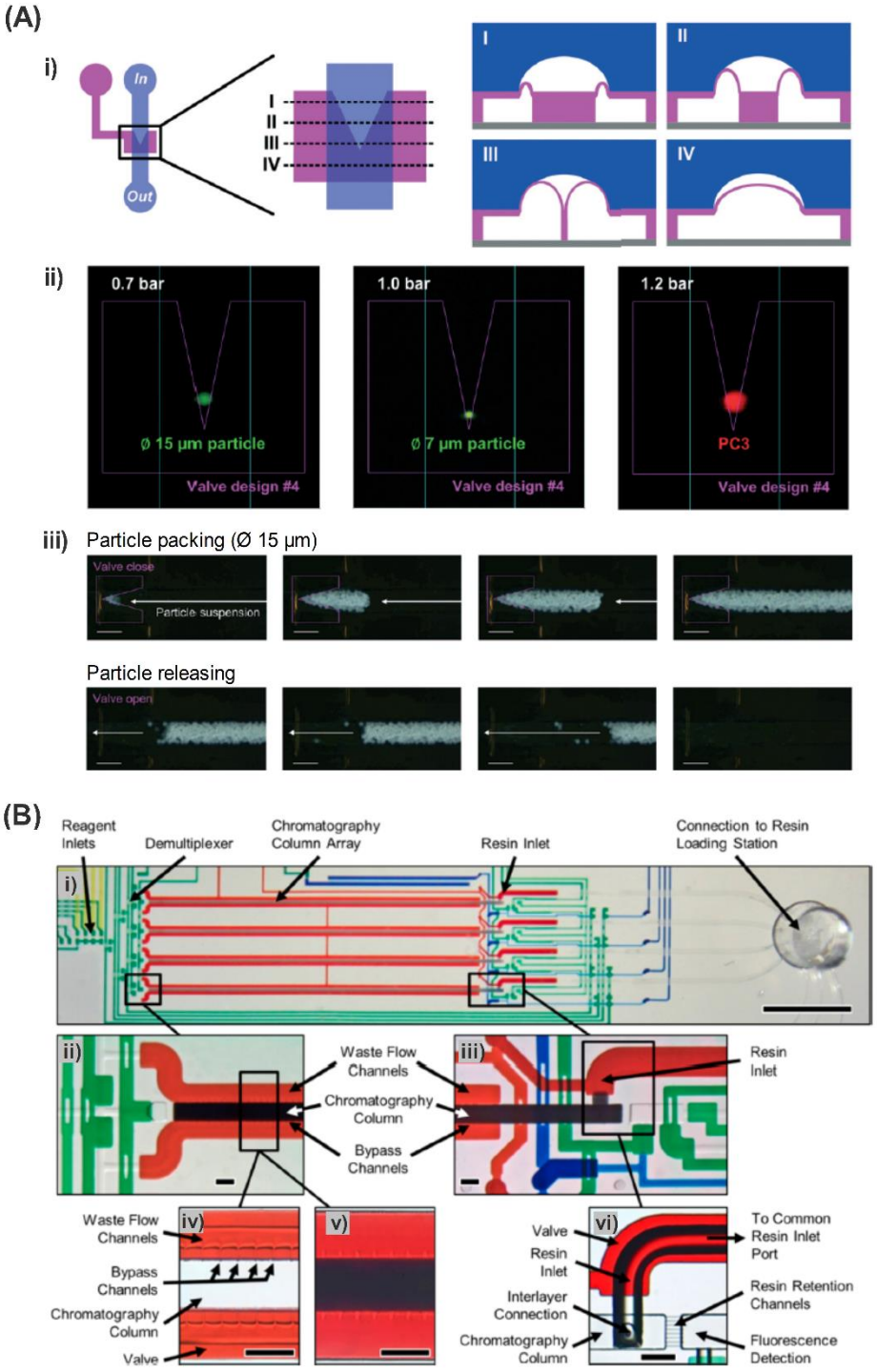

Figure 2.12 – Integration of miniaturized valves for chromatographic operations in microfluidic devices. **(A) (i)** Design (top view) and actuation (cross-sectional views at locations I, II, III, and IV) of v-type valves. **(ii)** Single particles captured by a v-type valve by applying 0.7 bar, 1.0 bar, and 1.2 bar for ∅ 15 µm particles, ∅ 7 µm particles and PC3 cells, respectively. **(iii)** Flexible particle packing and releasing. Adapted from Rho *et al.* [129] **(B) (i)** Micrograph of a microfluidic device having four separation channels for the packing of bead columns. **(ii)** Front of one microcolumn after packing (black channel). **(iii)** Back of a packed microcolumn with the resin inlet closed by a long microvalve (red). **(iv)** Bypass channels along a section of an unpacked microcolumn. **(v)** Section shown in (iv) after column packing. **(vi)** Resin inlet showing that resin is supplied through an interlayer connection and an inlet channel that connects to a common port. Scale bars are 5 mm for panel (i) and 200 µm for the remaining panels. Reproduced from Huft *et al.* [130].

"There's plenty of room at the bottom."

Richard Feynman

Chapter 3
Microfabrication and Handling of Microfluidic Devices

Microfluidic channels packed with nanoporous microbeads were systematically used throughout this thesis to perform the optimization of chromatography operating conditions using (i) fluorescence microscopy measurements or (ii) amorphous silicon (a-Si:H) *p-i-n* photodiodes. The configuration and design of the microfluidic structures evolved as different applications and functionalities were pursued. The main consideration for the design of the structures was the need to efficiently trap microbeads inside a channel, so all the structures were composed of two channels with different heights – a taller channel (height H_1) for bead packing and a shallower channel aligned beneath (height $H_2 << H_1$) for liquid flow. The height of the channels was defined considering the average diameter of the chromatography beads under study, so that the beads could easily flow inside the taller channel, creating a packed bed in the interface region between the two channels.

In this chapter, the microfabrication processes of the different microfluidic structures and miniaturized photodiodes are presented, as well as the general methodologies employed in the handling of the devices. This chapter contains sections reproduced from publications in which I was the leading author that will be appropriately referenced as footnotes.

3.1. Fabrication of microcolumns[§]

Microcolumns were fabricated through three main steps: (i) fabrication of an aluminum (Al) hard mask by direct write optical lithography (DWL); (ii) fabrication of an SU-8

This section is partially reproduced from the following publication:

[§]I.F. Pinto, C.R.F. Caneira, R.R.G. Soares, N. Madaboosi, M.R. Aires-Barros, J.P. Conde, A.M. Azevedo, V. Chu 2017 "The application of microbeads to microfluidic systems for enhanced detection and purification of biomolecules" *Methods* **116** 112-124.

mold with a taller channel (100 μm height) aligned on top of a shallower channel (20 μm height); and (iii) fabrication of polydimethylsiloxane (PDMS) structures and sealing. A detailed description of each of these steps is provided in the following subsections and shown in **Figure 3.1**.

3.1.1. Hard mask fabrication

The aluminum masks (**Figure 3.1-A**) were designed using AutoCAD software (Autodesk Inc., Mill Valley, CA/USA). Since the design required two different mask levels, all the following steps described in this section were performed in duplicate.

A glass (Corning® 1737) substrate was cleaned by sequentially rinsing with acetone, deionized (DI) water, immersion in Alconox™ solution (White Plains, NY, USA) for 15 min at 65 °C, and thoroughly rinsing with distilled (DI) water followed by drying with compressed air. Subsequently, a 200 nm Al layer was deposited using a Nordiko 7000 magnetron sputtering system. A positive photoresist (PFR 7790G) layer of 1.5 μm was spin-coated onto the deposited Al layer. The AutoCAD file was transferred to the photoresist by direct write lithography (DWLii, Heidelberg Instruments Inc.) using a diode laser at 405 nm. The resist was then developed exposing parts of the Al layer, which was later removed by wet etching with a standard aluminum etchant. Finally, the remaining photoresist was stripped away resulting in a patterned Al mask on the glass substrate. The previous microfabrication steps were all performed under class 100 clean-room conditions, except for the photolithography step, which was performed in class 10 conditions.

3.1.2. Master mold fabrication

The master mold (**Figure 3.1-B**) was fabricated using SU-8, a negative photoresist. Firstly, a silicon (Si) substrate (5 × 5 cm) was cleaned by sequential rinsing with acetone, isopropyl alcohol (IPA) and DI water to remove organic contaminants on the surface. Then, the substrate was immersed in a heated Alconox^{TM} bath (65°C) for 15 min, followed by a thorough rinsing with DI water and drying with compressed air. The substrate was then placed in a UVO cleaner (1444AX-220, Jetlight Company, Inc.) for 15 min to degrade any remaining organic contaminants. In order to fabricate the mold, SU-8 2015 (Microchem Corp.) was spin-coated onto the cleaned silicon substrate for 10 s at 500 rpm with an acceleration of 100 rpm/s, followed by 34 s at 1700 rpm with an

acceleration of 300 rpm/s, resulting in a 20 μm thick layer. After a 4 min pre-exposure bake at 95 °C using a hot plate, the substrate was allowed to cool down for 1 min and the hard mask with the design for the 20 μm channels was placed over the SU-8 layer with the Al side facing down, in order to prevent a loss in resolution due to scattering effects. The stack was exposed to a 400 W UV light with an energy per unit area of 178 mJ/cm^2, baked for 5 min at 95 °C, and cooled down to room temperature for 2 min. The development of the non-exposed photoresist was achieved by immersion in a propylene glycol monomethyl ether acetate (PGMEA) solution (Sigma-Aldrich) for 2 min with manual orbital agitation. After the development, the substrate was rinsed with IPA and dried with compressed air.

The second layer with 100 μm height was defined by spin-coating a SU-8 50 (Microchem Corp.) film on top of the previous layer at 10 s at 500 rpm with an acceleration of 100 rpm/s, followed by 30 s at 1000 rpm with an acceleration of 300 rpm/s. A pre-exposure bake process was then performed by baking the substrate at 65 °C for 10 min, followed by a gradual ramping-up of the temperature to 95 °C, at which the substrate was baked for 30 min. Then, the second hard mask for the 100 μm features was manually aligned on top of the previous layer using a stereomicroscope and exposed again to UV light with an energy per unit area of 416 mJ/cm^2. A post-exposure bake was performed at 65 °C for 1 min, followed by 10 min at 95 °C and 2 min of cooling down. The second photoresist layer was developed in PGMEA for 10 min with manual orbital agitation, rinsed with IPA and dried. Finally, the mold was hard baked for 15 min at 150 °C and left to slowly cool down on top of the hot plate until the temperature dropped below 50 °C.

3.1.3. Fabrication of PDMS microcolumns and sealing

To prepare the PDMS elastomer (Sylgard 184 elastomer kit, Dow Corning, Midland, MI, USA), a 10:1 weight ratio of PDMS to curing agent was mixed, degassed for 30 min and poured into a Petri dish containing the SU-8 mold (**Figure 3.1-C**). The Petri dish was then left to cure at 70 °C for 90 min. The cured PDMS was cut using a scalpel and peeled off from the mold. Access holes were punched with blunt 20 and 18 Gauge needles for the outlets and inlets, respectively. A PDMS slab (500 μm thick) was prepared by spin coating the PDMS mixture on top of a silicon wafer at 250 rpm for 25 s with an acceleration of 100 rpm/s. This membrane was then baked as previously described and cut into pieces with at least the size of the PDMS structures. Finally, the PDMS structures

were sealed against the PDMS slabs by first oxidizing both sides using an oxygen plasma cleaner (Harrick Plasma, Ithaca, NY, USA) at the medium power setting for 60 s. The membrane was placed in contact with the PDMS structure immediately after the plasma treatment. After the sealing, the PDMS becomes relatively hydrophilic for a few hours due to the plasma treatment. To allow hydrophobic recovery and stabilization by diffusion of the unreacted siloxane oligomers to the surface, the PDMS structures were stored for at least 24 h before being used.

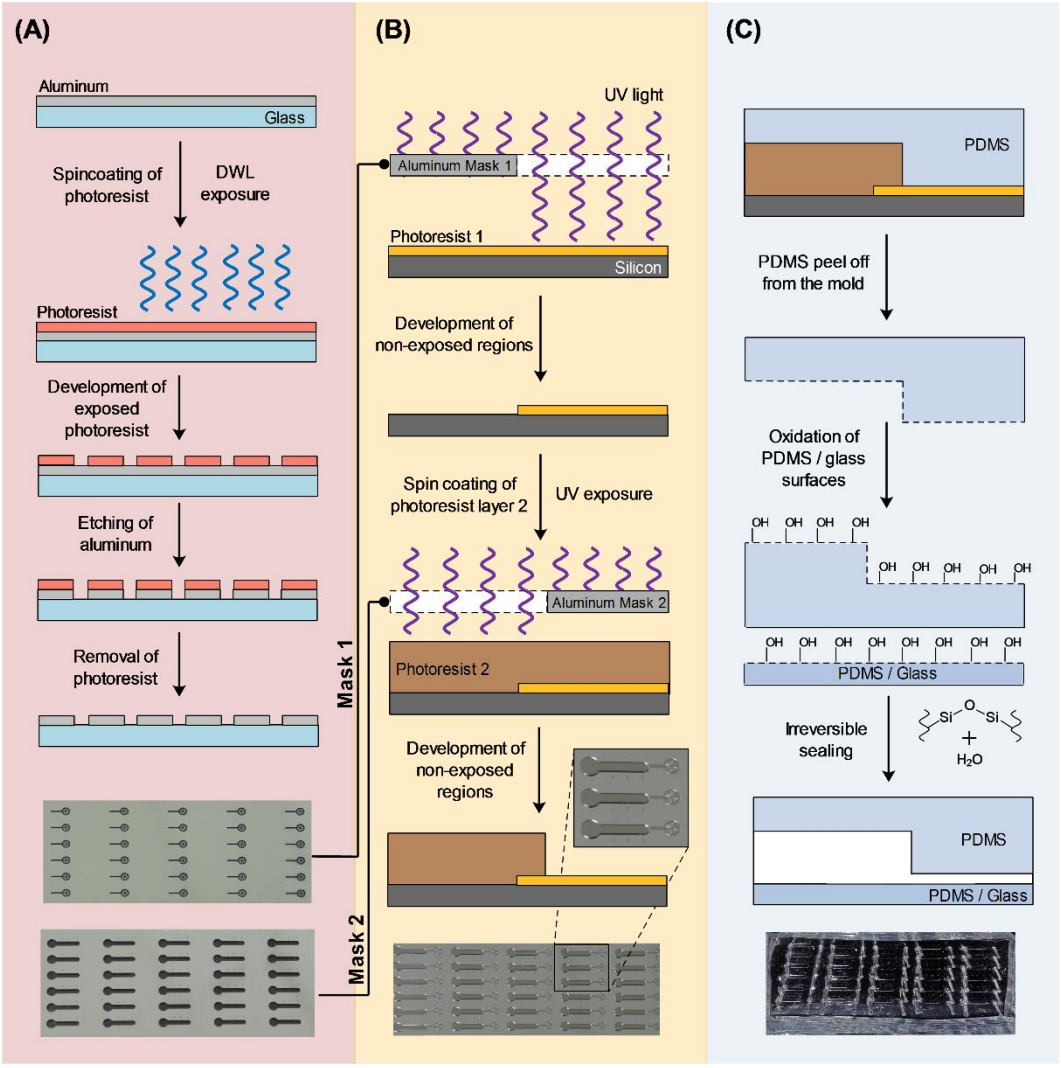

Figure 3.1 – Sequence of steps involved in the fabrication of the **(A)** aluminum hard mask; **(B)** SU-8 mold; and **(C)** PDMS structures used for trapping beads. The photoresists 1 and 2 correspond to SU-8 2015 and SU-8 50, respectively.

3.2. Fabrication of valve-integrated microcolumns[†]

Microfluidic devices comprising a microcolumn and integrated pneumatic valves were fabricated using polydimethylsiloxane (PDMS) multilayer soft-lithography (MLSL) (**Figure 3.2**). While the fabrication of the hard masks for these structures was performed exactly as described in section 3.1.1., the fabrication of the molds and PDMS structures was based on a significantly different and more complex process that will be described in the next subsections.

3.2.1. Mold fabrication for the fluidic layer

SU-8 features were first defined by spin coating SU-8 50 on top of a clean Si substrate for 10 s at 500 rpm with an acceleration of 100 rpm/s, followed by 30 s at 1000 rpm with an acceleration of 300 rpm/s, in order to obtain channels with 100 μm height (**Figure 3.2-A**). The SU-8 was baked for 10 min at 65 °C and the temperature was then ramped up to 95°C for 30 min. After this, the Al hard mask containing the features of the microcolumn was placed on top of the SU-8 film and the stack was exposed to UV light (365 nm, ~416 mJ/cm^2, 70 s). A post-exposure bake was performed at 65 °C for 1 min followed by 10 min at 95 °C, after which the mold was developed by immersion in propylene glycol monomethyl ether acetate (PGMEA) for 10 min, rinsed with IPA and hard baked at 150 °C for 15 min.

AZ features were then defined by spin coating AZ® 40 XT (MicroChemicals GmbH, Ulm, Germany) positive photoresist on top of the SU-8 features (**Figure 3.2-A**) for 10 s at 500 rpm with an acceleration of 100 rpm/s, followed by 21 s at 2000 rpm with an acceleration of 1000 rpm/s. The films were then baked for 5 min at 125 °C, by ramping up the temperature from 100 °C to 125 °C. The Al hard mask corresponding to the valve structures was aligned with the first SU-8 layer and the stack was exposed to UV light (365 nm, ~1.25 J/cm^2, 3 min 30 s), followed by a post-exposure bake at 105 °C for 2 min. The mold was then developed by immersion for 10 min in AZ® 400 K developer (MicroChemicals GmbH) previously diluted in distilled water (DI) to a ratio of 1:3, and then washed with DI water. Finally, a reflow step was performed by ramping up the

This section is partially reproduced from the following publication:

[†] I.F. Pinto, D.R. Santos, R.R.G. Soares, M.R. Aires-Barros, V. Chu, A.M. Azevedo, J.P. Conde 2018 A regenerable microfluidic device with integrated valves and thin-film photodiodes for rapid optimization of chromatography conditions, *Sens Actuators B Chem* **255** 3636-3646.

temperature from 100 °C to 125 °C and then baking for 5 min. After this process, microchannels with a round cross-section and a height of ~30 μm were obtained. It is important to note that the SU-8 features were defined first since the PGMEA can remove the AZ photoresist. On the contrary, the AZ® 400 K developer does not affect the previously patterned SU-8 features.

3.2.2. Mold fabrication for the control layer

For the control layer comprising pneumatic valves, a separate SU-8 mold (**Figure 3.2-A**) was fabricated by spin coating SU-8 50 (Microchem, Newton, MA, USA) on top of a clean Si substrate for 10 s at 500 rpm with an acceleration of 100 rpm/s, followed by 37 s at 2300 rpm with an acceleration of 300 rpm/s, in order to obtain channels with 50 μm height. The substrate was baked for 3 min at 65 °C and the temperature was then ramped up to 95°C for an 8 min bake. After this, the Al hard mask containing the design for the pneumatic channels was placed on top of the substrate and the stack was exposed to UV light (365 nm, ~300 mJ/cm^2, 25 s). A post-exposure bake was performed at 65 °C for 1 min followed by 7 min at 95 °C, after which the mold was developed by immersion in PGMEA for 6 min, rinsed with IPA and hard baked at 150 °C for 15 min.

3.2.3. Fabrication of valve-integrated PDMS structures and sealing

The replication of the mold patterns using PDMS multilayer soft-lithography is represented in **Figure 3.2-B**. The PDMS elastomer was prepared with a 10:1 ratio of base to curing agent, degassed, poured on top of the fluidic layer mold and baked at 70°C for 50 min. To create a thin PDMS layer to be pneumatically actuated as valves, PDMS was prepared with a 20:1 ratio of base to curing agent, degassed and spin coated on top of the mold of the control layer for 25 s at 300 rpm, resulting in a PDMS layer of 400 μm thick. The spinning conditions for the control valve layer were thoroughly optimized in order to ensure leakproofness (*i.e.* leakage occurs through the actuated valves if the membrane is too thick), reversible deflection (*i.e.* membrane is permanently actuated if it is too thin) and millisecond response times. The PDMS was then baked at 70 °C for 40 min (**Figure 3.2-B i**)). After curing, the PDMS was peeled off of the mold and access holes were punched using blunt syringe tips with diameters of 0.84 mm for inlets and 0.61 mm for the outlet of the micro-column. The fluidic layer was then aligned and placed on top of the control layer on the corresponding mold and baked together at 70 °C for 1.5 h (**Figure**

3.2-B ii)). After completing the curing process, the structures were cut and peeled off of the mold with the control channels irreversibly sealed beneath the fluidic channels. The inlets of the control channels were punched using blunt syringe tips with 0.61 mm diameter.

The sealing of the microfluidic structures was performed via a PDMS adhesive layer. This adhesive layer was obtained by spin coating PDMS 10:1 on top of a glass substrate for 4 min at 6000 rpm. This extremely thin layer of PDMS was then used to wet the bottom surface of the PDMS structures, by bringing the adhesive layer in contact with the stack consisting of the control and fluidic layers (**Figure 3.2-B iii**)). The stack was sealed against a 100 µm coverglass, in which PDMS was previously spin coated, resulting in a PDMS-PDMS sealing after a final bake at 70 °C for 1.5 h (**Figure 3.2-B iv**)).

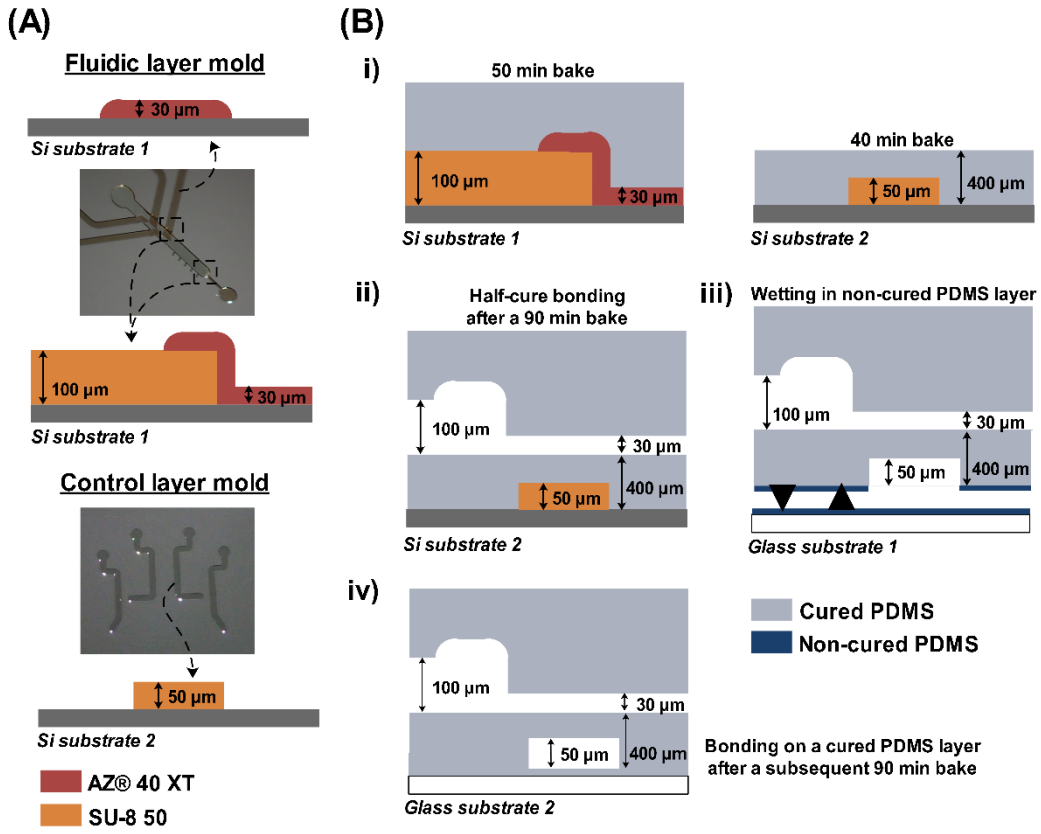

Figure 3.2 – Fabrication of valve-integrated microfluidic structures. **(A)** Fluidic and control layer molds. **(B)** Replication of mold patterns using PDMS multilayer soft-lithography and sealing using an adhesive layer.

3.3. Fabrication of a-Si:H *p-i-n* photodiodes[‡]

Hydrogenated amorphous silicon (a-Si:H) *p-i-n* photodiodes (200 × 200 μm of active area) were fabricated with an integrated a-SiC:H layer as an excitation absorption filter for fluorescence measurements. The Al back contact (200 nm) was fabricated with the same process as described in section 3.1.1 for the hard mask fabrication. The a-Si:H *p-i-n* junction was deposited by radio frequency plasma enhanced chemical vapor deposition (rf-PECVD) at a deposition pressure of 0.1 Torr and a substrate temperature of 250 °C. The photodiode comprised a 100 Å layer of n^+-a-Si:H (phosphine doped), a 5000 Å layer of undoped *i*-a-Si:H and a 100 Å layer of p^+-a-Si:H (diborane doped). Mesa junctions with dimensions of 200 × 200 μm were then defined by photolithography and reactive ion etching (Lam Research Rainbow Plasma Etcher). A passivation layer (1000 Å) of amorphous silicon nitride (SiN_x) was deposited by rf-PECVD at 100 °C and 0.1 Torr to passivate the sidewalls of the junctions. A via was opened in the passivation layer, by lift-off, to allow electrical contact between the p^+-a-Si:H layer and the indium tin oxide (ITO) transparent top contact (1000 Å), which was deposited by magnetron sputtering and defined by photolithography and lift-off. Aluminum lines, to connect the ITO to the contact pads, were deposited and defined as previously described. A second SiN_x passivation layer (2000 Å) was deposited by rf-PECVD and vias were opened by lift-off at the contact pads to allow wire bonding. An hydrogenated amorphous silicon carbide (a-SiC:H) filter with a thickness of 1.6 μm for fluorescence detection was deposited by rf-PECVD at 100 °C and 0.1 Torr and optimized to reduce the intensity of excitation light reaching the photodiode while passing the maximum level of emission light according to previous work by Lipovšek *et al.* [134].

3.4. Bead packing in microcolumns[§]

The procedure to pack the PDMS microcolumns is described in **Figure 3.3** and the most common problems that may arise from this operation are summarized in **Table 3.1**. Commercially available beads were provided as a slurry in a storage buffer (ethanol 20%),

---

These sections were partially reproduced from the following publications:

[‡] I.F. Pinto, D.R. Santos, R.R.G. Soares, M.R. Aires-Barros, V. Chu, A.M. Azevedo, J.P. Conde 2018 A regenerable microfluidic device with integrated valves and thin-film photodiodes for rapid optimization of chromatography conditions, *Sens Actuators B Chem* **255** 3636-3646.

[§] I.F. Pinto, C.R.F. Caneira, R.R.G. Soares, N. Madaboosi, M.R. Aires-Barros, J.P. Conde, A.M. Azevedo, V. Chu 2017 The application of microbeads to microfluidic systems for enhanced detection and purification of biomolecules, *Methods* **116** 112-124.

so the first step was to homogenize the bead stock using a pipette, ensuring thorough mixing. Then, a certain volume of stock solution was added to a 30% (w/w) polyethylene glycol (PEG) 8000 solution, to obtain a final solution with 1-2% bead volume. The use of a viscous solution allowed the beads to remain suspended and homogeneously dispersed without significant settling, thus avoiding problems of clogging when flowing the beads inside the microcolumns (**Table 3.1**). The pipette tip containing the bead suspension was inserted roughly half-way (**Table 3.1**) into the inlet access holes punched using the 18 Gauge blunt syringe and a syringe pump was subsequently turned on with the appropriate flow rate, pulling the liquid from the outlet of the microcolumn. Within approximately 40 s, it was possible to accumulate the beads at the interface region of the microchannels and fill the entire field of view of the microscope (**Figure 3.3**). After this step, the metal adapter connected to the syringe pump was removed before removing the pipette tip, to avoid trapping air bubbles at the interface between the liquid in the inlet hole and the subsequent solution due to the accumulated negative pressure. Subsequently, the PEG solution was washed from the microcolumns using an appropriate equilibration buffer and the specific sequence of steps comprising the assay was performed.

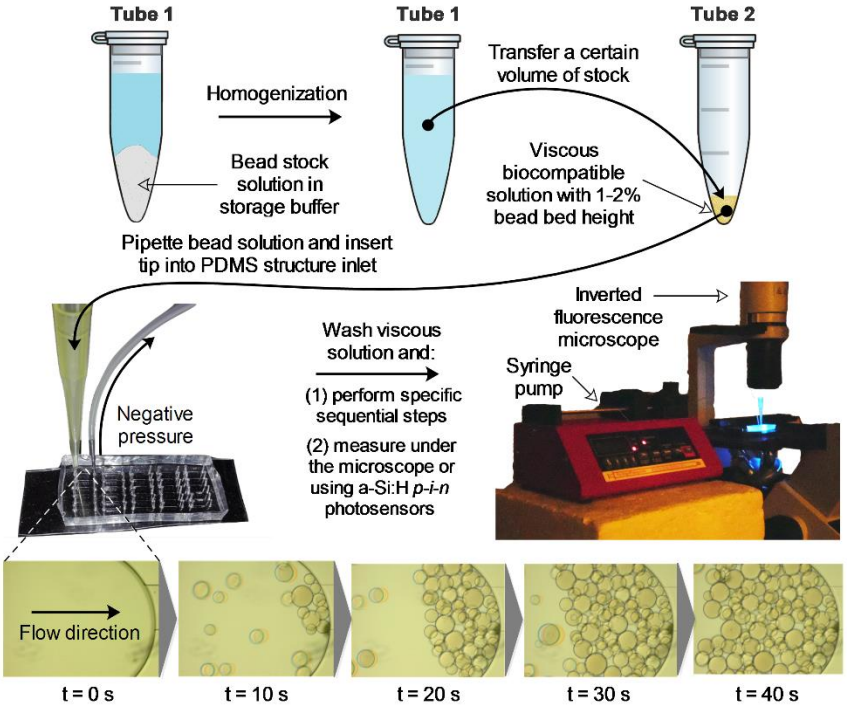

Figure 3.3 – General protocol for preparing the chromatography beads before insertion into the PDMS microcolumns. The bead solution was pulled from the microcolumn outlet using a syringe pump exerting a negative pressure. The time lapse of microscope bright field images shows the accumulation of beads in the interface region of the two channels with different heights within a few seconds. The measurements were performed either using an inverted fluorescence microscope or *in-house* fabricated a-Si:H *p-i-n* photodiodes.

Table 3.1 – Troubleshooting table for the most frequent problems encountered during bead packing and liquid handing in the microcolumns. Possible causes and solutions for each problem are presented.

Step	Problem	Cause	Solution
Bead solution preparation	Clogging of the channel due to the packing occurring too rapidly	Inhomogeneity of the bead solution or bead concentration too high	Homogenize the viscous solution with a 1-2% bead bed-height immediately before the packing
Liquid handling	Low quantity of beads packed inside the microchannel	Bead solution concentration is too low	Repeat the insertion step, adding more 0.3 µL of bead solution
	Air bubbles trapped or appearing inside the channel	Incomplete removal of air bubbles from the syringe and tubing, improper transition between solution flowing steps or flow rate set faster than the liquid can overcome the column resistance, leading to negative pressure build-up	Check thoroughly the syringe and tubing for air bubbles and successfully remove them. Always purge the syringe when inserting the metal coupler. Always release the metal adapter before inserting a new tip if negative pressure accumulated in the previous step
Solution preparation	Clogging of the channel	Debris and impurities that accumulate in free spaces between the packed beads	If required, when preparing the solutions, filter the solutions to remove impurities
Pipette tip insertion	Liquid not flowing	Liquid in the pipette tip not in contact with liquid column inside the inlet (< half-way through)	Make sure the end of the pipette tip contacts with the liquid column to avoid air gaps
		The inlet hole has a tear (> half-way through)	Make sure the larger part of the pipette tip does not tear the inlet hole
Metal coupler insertion	Liquid not flowing and negative pressure build-up	Metal coupler contacting the bottom PDMS sealing slab	Leave a small gap between the metal coupler and the sealing slab

3.5. Summary

This chapter summarizes the fabrication processes involved in the different devices used throughout this work and the general proceeding for operating the microfluidic devices. Overall, the simple design and the relatively straightforward soft-lithography based fabrication processes make this method a versatile technology that is compatible with various bead sizes and shapes. In particular, the soft-lithography processes are simpler and faster than other microfabrication processes involving, for example, silicon bulk micromachining and etching techniques [139-142]. In addition, even though the soft-lithography processes described in this thesis present a lower resolution than the referred methods, they allow to pattern complex 3D structures using a layer-by-layer strategy [143].

Due to the simplicity of the designs and smaller dimensions, it was possible to create a large number of patterned channels in a single 5×5 mold, thus allowing parallel fabrication of many devices for rapid and inexpensive prototyping. Considering the sealing of the PDMS structures, the use of an oxygen plasma is a simpler and more robust technique when compared to other standard techniques, such as lamination and adhesive layers. However, bonding using an adhesive layer was also successfully performed in valve-integrated structures, showing a good tolerance to dust and particles and a high strength of bonding, despite being a more time-consuming process.

The bead packing process took on average less than 1 minute, which is considerably faster than gravity or capillary-driven packing strategies [121, 144]. The interface region for bead trapping provided mechanical robustness, allowing the device to withstand higher pressures than, for example, traps made of hydrogels [145] or membranes [146].

Finally, the liquid flow was driven by applying a negative pressure at the outlet, thus generating a pressure differential between the inlet and the outlet. The use of a negative pressure provided a gradual increase in liquid flow velocity with minor distortion of the PDMS channel or deformation of the beads at the interface region, contrary to what is observed when a positive pressure is used. In fact, the use of positive pressure results in faster and less reproducible packing velocities, bulging of the microchannel and a higher likelihood of trapping air bubbles. Another advantage of using a negative pressure is the simplified operation and solution handling, since the solutions of interest are sequentially inserted using pipette tips and the liquid is pulled into the microcolumn, after which the tips are discarded, thus reducing issues due to mixing of reagents.

"In theory, theory and practice are the same. In practice, they are not."

Albert Einstein

Chapter 4
Nano-liter Scale Analysis of Multimodal Chromatography[§]

Multimodal chromatography has been extensively reported for the purification of monoclonal antibodies in both capture and polishing applications. However, the implementation of this type of technique depends on the full understanding of all the interactions enabled by the ligands, as well as on the ability to rapidly predict the optimal operating conditions to address a specific purification problem.

In this context, the development of high-throughput platforms has been gaining increasing attention for early stage evaluation of chromatography conditions. Most of these approaches are based on 96-well microtiter filter plates [12, 16] (resin volume 20-200 μL), but, more recently, miniature columns [109, 147] (resin volume ~200 μL) and micropipette tips (10 – 160 μL) operated in automated liquid handling stations have also been reported to improve assay reproducibility by reducing the variability in resin volumes. Although these approaches are able to deliver results comparable to preparative-scale, the parallelization and automation of assays in these platforms require the utilization of robotic systems, which are expensive, highly complex and have turnaround times in the range of several minutes to hours to obtain results. These technologies also lack the resemblance with conventional column chromatography operation, in the sense of having a continuous flow of a mobile phase through a stationary phase.

Microfluidic platforms comprising chromatography beads inside micro-columns represent a versatile solution to address this problem, while offering additional advantages such as the very low reagent consumption and the extremely rapid output of results. In fact, the confinement of beads inside microchannels has been previously

---

This chapter contains sections reproduced from the following publication:

[§]I.F. Pinto, R.R.G. Soares, S.A.S.L. Rosa, M.R. Aires-Barros, V. Chu, J.P. Conde, A.M. Azevedo, 2016 "High-throughput nanoliter-scale analysis and optimization of multimodal chromatography for the capture of monoclonal antibodies" *Anal Chem* **88**(16) 7959-7967.

reported for other applications, such as DNA hybridization onto probe-conjugated microbeads [148], catalytic reactions using enzymes immobilized on microbeads [149], and biosensing applications [150]. Additionally, the concept of packing chromatography beads within a microfluidic glass column for evaluation of the separation conditions and determination of the dynamic binding capacity has been reported [126]. In this case, the amount of resin used in the microfluidic columns was considerably lower (1.5 μL) compared to the high-throughput approaches previously mentioned. However, the fabrication of whole glass structures required complex and expensive methodologies, and the packing of the beads inside the microchannels also relied on elaborate handling.

This chapter focuses on the development of a microfluidic platform for the optimization of multimodal chromatography using the ligand Capto™ MMC (2-benzamido-4-mercaptobutanoic acid) towards the capture of a monoclonal antibody labeled with Alexa Fluor® 430. Capto™ MMC has been increasingly evaluated for the purification of several biological compounds, especially monoclonal antibodies, with successful results reported for its application either as a primary capture step [97] or as an intermediate step [151] in mAb purification from cell culture supernatants. Research studies are being performed targeting not only the identification of preferential binding sites [152] and mechanisms of interaction [153], but also the understanding of the driving forces controlling the adsorption/desorption of target molecules [154] in Capto™ MMC. With the goal of screening the behavior of this ligand in a high-throughput manner, micro-column arrays (resin volume ~70 nL) were fabricated using polydimethylsiloxane (PDMS) soft-lithography techniques, in order to measure binding kinetics in real time at resin-level using fluorescence microscopy. This approach aimed at providing information about adsorption and elution behaviors in a few seconds/minutes to expedite the optimization of chromatographic processes for the purification of monoclonal antibodies.

4.1. Experimental section

4.1.1. Buffer solutions and chromatography resins

Tris(hydroxymethyl)aminomethane, NaCl, Na_2CO_3 and $NaHCO_3$ were obtained from Sigma-Aldrich (St. Louis, MO/USA). K_2HPO_4 and KH_2PO_4 were purchased from Panreac Quimica Sau (Barcelona, Spain). Sodium acetate was obtained from Merck (Darmstadt, Germany). Acetic acid 100% (AnalaR Normapur®) was purchased from VWR BDH Prolabo (Radnor, PA/USA). All other chemicals were of analytical grade. Water used in all experiments was obtained from a Milli-Q purification system (Millipore, Bedford, MA/USA).

Chromatography resins were obtained from GE Healthcare (Uppsala, Sweden) in bulk and as pre-packed 1 mL columns, namely HiTrap Capto™ MMC (multimodal), HiTrap CM Sepharose FF (cation exchange) and HiTrap Phenyl FF High Sub (hydrophobic).

4.1.2. Production, purification and labeling of mAbs

Production – Anti-human interleukin-8 (anti-IL8) monoclonal antibodies (mAbs) were produced by Chinese Hamster Ovary cells (CHO DP-12 clone#1934, ATCC CRL-12445), containing a dihydrofolate reductase (DHFR) expression system, obtained from the American Type Culture Collection (LGC Standards, Middlesex, UK).

CHO cells were grown in a serum-free medium, ProCHO™5 (Lonza Group Ltd, Belgium), supplemented with 4 mM L-glutamine (Gibco, Life Technologies), 200 nM methotrexate (Sigma-Aldrich), 2.1 g/L sodium bicarbonate (Sigma-Aldrich), 10 mg/L recombinant human insulin (Lonza), 0.07% (v/v) lipids (Lonza), and 1% (v/v) antibiotics (100 U/mL penicillin and 100 μg/mL streptomycin, from Gibco). The initial cell density was 2.8×10^4 cells/cm^2 and the cultures were carried out in T-75 or T-175 flasks (BD Falcon, Franklin Lakes, NJ, USA) at 37°C and 5% CO_2. Cell passages were performed every 6 days, in which cells were detached from the flasks upon addition of a TrypLE™ Select solution (Gibco), for 3-4 min at 37°C. CHO cell suspensions were then centrifuged at 1250 rpm (12°C, 8 min) for medium clarification. The produced anti-IL8 mAb was characterized by an isoelectric point (pI) of ~9 and a concentration in the serum-free cell culture supernatants of ~50 mg/L.

Purification – The anti-IL8 mAbs were purified using protein A affinity chromatography. The purification assay was performed in an ÄKTA™ Purifier system, equipped with a Frac-950 fraction collector from GE Healthcare. Data acquisition and analysis was made using Unicorn 5.11 software.

The feedstock was directly loaded at native conditions onto a HiTrap MabSelect SuRe column (1 mL), at a flow rate of 1 mL/min, using a 50 mL Superloop M6 fitting from GE Healthcare. Adsorption and elution were performed with 10 mM PBS at pH 7.4, and 100 mM sodium citrate buffer at pH 3.6, respectively. Elution fractions were immediately neutralized using 1 M Tris-HCl at pH 8.0, to prevent antibody denaturation caused by the acidic elution conditions, pooled together (final volume of 22.5 mL) and 90× concentrated/diafiltered in PBS using Amicon Ultra-15 centrifugal filter units (MWCO of 50 kDa) from Merck Millipore, for 15 min at 5000 *g* in a fixed angle rotor centrifuge. The anti-IL8 mAb solution was further concentrated (~5.7×) and buffer exchanged into 0.1 M sodium bicarbonate buffer using Amicon Ultra-0.5 centrifugal filter units (MWCO of 10 kDa) also from Merck Millipore, for 7 min at 14000 *g*. After these steps, the final concentration of the mAb solution was 15.48 mg/mL.

Labeling – The anti-IL8 mAbs were then conjugated to the amine-reactive dye Alexa Fluor® 430 (A430) NHS ester, obtained from Thermo Fisher Scientific (Excitation = 430 nm; Emission = 545 nm). The purified and concentrated anti-IL8 mAb solution was added to the reactive dye solution in a 4:1 volume ratio, and the reaction was incubated in the dark for 1 hour at room temperature. The degree of labeling (DOL) was estimated to be 9.2 dye molecules/mAb molecule, considering the absorbance of the protein-dye conjugate at 280 nm (A_{280}) and 430 nm (A_{430}), and the extinction coefficient of the dye at 430 nm ε_{dye}, according to **Equation 4.1**, where MW is the molecular weight of IgG and CF is a correlation factor for the contribution of the Alexa Fluor® 430 dye in the absorbance of the protein-dye conjugate at 280 nm. The constant 1.4 is used to correlate the absorbance values with the protein concentration in mg/mL and it is only correct for IgG antibodies. The values of CF and ε_{dye} were considered to be 0.28 and 16,000, respectively, according to information provided by the supplier of the amine-reactive dye (Life Technologies). The non-conjugated dye was removed in a series of 10 diafiltration steps with PBS using Amicon Ultra-0.5 centrifugal filter units (MWCO of 10 kDa), until a clear permeate was obtained.

$$DOL = \frac{A_{430} \times MW}{1.4(A_{280} - A_{430} \times CF) \times \varepsilon_{dye}}$$ **Equation 4.1**

4.1.3. Micro-column packing and liquid handling

The procedure for bead preparation and packing in the micro-columns is described in detail in chapter 3, section 3.4. Briefly, chromatography agarose beads were suspended (1-2% (v/v)) in a 33% (w/w) polyethylene glycol (PEG) 8000 solution (Sigma-Aldrich, St. Louis, MO/USA). Suspended beads were then packed inside the micro-columns by pulling the liquid from the outlet, using a syringe pump (Model NE-1002X, New Era Pump System, Inc.). All solutions were flowed through the micro-columns by applying a negative pressure at the outlet.

After the packing step, the micro-columns were washed with 50 μL of the corresponding adsorption buffer, to completely remove the PEG solution. Adsorption was performed with 30 μL of an anti-IL8-A430 solution (50 μg/mL), and elution was accomplished with 30 μL of the corresponding elution buffer. Screening conditions for adsorption studies included different buffers with pH values ranging from 5.5 – 9.5, and conductivity values ranging from 1 – 21 $mS.cm^{-1}$ upon addition of NaCl (0 – 200 mM). For the elution studies, the screened conditions comprised buffers with pH values in the range 7.5 – 9.5, and conductivity values from 0.6 – 147 $mS.cm^{-1}$ upon addition of NaCl (0 – 2 M). Conductivities were measured using an ECTestr Low conductivity tester (OAKTON Instruments, Vernon Hills, IL/USA).

4.1.4. Fluorescence monitoring and analysis

Adsorption and elution assays were continuously monitored and recorded using an inverted fluorescence microscope (Olympus CKX41) coupled to a CCD color camera (Olympus XC30). The filter cube provided a band pass excitation of 460-490 nm and a long pass emission of 520 nm. Fluorescence signal from the beads inside the micro-columns was acquired with an exposure time of 500 ms, 5× gain and 100× total magnification. Images were analyzed using ImageJ software (National Institutes of Health, USA), and the fluorescence emission values were obtained by averaging the entire end-section of the micro-columns.

4.1.5. Standard column chromatography assays

The microfluidic results were validated and compared to results obtained using a pre-packed HiTrap Capto™ MMC column (1 mL) in an ÄKTA™ Purifier system. A purified anti-IL8 mAb solution with a concentration of 20 μg/mL was loaded at a flow rate of 1 mL/min, using a 500 μL loop. Recovery yield studies were performed using 50 mM acetate buffer at pH 5.5 as binding buffer and testing different elution buffers, namely (i) 50 mM carbonate buffers at pH 9.5 containing 0 M, 1 M and 2 M NaCl, (ii) 50 mM Tris buffers at pH 8.5 containing 1 M and 2 M NaCl, and (iii) 50 mM phosphate buffers at pH 7.5 containing 1 M and 2 M NaCl. Column equilibration, washing and elution were performed over 5 CV, 5 CV, and 7 CV, respectively.

Flowthrough and eluate pools were collected and further analyzed to determine IgG concentration by analytical protein A chromatography using a POROS PA ImmunoDetection sensor-cartridge from Applied Biosystems (Foster City, CA/USA) [155]. For the analytical quantification, adsorption was performed using 50 mM sodium phosphate buffer at pH 7.4 containing 150 mM NaCl over 10 CV. Elution was then performed using 12 mM HCl containing 150 mM NaCl at pH 2-3 over 25 CV. All analyzed samples were previously diluted five times in binding buffer and the absorbance was monitored at 215 nm.

For each evaluated condition, chromatography runs were carried out in duplicate, while the corresponding microfluidics experiments were carried out in triplicate.

4.2. Operating procedure in the micro-columns

The microfluidic columns (210 nL volume) (**Figure 4.1-A**) were designed to allow the packing of beads in a region confined by the height difference of two microchannels. The heights of the microchannels were defined considering the average diameter of the agarose beads (75 - 90 μm), in a way that a shallower channel (20 μm height) prevented the flow of the beads downstream, creating a packed-bed with the interface region of a taller channel (100 μm). Thirty of these nano-liter scale columns were distributed in a 15×40 mm PDMS chip (**Figure 4.1-B**), allowing the evaluation of different adsorption/elution conditions simultaneously within a few minutes.

The liquid flow was driven by applying a negative pressure at the outlet, which provided a more gradual increase in liquid velocity with minor distortion or compression of the beads against the 20 μm gap (**Figure 4.1-C**).

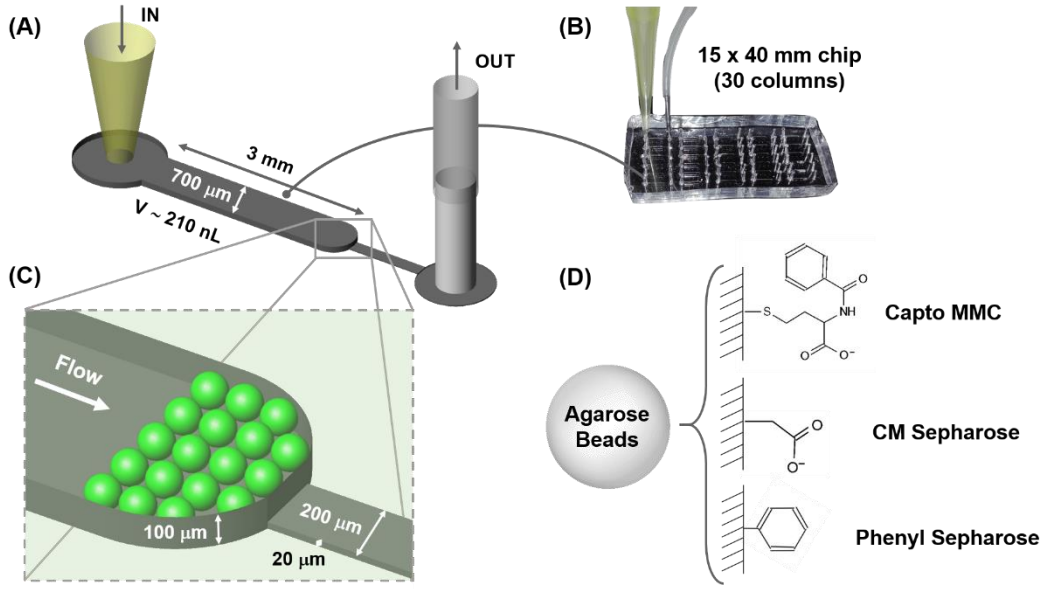

Figure 4.1 – Schematics of the microfluidic columns used for the optimization experiments. **(A)** Detail of a single micro-column exhibiting the inlet (pipette tip) and outlet (metal adapter) through which the liquid was flowed by applying a negative pressure at the outlet. **(B)** PDMS structure comprising 30 microcolumns within an area of 6 cm^2. **(C)** Magnification of the interface region between the two channels at different heights. The shallower channel arrests the beads in place and prevents their movement downstream throughout the assay. **(D)** Molecular structure and name of the analyzed chromatography ligands, commercially available in functionalized agarose beads.

4.3. Analysis of adsorption and elution kinetics

The assays to evaluate the adsorption and elution kinetics of the target antibody were performed in plain buffer solutions rather than complex matrices such as serum-free or serum-containing cell culture supernatants. By using buffer solutions it is possible to avoid the intrinsic variability related to secondary interactions with the matrix components, which are specific to each formulation. In addition, since each matrix has its own native pH and conductivity conditions, these would limit the range of pH and conductivity values that could be tested in the microfluidic experiments.

4.3.1. Fluorescence measurements and signal quantification

The microfluidic assays were designed to optimize conditions for chromatographic operation at the macroscale, so it was necessary to first confirm that the presence of a fluorophore did not significantly influence the binding behavior of the mAb to the

multimodal ligand. This study was performed in a standard 1 mL chromatography column by loading labeled and unlabeled IgG at the exact same concentration (5 µg/mL). The chromatographic profiles (**Figure 4.2**) were similar, in terms of both retention time (t_r = 10.11 ± 0.0071 min) and area (A = 6.38 ± 0.013 mAU.min) of the elution peaks, so for all the optimization experiments the fluorophore was considered to play a negligible role in the antibody-ligand interactions. This conclusion was also supported by previous findings by Linden *et al.* [156] and Harinarayan *et al.* [125], in which multiple fluorophore conjugates did not have a significant impact on protein adsorption and diffusion through ion exchange agarose resins.

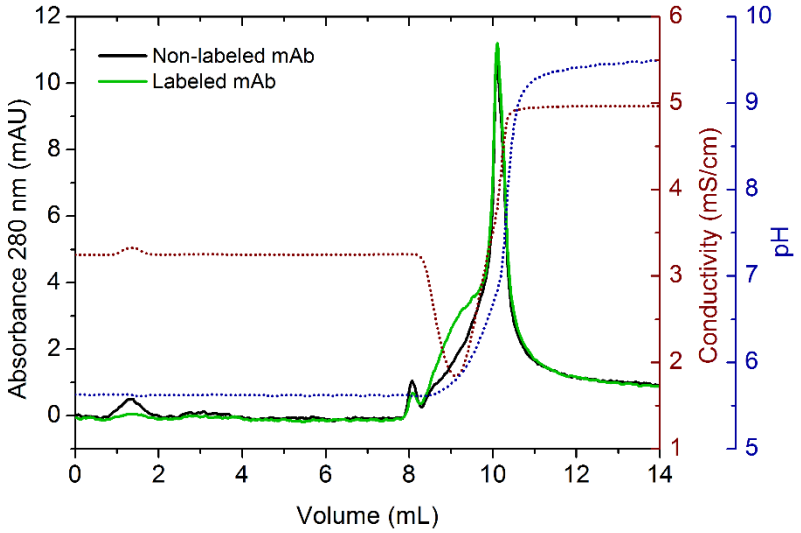

Figure 4.2 – Chromatographic profiles obtained by loading 0.5 µg of a labeled and unlabeled anti-IL8 IgG solution at a concentration of 5 µg/mL onto a pre-packed HiTrap Capto™ MMC column. Adsorption was performed with 50 mM acetate buffer at pH 5.5, and elution was performed with 50 mM carbonate buffer at pH 9.5.

Another aspect that was necessary to investigate was whether the different pH values and NaCl concentrations that were going to be used in the screening studies influence the fluorescence emission of the antibody solution. For that, a fixed concentration of IgG-Alexa 430 (5 µg/mL) was spiked in 100 µL of each of the different buffers and measured in a 96-well plate spectrofluorimeter (Varian Cary Eclipse). The excitation and emission wavelengths were set at 430 and 540 nm, respectively. The results obtained are shown in **Figure 4.3** for the buffers used in the adsorption **(A)** and elution **(B)** assays. It is possible to see that there is a random distribution of points around an average value of fluorescence, both for adsorption (140 ± 11 A.U.) and elution (135 ± 11 A.U.) conditions. Although there is some variability, these results confirm that there is no particular trend in terms of conductivity or pH for the variation of the fluorescence intensity.

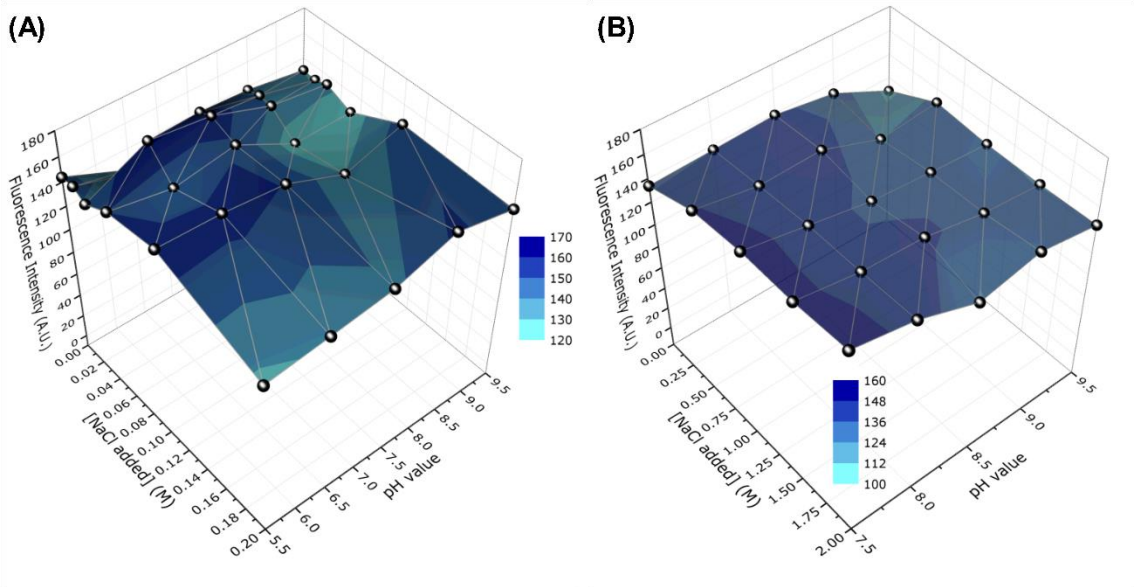

Figure 4.3 – Distribution of the fluorescence intensity as a function of the different pH values and NaCl concentrations evaluated in the adsorption **(A)** and elution **(B)** microfluidic assays.

The analytical quantification of the fluorescence measurements was always performed by imaging the entire interface region of the two microchannels with different heights, based on the fact that there is no significant antibody depletion along the micro-column. This lack of depletion was achieved by using a relatively high flow rate (15 μL/min) and low residence time (0.28 s) in the experiments. The reliability of the fluorescence quantification and lack of depletion is clearly demonstrated by analyzing different areas of the imaged region and plotting the fluorescence intensity over time. **Figure 4.4** shows that for different and randomly selected areas of quantification, the adsorption curves are very similar, which reinforces that the fluorescence signal in the packed beads is uniformly distributed.

It is important to note that, in the real-time monitoring of the fluorescence emission, the background signal of the solution flowing in the channel was very low compared to the signal provided by the beads, as also reported by Cohen *et al*. [157]. In fact, the fluorescence of the solution was not significantly different from the fluorescence of the bare channel or beads, which allowed a quantitative analysis of the fluorescence intensity independent of background signal subtraction and without resorting to more complex imaging techniques such as fluorescence polarization [158, 159].

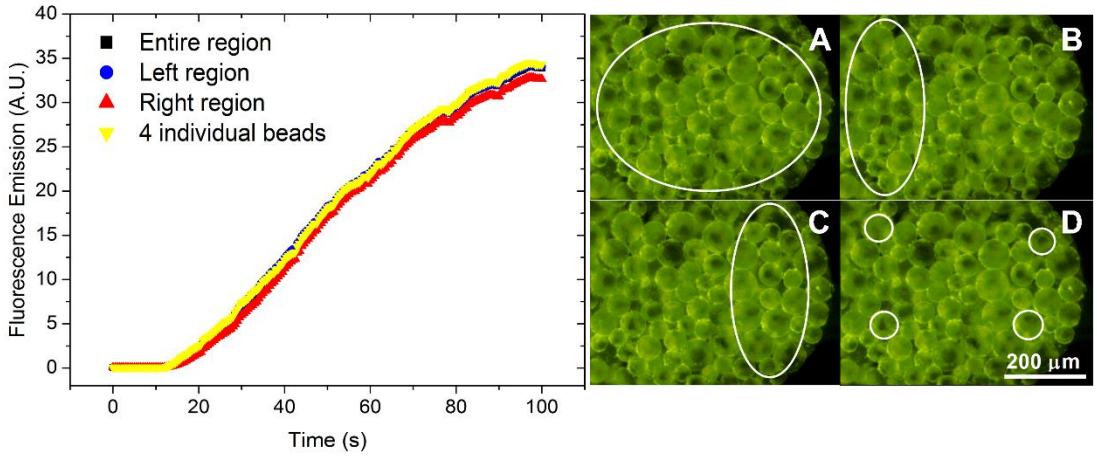

Figure 4.4 – Fluorescence emission of the packed beads as a function of the assay time considering different areas for quantification, namely (A) the average of the entire field of view, (B) the average of the left region of the field of view, (C) the average of the right region of the field of view, and (D) the average of the fluorescence intensity of four individual beads. Imaging conditions: 100x total magnification, 500 ms exposure time, 5x gain.

4.3.2. Determination of the response parameters

Adsorption and elution curves were obtained by individually measuring the fluorescence emission over time under different operating conditions, as exemplified in **Figure 4.5**. The adsorption experimental data points were fitted with a non-linear function based on a sigmoidal dose-response model, according to **Equation 4.2**, where F_{em} is the fluorescence emission, F_0 is the background fluorescence, F_{max} is the maximum fluorescence, $t_{1/2}$ is the time at the inflexion point, and k_s is the sigmoidal slope.

$$F_{em} = F_0 + \frac{F_{max} - F_0}{1 + 10^{(t_{1/2} - t)k_s}} \qquad \textbf{Equation 4.2}$$

The response parameter ($k_{1/2}$) chosen to compare the different adsorption kinetics was the first derivative of **Equation 4.2** calculated at the inflexion point ($t_{1/2}$) of the fitted curve, according to **Equation 4.3**.

$$k_{1/2} = \frac{k_s . ln10 . (F_{max} - F_0)}{4} \qquad \textbf{Equation 4.3}$$

Considering that the slope of the adsorption curve provides more meaningful information on the antibody-ligand binding kinetics than the plateau that is reached after ~150 s, only data points over the first 80 s were included in the fitting, which also reduces the time required for the optimization studies.

During elution, it was observed that the fluorescence drops very rapidly, within less than 4-5 seconds, as the eluent flows through the beads. Therefore, a non-linear fit would not

provide reproducible results due to the very pronounced influence of inter-assay variability in liquid velocity in the first few seconds after the application of a negative pressure. Thus, in order to average the initial variability, the selected response parameter (Y_R) was the ratio between the fluorescence intensity at 20 s (Min_{20s}) after the beginning of the elution process and the initial fluorescence (Max_{0s}) according to **Equation 4.4**. It is important to note that the 20 s time was selected as it allows sufficient time for the elution to take place and simultaneously avoids any pronounced bleaching effects.

$$Y_R = \left(1 - \frac{Min_{20s}}{Max_{0s}}\right) \times 100 \qquad \textbf{Equation 4.4}$$

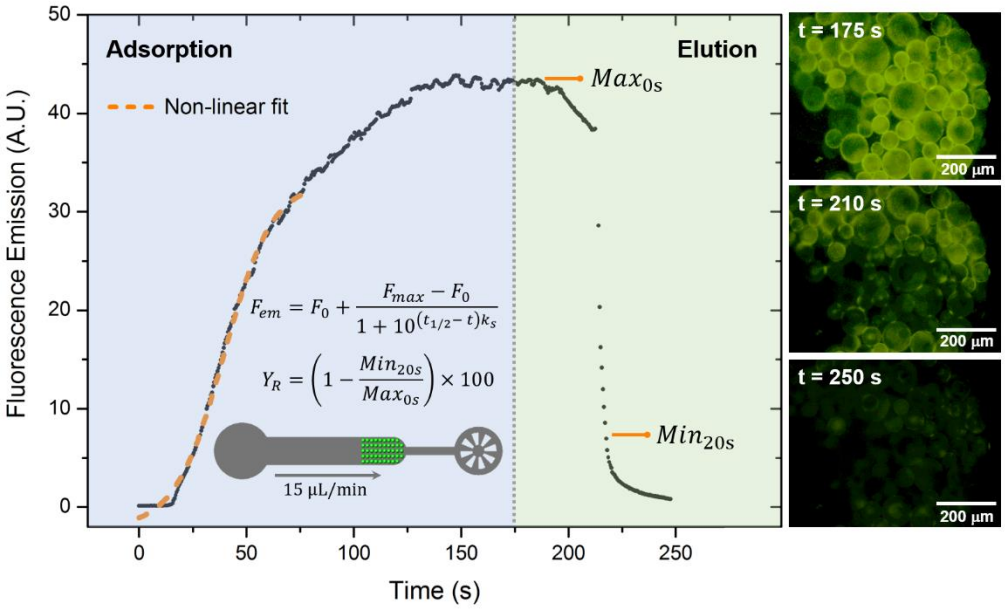

Figure 4.5 – Example of adsorption and elution kinetic curves obtained by continuously measuring the fluorescence emission (F_{em}) of the packed beads over time. The online measurements were performed at a flow rate of 15 µL/min and the signal was recorded using an exposure time of 500 ms. Dashed line represents the non-linear fit of the adsorption curve over the first 80 seconds.

4.4. Optimization of adsorption conditions

For the optimization of adsorption on Capto™ MMC, several buffers were used to screen a wide range of pH (5.5 – 9.5) and conductivity (0 – 200 mM NaCl) conditions. Considering that the buffering agent itself also has an intrinsic conductivity, the same concentration of NaCl gave slightly different global conductivity values for the different pH conditions under study (Appendix A).

The kinetic response parameters ($k_{1/2}$) for the adsorption on Capto™ MMC were displayed in a contour plot (**Figure 4.6-A**). It can be observed that an increase in buffer

pH resulted in a reduced binding of the mAb, regardless of the buffer conductivity. Considering that the mAb isoelectric point (pI) is ~9, as the pH of the binding buffer approaches this value the number of positive patches on the surface of the mAb decreases, which directly influences the ability of the antibody to electrostatically bind to the ligand. Among the conditions tested, the optimal pH value for adsorption was 5.5, which is about 3.5 units below the isoelectric point of the antibody. These observations are in accordance with previous studies reporting that having a difference of 3.5 units between mAb pI and load pH leads to the maximum dynamic binding capacity for basic mAbs (pI in a range of 8.2 – 9.3) [97].

Another observation is that at the optimal pH value (pH = 5.5) the ligand shows a high salt tolerance at conductivities as high as 20 mS.cm^{-1}, with the measured $k_{1/2}$ value remaining approximately constant, which is also in accordance with the reported literature [55, 96]. Salt tolerance was also found to decrease dramatically with increasing pH values, as can be seen in the adsorption kinetic profiles in **Figure 4.6-B** for a pH value of 6.5.

To further explore the interactions between mAbs and Capto™ MMC, the most relevant moieties of this multimodal ligand were individually evaluated, namely the carboxyl and the phenyl groups, within the same range of pH values and conductivities. The contour plot for the carboxyl resin (**Figure 4.6-C**) shows a typical behavior of a cation exchanger where a slight increase in conductivity, at a certain pH, strongly reduces the binding capacity. In this context, a 3.7-fold decrease in $k_{1/2}$ was observed when the conductivity was increased from 3.6 mS.cm^{-1} to 6.1 mS.cm^{-1}, at pH 5.5. On the other hand, at a constant conductivity value, the lower the pH (meaning a higher difference between the mAb pI and the pH value), the higher the $k_{1/2}$ value. Interestingly, at very low conductivities (no NaCl addition to binding buffer), the observed trend for the adsorption kinetics with increasing pH is very similar to that achieved for the multimodal resin, suggesting that for low conductivities the multimodal ligand behaves as a cation exchanger.

In the case of the phenyl ligand, it is important to highlight that the range of measured $k_{1/2}$ values is nearly one order of magnitude lower than that obtained for the other ligands. This is due to the working range being considerably outside of the appropriate operating conditions to promote hydrophobic interactions (*e.g.* 1.5 M ammonium sulfate) and also to the considerably low dynamic binding capacities of HIC in comparison to IEX [160].

Nevertheless, despite the lower values of $k_{1/2}$, it is possible to clearly observe a trend in the results. By observing the contour plot in **Figure 4.6-D**, the results indicate that the phenyl ligand is characterized by a high degree of salt tolerance up to pH values of ~7.5, together with an overall decrease in binding with increasing pH. Considering the low conductivities used, relative to the optimal conductivity conditions typically applied to a hydrophobic ligand, the binding mechanism to the phenyl ring is most likely to occur by cation-π interactions [67]. The results also highlight an expected property of the phenyl ligand at pH values near the pI of the mAb (pH 8.5-9.5), which is the promotion of hydrophobic interactions at higher conductivities (~20 mS.cm^{-1}).

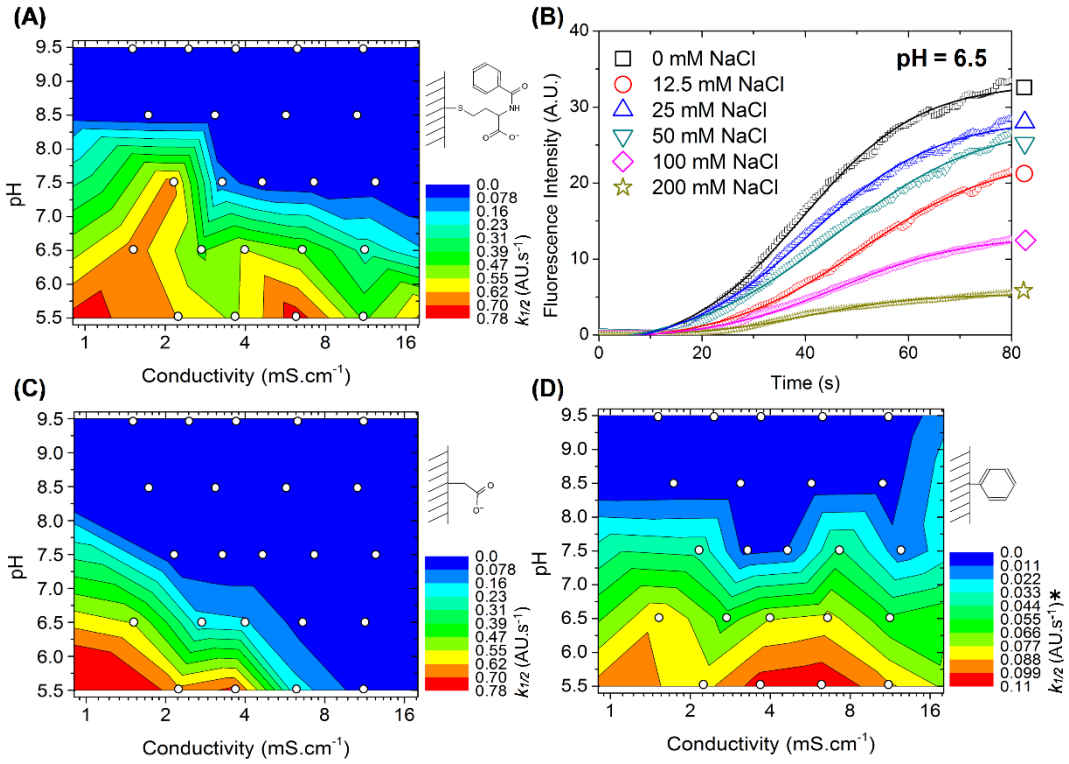

Figure 4.6 – Screening results based on the kinetic response parameter ($k_{1/2}$) for the adsorption of the anti-IL8 mAb performed at different pH (5.5 – 9.5) and conductivity (0 – 200 mM NaCl) conditions using **(A)** multimodal, **(C)** electrostatic, and **(D)** hydrophobic beads. Only some of the experimental data points corresponding to the tested conditions are indicated in the plots. The extreme conductivity points are outside the scale range, in order to provide a uniform contour surface. **(B)** Adsorption kinetic curves obtained using Capto™ MMC multimodal beads at pH 6.5 for different salt concentrations in the binding buffer. The asterisk (∗) highlights the different scale in the case of the phenyl ligand.

Overall, the profiles observed in the three contour plots suggest an additive contribution of both the electrostatic and hydrophobic moieties to describe the binding mechanism in the multimodal ligand. In particular, the binding to the multimodal ligand seems to be mostly driven by the electrostatic moiety, considering the magnitude of $k_{1/2}$ in **Figure 4.6-A** and **C**, while the hydrophobic moiety promotes a synergic effect in binding at

higher conductivities, thus endowing Capto™ MMC with additional salt tolerance. This hypothesis is corroborated by recent findings by Karkov and co-workers [8] using in-silico and site-directed mutagenesis approaches. The combined adsorption results obtained with the three resins allowed the selection of a common adsorption condition to perform the subsequent elution studies. This condition (pH 5.5, ~ 4 mS.cm^{-1}) was chosen based on the need to fix one buffer composition that provides high $k_{1/2}$ values for all the three resins, in order to allow meaningful comparison during the elution studies.

4.5. Optimization of elution conditions

For the elution studies, pH values closer to the mAb pI were used as these conditions are unfavorable to electrostatic interactions, which are the main responsible for the binding as discussed in section 4.4. For this reason, the screening conditions included pH values in the range of non-binding pH conditions, *i.e.* from 7.5 to 9.5. The conductivity values were selected in order to test more extreme NaCl concentrations (0 – 2 M NaCl), to further evaluate the contribution of each moiety under conditions that disrupt or promote each of their individual modes of action.

Figure 4.7-A shows the elution from Capto™ MMC. It can be observed that the maximum antibody recovery (Y_R > 94%) occurs at a pH of 9.5 and at the lowest tested conductivity (6.5 mS.cm^{-1}). These results indicate that the conditions that more strongly promote the elution of the antibody are those where the antibody is negatively charged (pH > pI), inducing a charge repulsion, together with unfavorable conditions for promoting hydrophobic interactions. The latter effect can be clearly seen as a gradual decrease in Y_R with an increase in conductivity from 6.5 to 147.2 mS.cm^{-1}. The same trend can be observed in the kinetic curves plotted in **Figure 4.7-B**. As the pH is changed in the range between 7.5 and 9.5, at a fixed concentration of 0 mM NaCl in the elution buffer, the Y_R values decrease significantly as the antibody charge changes from positive to neutral and from neutral to negative.

Analyzing each of the individual moieties, the purely electrostatic ligand (**Figure 4.7-C**) shows a typical elution behavior, in which at low conductivities the antibody remains strongly bound to the beads, until the pH equals the pI (neutral charge conditions) or surpasses the pI (charge repulsion). Also consistent with a typical cation exchange interaction is the profile obtained at NaCl concentrations ≥500 mM (45.5 –

49.9 mS.cm^{-1}) where the elution is triggered by the shielding of the surface charge. On the other hand, the phenyl resin (**Figure 4.7-D**) shows considerably lower removal yields for higher concentrations of salt (≥ 1 M NaCl, *i.e.* 83.5 – 86.2 mS.cm^{-1}), regardless of the pH value, which is an expected behavior for a hydrophobic interaction ligand, since high salt concentrations lead to salting-out effects [73], which promote hydrophobic interactions with the sorbent thus impairing the elution. It is important to note the difference in the range of Y_R values measured for the phenyl ligand, since for conductivities higher than ~50 mS.cm^{-1} the antibody remains strongly adsorbed to the beads, leading to a recovery yield that is considerably lower than the minimum percentage displayed in the other two contour plots. Interestingly, at a low conductivity (0 M NaCl in the elution buffer) the Y_R has a maximum at pH 9.5, similar to what was observed for the multimodal and cation exchange ligands. For the phenyl resin, this condition corresponds to the elimination of both hydrophobic and cation-π interactions.

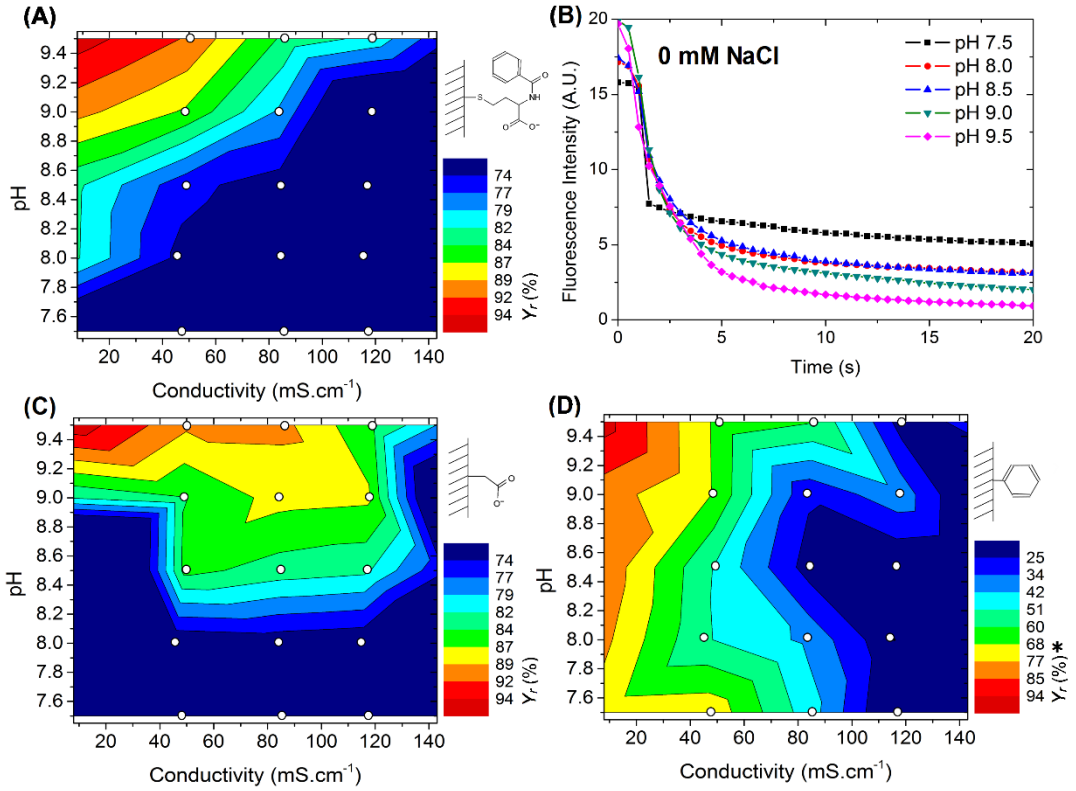

Figure 4.7 – Screening results based on the recovery yield parameter (Y_R) for the elution of the anti-IL8 mAb performed at different pH (7.5 – 9.5) and conductivity conditions (0 M – 2 M NaCl) using **(A)** multimodal, **(C)** electrostatic, and **(D)** hydrophobic beads. Only some of the experimental data points corresponding to the tested conditions are indicated in the plots. The extreme conductivity points are outside the scale range, in order to provide a uniform contour surface. **(B)** Elution kinetic curves obtained using Capto™ MMC multimodal beads for different pH values of the elution buffer with no salt addition (0 mM NaCl). The asterisk (∗) highlights the different scale in the case of the phenyl ligand.

Overall, comparing the elution profiles obtained for the multimodal ligand and for each of the individual moieties, the result suggests a decreased elution yield at high conductivities, which is essentially due to the phenyl moiety, considering that at high salt concentrations the electrostatic interactions are blocked and thus the ion exchange moiety is cancelled out. On the other hand, the trend observed at constant conductivities (pH effect only) was similar for both moieties, highlighting both the reduced binding at pH values close to the mAb pI, which correlates to an overall decrease in positive charges in the case of the electrostatic resin, and also the reduced cation-π interactions in the case of the hydrophobic resin.

4.6. Validation in standard column chromatography

The validation of some conditions derived from the miniaturized assays was performed using a standard chromatography column pre-packed with the multimodal resin (Capto™ MMC). A solution of anti-IL8 mAb at a concentration of 20 g/mL was loaded at the optimal condition obtained from the adsorption experiments in microfluidics (pH 5.5, 0 mM NaCl), and different elution buffers were tested, namely pH 9.5 containing 0, 1, 2 M NaCl, pH 8.5 containing 1, 2 M NaCl and pH 7.5 containing 1, 2 M NaCl.

As an example, the chromatographic profiles obtained at pH 9.5 are represented in **Figure 4.8**, clearly highlighting a pronounced decrease on the recovery yield values as the conductivity is increased. It is possible to observe that no peaks were detected in the flowthrough, which means that the binding of the antibody occurred with minimal losses, and so that the observed differences in performance can be attributed only to the different ability of the elution buffers to remove the bound antibody. Using an elution buffer at pH 9.5 with no added NaCl (**Figure 4.8-A**), desorption takes place as the pH begins to increase, gradually approaching and crossing the pI of the mAb. In this case, the elution occurs due to a pH effect only, since the conductivity values in the column are constant throughout the entire run. On the other hand, when 1 or 2 M of NaCl are present in the elution buffer at pH 9.5 (**Figure 4.8-B**), it is the increase of conductivity that readily promotes the elution of the mAb, since the increase in pH occurs only after the elution peak. This observation is further supported by a shift in the mAb retention time from 9.90 ± 0.04 min at 0 M NaCl to 9.22 ± 0.02 min at 1 or 2 M NaCl. The delay in the pH increase is due to an initial acid-base titration that occurs in the mixing chamber (0.6 mL). In

addition, it can be observed that the areas of the elution peaks, as well as the corresponding recovery yields ($Y_{0,1,2M}$) decrease as the concentration of NaCl increases in the elution buffer. The trend that a higher salt concentration in the elution buffer decreases the elution efficiency is further observed at pH 8.5 and 7.5. This is in accordance to the results shown in **Figure 4.7-A** where it was observed that the recovery yield values tend to decrease as the elution pH decreases to values increasingly below the antibody isoelectric point and at higher salt concentrations.

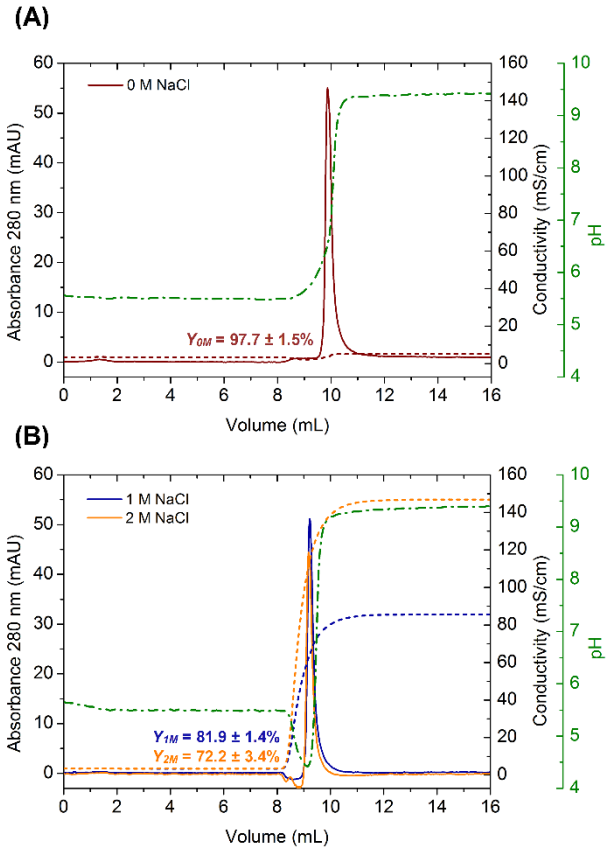

Figure 4.8 – Chromatographic profiles obtained by loading 10 µg of anti-IL8 mAb at a concentration of 20 µg/mL onto a pre-packed HiTrap Capto™ MMC column. Adsorption was performed with 50 mM acetate buffer at pH 5.5 and elution was performed with 50 mM carbonate buffer at pH 9.5 containing 0 M NaCl **(A)**, 1 M or 2 M NaCl **(B)**. Dashed lines correspond to conductivity and pH.

Table 4.1 summarizes and compares the results obtained in the microfluidic and macroscale approaches and it can be observed that both exhibit the same trends. The recovery yield values are also highly consistent between microfluidic and macroscale approaches since the average values obtained for each approach are not statistically different at a confidence level of 95% (p-value > 0.05). It can also be noted that in this particular case, the recovery yield values calculated at the macroscale and those obtained

in the microscale can be directly compared, since they are both relative to the total amount of antibody present in the beads.

A comparison of some operating parameters employed in the micro- and macroscale approaches is also presented in **Table 4.1**. It is possible to observe that major differences can be found in the amount of reagents consumed and the time required for each assay, which directly correlates with cost and time savings. In the microfluidic experiments, the velocity at which the liquid flowed was much higher (~10-fold difference) than in the macroscale assays, which translated in a much lower residence time. This low residence time (0.28 s) in the microscale assays does not present a problem in this case, since the main purpose was to rapidly reach an equilibrium condition, regardless of possible antibody losses, in order to obtain a response parameter to decide the optimal operating conditions. Also attractive from a high-throughput point of view are the low amounts of resin and antibody molecules that were required to perform the screening of conditions in the microscale, corresponding to approximately a 10^4-fold and 10-fold decrease, respectively. Furthermore, the experiments at microscale are amenable to parallelization, resulting in even lower times per experiment, from 2 minutes down to a few tens of seconds.

Table 4.1 – Comparative analysis of some operating and performance parameters[(a)] from the experiments performed in micro- and macroscale.

	Microscale	**Macroscale**		**Microscale**	**Macroscale**
	(i) Operating Parameters			(ii) Recovery Yield (Y_R) (%)	
Packed-bed height	~ 1 mm	25 mm	pH 9.5 + 0 M[(c)]	94.6 ± 5.2	97.7 ± 1.5 (p = 0.23)
Packed-bed volume	~ 70 nL	1 mL	pH 9.5 + 1 M	86.2 ± 4.7	81.9 ± 1.4 (p = 0.15)
Flow rate	15 µL/min	1 mL/min	pH 9.5 + 2 M	78.3 ± 3.7	72.2 ± 3.4 (p = 0.091)
Velocity	21.4 cm/min	25.9 mm/min	pH 8.5 + 1 M	75.9 ± 3.5	81.7 ± 3.3 (p = 0.092)
Residence time	0.28 s	1 min	pH 8.5 + 2 M	66.0 ± 8.8	79.1 ± 1.6 (p = 0.063)
Mass of mAb per assay	1.5 µg	10 µg	pH 7.5 + 1 M	69.1 ± 5.2	79.0 ± 3.7 (p = 0.058)
Assay time	~ 2 min	~ 26 min[(b)]	pH 7.5 + 2 M	56.2 ± 11.1	67.5 ± 8.3 (p = 0.17)

[(a)] Recovery yield values are displayed as mean ± SD. Chromatography runs were performed in duplicate, while the corresponding microfluidic experiments were performed in triplicate. The p-values to evaluate the probability of the two average recovery yields being different were calculated assuming a two-tailed t student distribution with two degrees of freedom.
[(b)] Assuming a run time of 16 min + 5 min for column equilibration + 5 min for column re-equilibration.
[(c)] 0, 1 and 2 M refer to concentrations of NaCl.

4.7. Summary

This chapter reports the development of a microfluidic analytical method to screen adsorption and elution conditions within a few minutes for optimization of multimodal chromatography. In addition to optimizing the binding conditions of an anti-IL8 mAb to a commercial multimodal resin (Capto™ MMC), it was also possible to explore the source of the complex kinetic properties of this resin by analyzing its ionic and hydrophobic moieties individually. This multimodal resin was observed to have a mostly electrostatically driven adsorption with the hydrophobic moiety providing additional salt tolerance, in accordance to several previous studies using conventional optimization approaches. Optimal elution conditions were achieved for a pH value (pH = 9.5) slightly above the antibody isoelectric point and, in this case, addition of a neutral salt (NaCl) reduced the antibody recovery. Overall, the best recovery conditions resulted in a yield of (94.6 ± 5.2) %, which is comparable to the optimal value of (97.7 ± 1.5) % obtained using a conventional chromatography column.

The obtained results demonstrated that microfluidic chromatography coupled to fluorescence measurements directly on the resin under study can be a powerful and versatile tool to speed up the screening of binding kinetics and to provide insights on the mechanisms of interaction. Furthermore, this technique can potentially be used with any target molecule or resin assuming a previous labeling procedure with a photostable and environment-independent fluorophore.

"In the middle of difficulty lies opportunity."

Albert Einstein

Chapter 5
Multiplexed and Quantitative Screening of Ligands and Target Molecules[§]

The increasing number of novel commercially available chromatography ligands has been motivating the use of high-throughput screening platforms, particularly during the early stages of process development. As discussed in section 2.4, the approaches to perform a high-throughput optimization of chromatographic operating conditions are normally based on microtiter plates, micropipette tips and miniature columns operated in robotic platforms for automation and parallelization of processes. However, to further reduce time, costs and molecule consumption, the use of microfluidic platforms has been reported within this context, for quantifying protein breakthrough [20, 126] and real-time tracing of adsorption isotherms [21]. Microfluidics allows to explore different types of stationary phases within a microchannel, from monolithic structures [161-163] to bead-packed channels [19, 126, 164]. Additionally, the use of microfluidic devices for chromatographic separations has the potential to parallelize and automatize the process operation, from sample injection to signal read-out, without resorting to complex, expensive and bulky equipment. For complex separations, in particular, it is advantageous to optimize the chromatography operation by bead-level monitoring, while simultaneously analyzing the behavior of multiple target molecules. Despite the progress made in miniaturizing the different components of liquid chromatography, this type of multiplexed study and quantitative analysis associated with multiple target compounds has so far not been demonstrated.

This chapter reports the development of a microfluidic device to perform a multiplexed screening of different chromatography resins – packed in three chambers in series with

---

This chapter contains sections reproduced from a manuscript currently submitted to *Journal of Chromatography A*:

[§]I.F. Pinto, R.R.G. Soares, M.R. Aires-Barros, V. Chu, J.P. Conde, A.M. Azevedo, "Optimizing the performance of chromatographic separations using microfluidics: multiplexed and quantitative screening of ligands and target molecules" (*submitted*).

the liquid flow – and target molecules. An artificial mixture of an anti-IL8 monoclonal antibody and BSA was used as a model system to perform a comprehensive optimization of separation conditions using multimodal ligands. A quantitative analytical method was developed to determine the recovery yield and purity of the separation, based on fluorescence measurements of the molecules of interest directly at bead-level. The performance of the separation was then sequentially optimized through a (i) capture step, in which the selective binding of IgG to the beads was maximized, followed by a (ii) polishing step, in which remaining amounts of BSA were further removed by interaction with the beads.

5.1. Experimental section

5.1.1. Buffer solutions and chromatography resins

Acetate buffers at pH 4.5 and 5.5 were prepared using sodium acetate from Merck (Darmstadt, Germany) and acetic acid (100%, AnalaR Normapur) from VWR BDH Prolabo (Radnor, PA, USA). Phosphate buffers at pH 6.5 and 7.5 were prepared using potassium dihydrogen phosphate and dipotassium phosphate from Panreac Quimica Sau (Barcelona, Spain). Tris buffer at pH 8.5 was prepared using Tris(hydroxymethyl) aminomethane from Sigma-Aldrich. Carbonate buffer at pH 9.5 was prepared using sodium bicarbonate and sodium carbonate also from Sigma-Aldrich. For each pH condition (50 mM buffering agent), different conductivities were achieved by adding sodium chloride (Sigma-Aldrich) at the following concentrations: 0, 50, 100, 200, 500, 1000 mM.

CM Sepharose Fast Flow, Q Sepharose Fast Flow, MabSelect SuRe (Protein A), Capto™ MMC and Capto™ adhere resins were obtained from GE Healthcare (Uppsala, Sweden) in bulk and as prepacked 1 mL columns. MEP HyperCel™ and HEA HyperCel™ were obtained from Pall Corporation (Port Washington, NY, USA) in bulk and as prepacked 1 mL columns. Toyopearl Sulfate-650F and Toyopearl NH2-750F bulk resins were kindly provided by Tosoh Bioscience GmbH (Darmstadt, Germany).

5.1.2. IgG purification and protein labeling

Anti-interleukin 8 monoclonal antibodies (anti-IL8 IgG, pI = 9) were produced by Chinese hamster ovary (CHO) cells grown in a serum-containing medium, as described

in detail in [165]. Purified IgG was obtained by loading the cell culture supernatant onto a protein A (MabSelect SuRe) column using an ÄKTA™ Purifier system from GE Healthcare. Recovered IgG was concentrated using Amicon centrifugal units (10 kDa cutoff) before conjugation to a fluorophore.

IgG and BSA (Sigma-Aldrich) were conjugated to the thiol-reactive dyes BODIPY FL (Ex = 488 nm, Em = 503 nm) and BODIPY TMR (Ex = 545 nm, Em = 570 nm), respectively, from Thermo Fisher Scientific. The conjugation reactions were performed as follows: (i) IgG and BSA were prepared at a final concentration of 8.5 and 15 mg/mL, respectively, in PBS; (ii) BODIPY dyes were added to the protein solutions in a proportion of 20 mol dye/mol protein; (iii) solutions were mixed in the vortex for 2-3 s and incubated in the dark for 2 h with constant orbital agitation; (iv) free dye molecules were removed using Amicon centrifugal devices (0.5 mL, 10 kDa cutoff) using at least 10 diafiltration volumes. The degree of labeling for the conjugation reaction of IgG and BSA was measured spectrophotometrically as 0.5 and 2.2 mol dye/mol protein, respectively.

5.1.3. Liquid handling and operation in the microfluidic device

The microfluidic structures were fabricated according to the described in chapter 3, section 3.1, and the different types of chromatography beads were prepared as described in section 3.4. The bead solutions were then simultaneously introduced into the three microchambers by inserting pipette tips in the inlets of the chambers and applying a negative pressure at both the inlet and outlet of the 20 μm tall channel using a syringe pump. The inlets of the microchambers were then closed with a steel plug and the beads were washed with 50 μm of PBS (Sigma Aldrich) by flowing the buffer through the 20 μm tall channel crossing the three chambers. Adsorption studies in the multiplexed microfluidic device were performed by flowing mixtures of fluorescently labeled IgG (25 μg/mL) and BSA (250 μg/mL) under different buffer conditions at 10 μL/min for 150 s. Due to the high concentration of BSA used in these studies and relatively high photoluminescence of the BODIPY-TMR fluorophore, 3 μg/mL of labeled BSA were diluted with 247 μg/mL of non-labeled BSA, to avoid signal saturation during the fluorescence measurements. Elution studies were performed in single-column microfluidic channels (fabricated as described in chapter 3, section 3.1), by first adsorbing

the molecules under appropriate conditions for 180 s and then flowing the elution buffer for 150 s, both at a flow rate of 10 μL/min.

5.1.4. Image acquisition and processing

Fluorescence measurements were performed using an Olympus CKX41 inverted microscope coupled to a CCD color camera (Olympus XC30) equipped with a filter cube providing blue-excitation (band-pass excitation: 460 – 490 nm; long-pass emission: 520 nm) and green-excitation (band-pass excitation: 480-550 nm; long-pass emission: 590 nm). These filter cubes will be henceforth referred as B and G filters. The signal corresponding to the fluorescence emission of IgG and BSA in the artificial mixture was acquired using the B and G filters, respectively, in intervals of 20 s using an exposure time of 1.5 s, 5 dB gain and 40× total magnification. Images were analyzed using ImageJ software (National Institutes of Health, USA), and the fluorescence emission values were obtained by averaging the entire area (200 × 400 μm) corresponding to the intersection of each microchamber with the transversal 20 μm channel.

5.1.5. Assays in 1-mL chromatography columns

Chromatography assays were performed using either pre-packed or *in-house* packed columns (1 mL) in an ÄKTA™ Purifier system. UV absorbance at 280 nm, conductivity and pH of the outlet stream were continuously monitored using a UV-900 and pH/C-900 module, respectively. Flowthrough and elution fractions were collected using a Frac-920 fraction collector (GE Healthcare).

In the assays using artificial mixtures, the capture and polishing steps for the different purification sequences were performed in separate. Similarly to the approach followed in the microfluidic experiments, the performance parameters (yield, purity) of the first step were used to determine the composition of the mixture to load on the second step. Chromatography runs were performed at a flow rate of 1 mL/min using a 500 μL injection loop. The artificial mixtures were prepared in the adsorption buffer of the corresponding purification step (capture or polishing) under study.

Purification using a serum-containing cell culture supernatant was accomplished by performing the capture and polishing steps sequentially. Capture was performed in a Toyopearl Sulfate column by loading the cell culture supernatant using a 5 mL injection loop, adsorbing the molecules at pH 6.5 + 50 mM NaCl and eluting at pH 9.5 + 500 mM

NaCl. Polishing was then performed in a Toyopearl NH_2 column by loading the elution pool of the capture step using a 2 mL injection loop, adsorbing the molecules at pH 9.5 + 500 mM NaCl and eluting/regenerating with 0.5 M NaOH. Both capture and polishing runs were performed at a flow rate of 1 mL/min.

5.1.6. Post-chromatography quantification of IgG and total protein

Flowthrough and elution fractions collected in conventional chromatography assays (non-microfluidic) were analyzed with respect to IgG and total protein concentrations. IgG concentration was determined by analytical protein A chromatography, using a POROS PA ImmunoDetection sensor-cartridge from Applied Biosystems (Foster City, CA, USA), as described by Azevedo *et al.* [155]. Total protein content was determined by the Bradford method using a Coomassie assay reagent from Pierce (Rockford, IL, USA).

5.1.7. Protein gel electrophoresis

Reducing sodium dodecyl sulfate-polyacrylamide gel electrophoresis (SDS-PAGE) was performed with samples collected in the chromatographic assays using a serum-containing cell culture supernatant. The samples were prepared in reducing conditions as previously described by Pinto *et al.* [165] and loaded in a 12% acrylamide gel polymerized using 40% acrylamide/bisacrylamide solution (29:1) from Bio-Rad (Hercules, CA, USA). Gels were run at 90 mV using a running buffer containing 192 mM glycine, 25 mM Tris-HCl and 0.1% SDS at pH 8.3. Gels were silver stained as follows: (i) 2h fixation in 30% ethanol, 10% acetic acid; (ii) 10 min wash with 30% ethanol; (iii) 2×10 min wash with MilliQ water; (iv) 1 min sensitization with 0.02% sodium thiosulfate; (v) 3×30 s wash with MilliQ water; (vi) 30 min staining with 0.15% silver nitrate; (vii) 1 min wash with MilliQ water; (viii) development in 3% sodium carbonate, 0.05% formaldehyde; (ix) 15 min wash with 5% acetic acid.

5.1.8. Isoelectric focusing

Isoelectric focusing (IEF) was performed to analyze the isoelectric point of IgG and BSA after labeling with BODIPY fluorophores. The IEF was performed in a Pharmacia PhastSystem separation module using a precast homogeneous polyacrylamide gel (PhastGel® IEF 3-9) from GE Healthcare. The program for running the gel included a 75 Vh prefocusing step at 2000 V, sample application at 200 V for 15 Vh, and a focusing

step at 2000 V for 410 Vh, as reported by Olsson *et al.* [166]. The gel was subsequently silver stained, according to the proceeding also described in [166].

5.2. Design and operation of the multiplexed microfluidic device

The microfluidic structure designed for the multiplexing experiments is shown in **Figure 5.1**. The device consisted of three individual microchambers in which three different types of chromatography beads were packed. Each chamber had a useful volume of ~10 nL and was placed in series with the flow of the solution. By having the chambers placed in series, it was possible to ensure that the liquid velocity was the same through the three chambers, independent of any variations in the bulk density of the bead packing in each chamber.

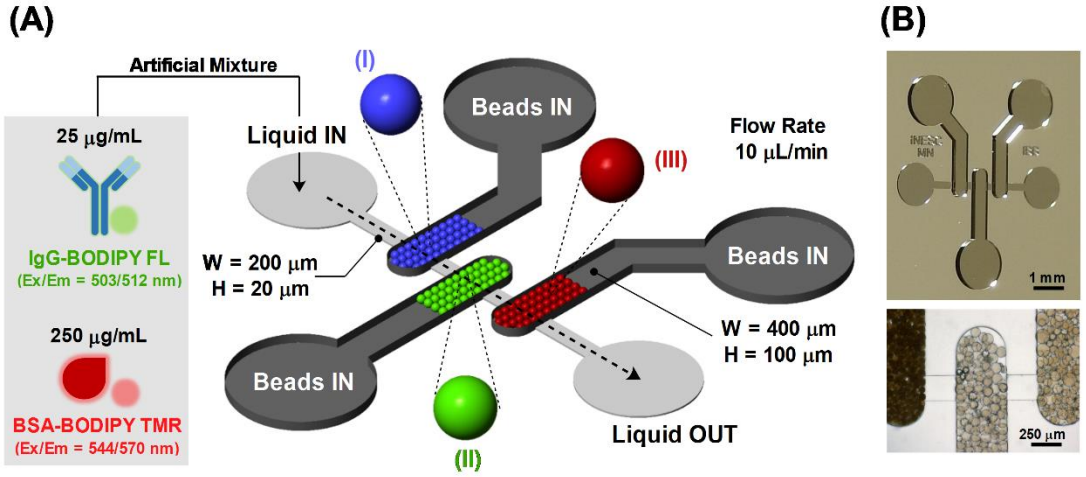

Figure 5.1 – Microfluidic structure used in the multiplexing experiments. **(A)** Schematics of the microchambers with three different types of chromatography beads packed in series with the flow of the solution. An artificial mixture of IgG-BODIPY FL and BSA-BODIPY TMR was flowed through the three chambers at different operating conditions. **(B)** SU-8 mold of the microfluidic structure (*top*) and bright field microscopy image of the PDMS structure showing the beads packed inside the microchambers (*bottom*).

Preliminary experiments performed with the same type of beads (Capto™ MMC) in the three chambers showed that at a flow rate of 10 μL/min no significant depletion of the target molecules in solution is observed (**Figure 5.2**). This is essential for performing a multiplexed analysis of different types of beads subjected to the same concentration of target molecule in solution under the same operating conditions.

An artificial mixture composed of IgG (25 μg/mL) and BSA (250 μg/mL), in concentrations similar to those in a serum-containing cell culture supernatant, was used

as a model to optimize the performance of the separation. IgG and BSA were previously labeled with different thiol-reactive neutral dyes – BODIPY FL and BODIPY TMR, respectively – to allow fluorescence measurements of the adsorption and elution events in real-time and at bead-level.

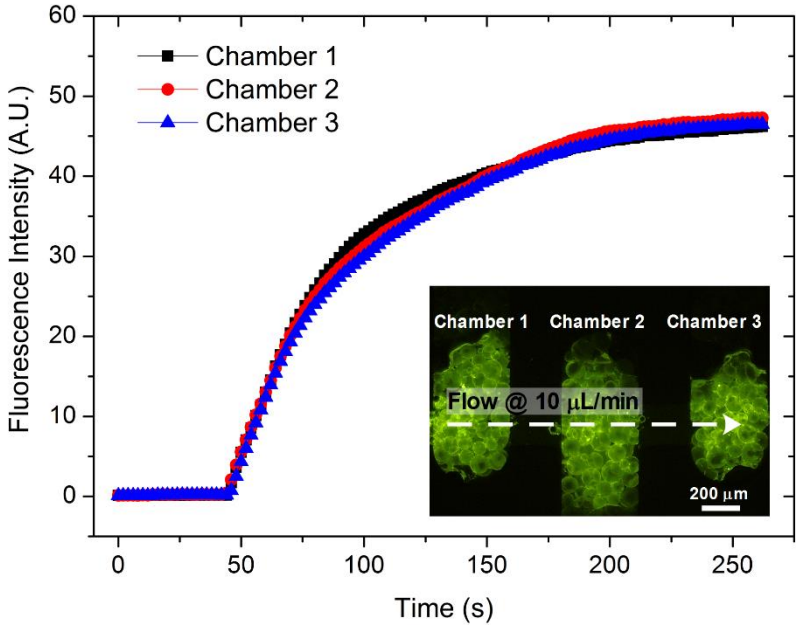

Figure 5.2 – Fluorescence emission of the packed beads in the three microchambers simultaneously monitored over time using a microscope. The chambers were packed with a single type of chromatography beads (Capto™ MMC) and a solution of fluorescently labeled IgG (50 µg/mL) was flowed at 10 µL/min. The fluorescence intensity of the three chambers was homogeneous over time, which indicates that there is no depletion of IgG molecules in solution at the used flow rate, implying reaction-limited conditions.

The fluorophores used to label the proteins were selected based on their excitation/emission spectra, to avoid signal cross-contamination when performing the simultaneous detection of IgG and BSA in the same solution. In **Figure 5.3-A** and **B** the spectral properties of the fluorophores overlapped with the used set of fluorescence filter cubes are shown. The bandpass excitation of the B and G filters excites both BODIPY FL and TMR fluorophores, although TMR is excited with a relatively low efficiency by the B filter. On the other hand, while with the B filter the emission of both fluorophores is measured, the fluorescence emission measured with the G filter is uniquely derived from the BODIPY TMR fluorophore. This allows the deconvolution of the signal measured with the B filter in order to obtain the fluorescence intensity derived only from the BODIPY FL fluorophore. The fluorescence signal deconvolution is shown schematically in **Figure 5.3-C** and this approach was systematically used to construct calibration curves for each of the conjugates, enabling an analytical quantification of the mass of IgG/BSA bound per volume of resin for each operating condition tested.

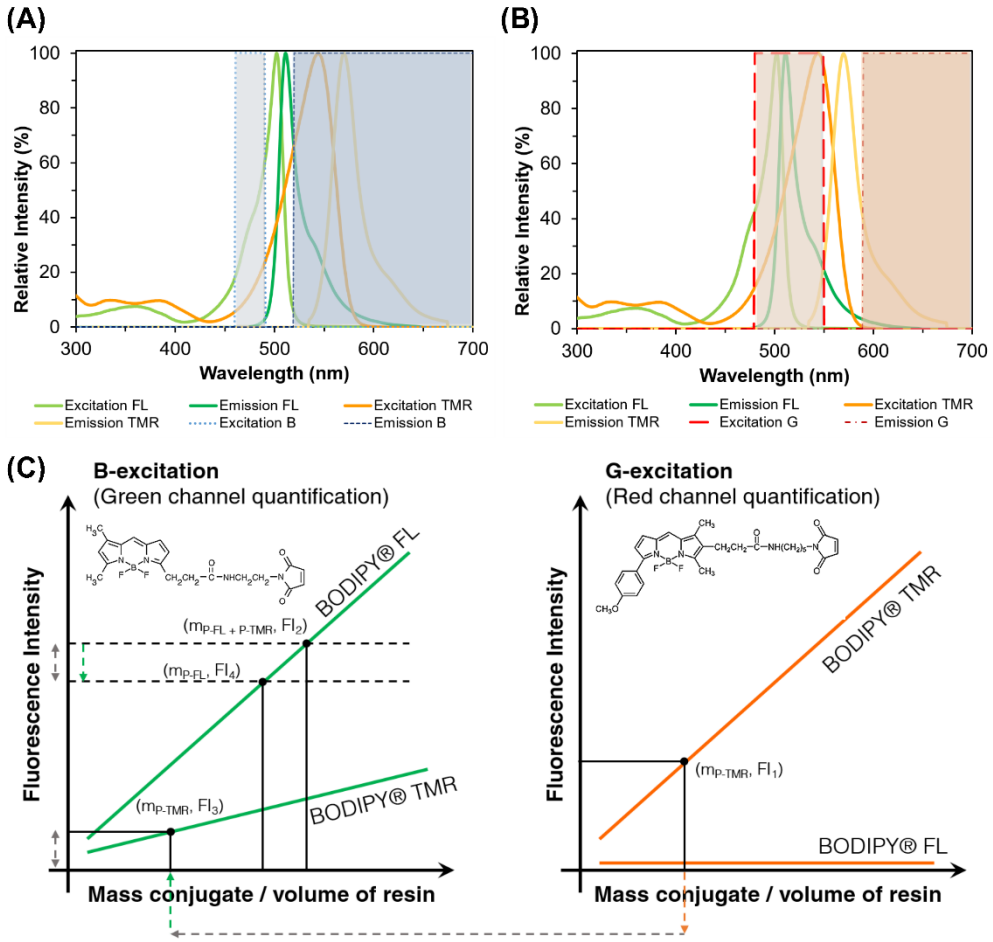

Figure 5.3 – Excitation/emission spectra of the BODIPY FL and BODIPY TMR fluorophores overlapped with the intervals of excitation/emission provided by the **(A)** B filter (band-pass excitation: 460 – 490 nm; long-pass emission: 520 nm) and **(B)** G filter (band-pass excitation: 480-550 nm; long-pass emission: 590 nm) in the fluorescence microscope (Olympus CKX41). **(C)** Schematics of the strategy followed for signal deconvolution in the calibration curves obtained with the protein conjugates, caused by the simultaneous excitation/emission of both IgG and BSA molecules in the blue region. The fluorescence signal measured at a long-pass emission of 520 nm is a contribution of both IgG and BSA molecules that can be corrected considering that the fluorescence signal measured in the green region corresponds uniquely to the labeled BSA molecules.

The selection of the thiol reactive BODIPY fluorophores was motivated by their environment-independent quantum yields, their reactivity with neutral -SH groups in the protein, their neutral charge and their relatively low molecular weight (< 600 Da). Thus, the labeling of IgG and BSA with BODIPY FL and TMR did not alter the overall charge of the protein (**Figure 5.4)**, minimizing the effect that tagging the molecules of interest would have in their interaction with the chromatographic beads. This was particularly important considering that the optimization studies performed in the microfluidic device were intended to serve as guidelines for the separation of IgG (target) from BSA (impurity) at a conventional scale, when the target proteins are in their native state.

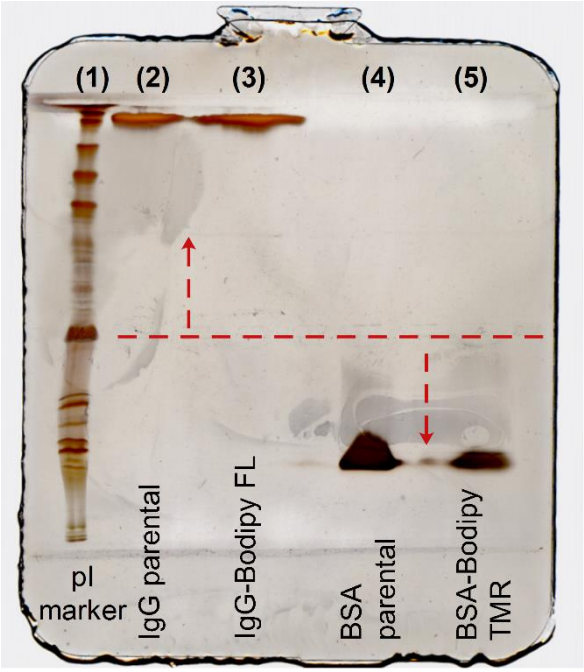

Figure 5.4 – Isoelectric focusing (IEF) gel performed with labeled and unlabeled IgG and BSA. Lanes ID: (1) – pI broad standards 3-10 (GE Healthcare); (2) – parental IgG; (3) IgG conjugated to BODIPY FL; (4) parental BSA; (5) BSA conjugated to BODIPY TMR. Samples were loaded in the central part of the gel (dashed line) and migrated up or downwards according to their isoelectric point (pI). The gel shows that the presence of the fluorophore did not alter the overall charge of the proteins. pI (IgG) = 9; pI (BSA) = 4.6.

5.3. Mass balance calculations

Prior to performing the experiments in the multiplexed microfluidic device, it was necessary to calibrate the mass of each conjugate captured by the beads with respect to the fluorescence intensity measured at bead-level in microfluidic devices. This analytical method was based on a mass balance followed by a signal deconvolution strategy (as shown in **Figure 5.3**) and allowed to determine the recovery yield and purity of the separation under different operating conditions.

Two separate mass balances were performed, one for IgG and other for BSA conjugates, using protein A and Q Sepharose chromatography beads, respectively. The mass balance approach relates the intensity of the fluorescence signal with the amount of molecules bound to the beads inside the microcolumn, after flowing a given amount of IgG/BSA conjugates. The intensity of the fluorescence signal is proportional to the total mass of IgG/BSA inside the microchannel ($m(IgG/BSA)_{total}$), either specifically bound to the beads ($m(IgG/BSA)_{beads}$) or non-specifically bound to the PDMS walls ($m(IgG/BSA)_{PDMS}$), according to **Equation 5.1**:

$$m(IgG/BSA)_{beads} = m(IgG/BSA)_{total} - m(IgG/BSA)_{PDMS}$$ **Equation 5.1**

The mass that adsorbs non-specifically to the PDMS walls was accounted for by flowing the same amount of protein conjugates through (i) a channel packed with beads (*p*) and (ii) a bare channel (*b*) under the same conditions, which allows to rewrite **Equation 5.1** as follows:

$$m(IgG/BSA)_{beads} = \left[m(IgG/BSA)_{IN} - m(IgG/BSA)_{OUT,p}\right] - \left[m(IgG/BSA)_{IN} - m(IgG/BSA)_{OUT,b}\right]$$ **Equation 5.2**

where $m(IgG/BSA)_{OUT,p}$ is the mass of IgG/BSA collected at the outlet of the channel with packed beads (V = 10 µL), $m(IgG/BSA)_{OUT,b}$ is the mass of IgG/BSA collected at the outlet of the bare channel (V = 10 µL), and $m(IgG/BSA)_{IN}$ is the mass of IgG/BSA that is loaded onto the channels. The only term of the mass balance that is *a priori* known is $m(IgG/BSA)_{IN}$, as the solutions of IgG/BSA conjugates at different concentrations were prepared from stock solutions. Taking this into account, initial calibration curves were obtained using increasing concentrations of IgG (Figure 5.5-**A**) and BSA (**Figure 5.5-B**) conjugates, in order to correlate the signal intensity with the conjugate concentration and, subsequently, determine the $m(IgG/BSA)_{OUT}$ in each case.

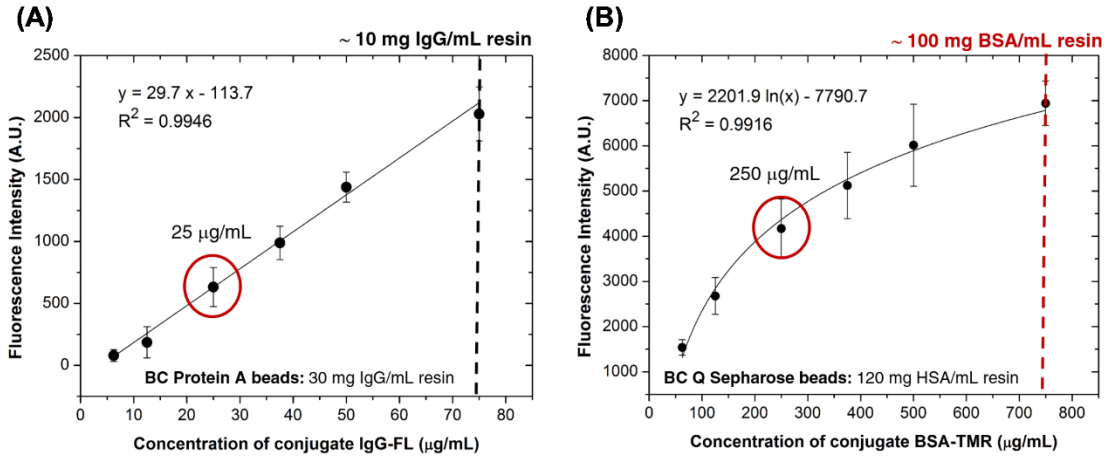

Figure 5.5 – Calibration curves of initial solutions with known concentrations of **(A)** IgG and **(B)** BSA conjugates used for determination of $m(IgG)_{OUT}$ and $m(BSA)_{OUT}$ in the mass balance. Protein A and Q Sepharose beads were packed in microfluidic channels to bind IgG and BSA, respectively, at different concentrations. Maximum binding capacities (BC) for the two ligands are indicated in the plots, according to the information provided by the manufacturer. The concentrations of IgG (25 µg/mL) and BSA (250 µg/mL) used to prepare the artificial mixtures in the optimization studies are highlighted. Dashed lines indicate the concentration of conjugate in solution corresponding to a mass of 10 mg IgG and 100 mg BSA captured per mL of resin.

The calibration curve and the quantification of signal intensity of the outlet solutions were performed using a fluorescence microscope (Olympus CKX41) but the procedure is valid for any other equipment, *e.g.* a fluorimeter device. For the calibration of the fluorescence signal, IgG-BODIPY FL conjugates were used in the following concentrations: 6.25, 2.5, 25, 37.5, 50, 75 μg/mL, whereas BSA-BODIPY TMR conjugates were used in the following concentrations: 62.5, 125, 250, 375, 500, 750 μg/mL.

According to the results in **Figure 5.6**, the mass of IgG and BSA non-specifically bound to the PDMS walls was shown to be negligible, as *p*-values > 0.05 were obtained for all the concentrations under study, meaning that $m(IgG/BSA)_{IN}$ and $m(IgG/BSA)_{OUT,b}$ were not significantly different for all tested concentrations, and so the mass balances were simplified according to **Equation 5.3**.

$$m(IgG/BSA)_{beads} = \left[m(IgG/BSA)_{IN} - m(IgG/BSA)_{OUT,p}\right] \qquad \textbf{Equation 5.3}$$

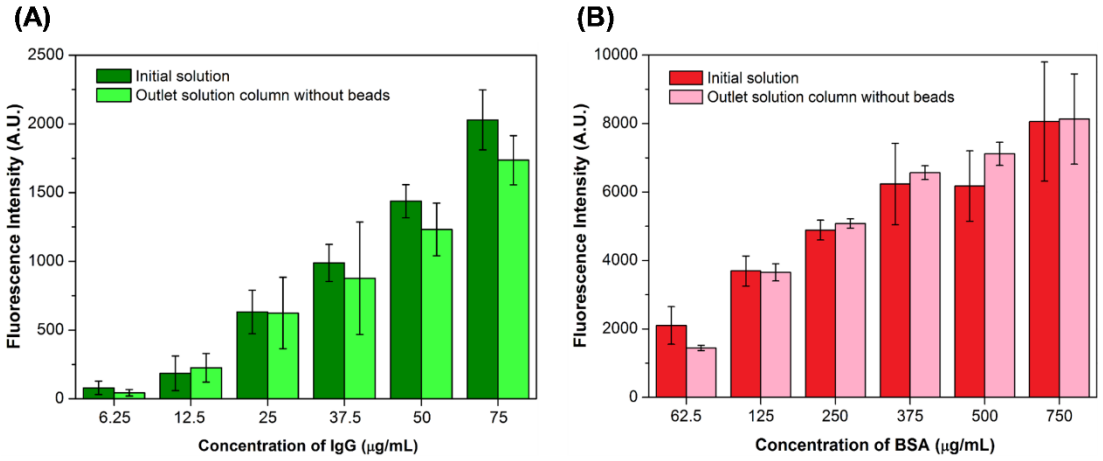

Figure 5.6 – Measurement of **(A)** IgG and **(B)** BSA conjugates non-specifically bound to the PDMS walls for fluorescence assays at increasing concentrations of conjugates in the initial solution and in the outlet solution collected from a microchannel without beads. The error bars in all plots correspond to the standard deviation of three individual measurements. A negligible amount of protein conjugates is non-specifically bound to the PDMS walls, so $m(IgG)_{PDMS}$ and $m(BSA)_{PDMS}$ were not taken into account for the mass balance equations.

Based on these calculations, it was possible to obtain the calibration curves in **Figure 5.7**, in which the intensity of the fluorescence signal is related to the mass of IgG or BSA bound per volume of resin (q_{IgG}/q_{BSA}). The minimum detectable mass values of labeled IgG and BSA were 0.66 ± 0.24 ng/nL$_{resin}$ and 1.86 ± 1.36 ng/nL$_{resin}$, respectively.

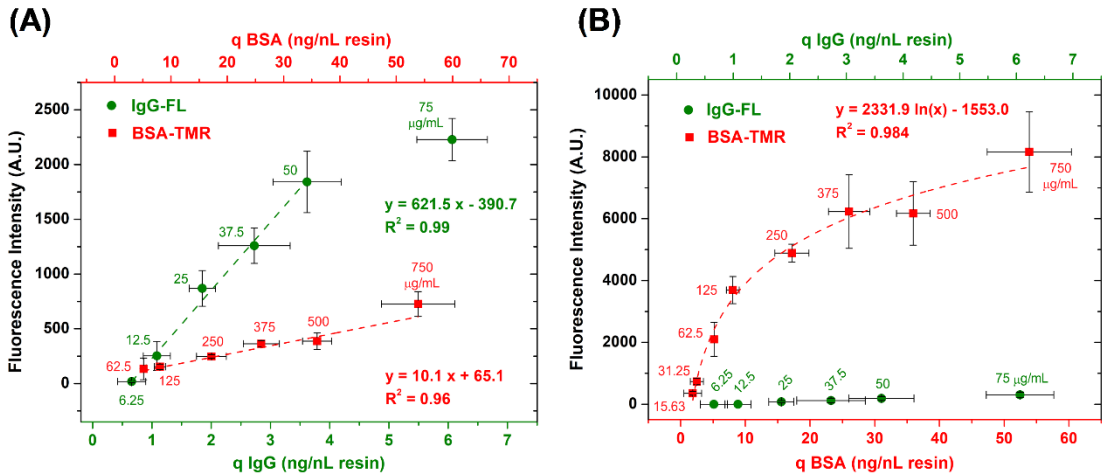

Figure 5.7 – Calibration curves obtained for the fluorescence intensity upon **(A)** blue-excitation and **(B)** green-excitation as a function of the mass of IgG and BSA conjugates bound per volume of chromatography resin inside the microchannel. The minimum detectable mass values of labeled IgG and BSA were 0.66 ± 0.24 ng/nL$_{resin}$ and 1.86 ± 1.36 ng/nL$_{resin}$, respectively.

5.4. Experiments using affinity and single-mode ligands

Preliminary experiments were performed using affinity and single-mode chromatography ligands, namely Protein A (affinity), Carboxymethyl Sepharose (cation exchanger) and Q Sepharose (anion exchanger), whose interactions with IgG and BSA are well described in the literature [34, 167, 168], in order to demonstrate the potential and feasibility of the multiplex structure to screen different chromatographic conditions and to find optimal working windows.

Figure 5.8-A i-iii shows the kinetic profiles for the adsorption of IgG and BSA at pH 5.5, by plotting the mass of protein bound per volume of resin over 150 s. The three chambers were imaged simultaneously during the experiment upon excitation in the blue and green region for quantification of IgG and BSA, respectively (**Figure 5.8-A iv**). The slope (k_{IgG} or k_{BSA}) of the linear fit of experimental data points can be used as a kinetic response parameter to evaluate the capture performance at a given operating condition. The contour plots in **Figure 5.8-B** show the overall performance of the three chromatographic resins under nine operating conditions obtained by combination of three pH values (5.5, 7.5, 9.5) and three conductivities (0, 50, 100 mM NaCl).

For the protein A resin, the results in **Figure 5.8-B i, iv** show that binding of IgG was not significantly affected by the operating conditions, being more favorable at neutral pH values, while binding of BSA was negligible. These results are consistent with what is expected, since protein A is well-known for capturing IgG molecules with high selectivity

and efficiency. In the case of Carboxymethyl Sepharose, proteins bind to the resin mostly by electrostatic interactions with the ligand, so a separation of the proteins in the mixture based on their isoelectric points is expected. In fact, IgG showed a strong interaction at pH values significantly below its isoelectric point (pI = 9) and conductivities between 6-9 mS.cm^{-1}. Higher conductivities preclude binding of this protein, as well as pH values approaching its isoelectric point. On the other hand, binding of BSA (pI = 4.7) was not observed for any of the conditions tested (pH ≥ 5.5).

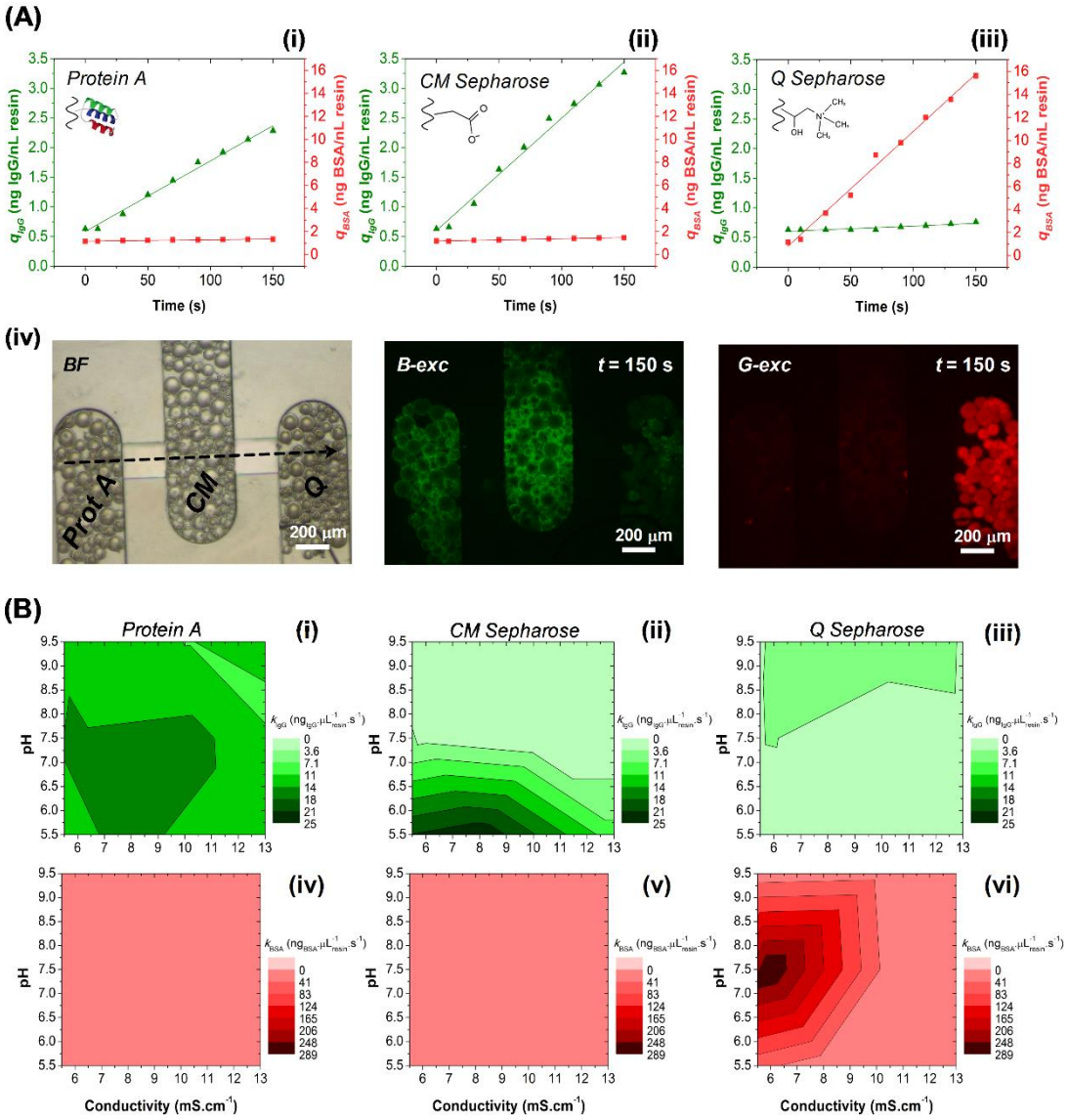

Figure 5.8 – Separation of IgG and BSA using affinity and single-mode electrostatic ligands. **(A)** Kinetic profiles for the adsorption at pH 5.5 in **(i)** Protein A; **(ii)** Carboxymethyl Sepharose; and **(iii)** Q Sepharose resins. Microscopy images **(A-iv)** of the three microchambers imaged in the bright field (BF), and upon excitation in the blue region (B-exc) and in the green region (G-exc). **(B)** Contour plots of the adsorption of IgG **(i-iii)** and BSA **(iv-vi)** on protein A, Carboxymethyl Sepharose and Q Sepharose resins.

The opposite was observed in the case of Q Sepharose, with IgG showing mostly negligible binding in the majority of conditions and BSA showing increasing interaction with the ligand as the pH increases above its pI at conductivities below ~10 $mS.cm^{-1}$. It is interesting to observe that for pH ≥ 7.5, binding of BSA starts to gradually decrease possibly due to the competitive interaction of IgG with the ligand at these conditions. In addition, conductivities higher than 10 $mS.cm^{-1}$ showed a significant negative impact in the binding of BSA, regardless of the pH conditions, due to the screening of electrostatic interactions induced at high NaCl concentrations.

Overall, the results obtained for both IgG and BSA were in good agreement with what would be expected from the molecule and bead properties, indicating that this approach can potentially be used to optimize the separation using intricate multimodal ligands, in which there is an interplay of different functional groups governing the binding of the proteins.

5.5. Multimodal chromatography process development

A purification process for antibodies based on multimodal chromatography was developed at a microfluidic scale using two different microfluidic devices, the multiplexed structure shown in **Figure 5.1**, and a single-column structure previously reported in chapter 4. Optimization studies were divided into capture and polishing studies, according to the schematics in **Figure 5.9**. For each study, a group of three multimodal resins was chosen so that purification could be achieved using two orthogonal chromatographic steps, in which the first step (capture) exploits the interaction of molecules with a negatively charged ligand and the second step (polishing) uses a positively charged ligand to further improve the performance of the separation.

The optimization of the capture step comprised adsorption and elution studies, which were performed in two different microfluidic structures. For the adsorption studies, the multi-chamber microfluidic device was used in order to simultaneously evaluate three multimodal resins, namely Capto™ MMC, MEP Hypercel™ and Toyopearl Sulfate, using an artificial mixture of fluorescently labeled IgG and BSA. The most promising adsorption conditions for each resin were selected based on the ability to maximize binding of IgG, while minimizing binding of BSA to the beads. Since the optimal conditions to fulfil these criteria were different for each resin, it was necessary to individualize the elution studies using single-column microfluidic channels as

represented in **Figure 5.9**. At this point, optimal conditions were selected based on the ability to successfully desorb the IgG from the beads, and avoiding co-elution of any bound BSA.

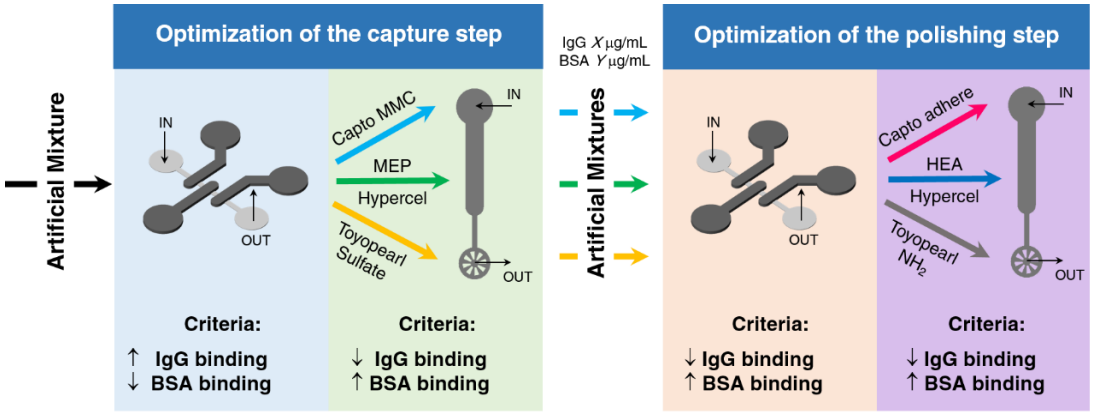

Figure 5.9 – Strategy followed in the optimization studies. Two different microfluidic devices were systematically used to perform the optimization of the capture and polishing steps, depending on the type of analysis required. The panel of three multimodal resins used in each step of the optimization process is also indicated.

The next stage in the optimization process was to evaluate the polishing step, taking into account the recovery yield and purity parameters obtained after the first capture step. Artificial mixtures of IgG and BSA with different compositions, resulting from the most promising conditions evaluated in the previous step (capture), were prepared and flowed through the multi-chamber device packed with three multimodal resins, namely Capto™ adhere, HEA Hypercel™ and Toyopearl NH_2. Optimization studies aimed at defining an operating window for these resins in which binding of BSA was maximized while minimizing interaction of IgG with the ligand. Analogous to the strategy used in the capture step, optimal conditions derived from the screening studies using the multi-chamber device were individually evaluated in single-column microfluidic channels to determine the performance of the polishing step.

The results obtained in each of these steps are presented and discussed in detail in the following subsections.

5.5.1. Capture studies

Figure 5.10 shows the results obtained for the optimization of the capture step. In the adsorption studies (**Figure 5.10-A**), both Capto™ MMC and Toyopearl Sulfate provided similar binding trends for both IgG and BSA. The most relevant differences are related to the extended salt tolerance of Capto™ MMC, which is able to bind IgG and BSA at

conductivities up to 64 mS.cm^{-1}, and the higher binding capacity of Toyopearl Sulfate towards IgG in a range of pH values from 5.0 – 7.0. The results obtained with MEP Hypercel™ showed a poor binding of IgG in the conditions evaluated, although better results were obtained at near-neutral pH values, in accordance with previous reports [169, 170].

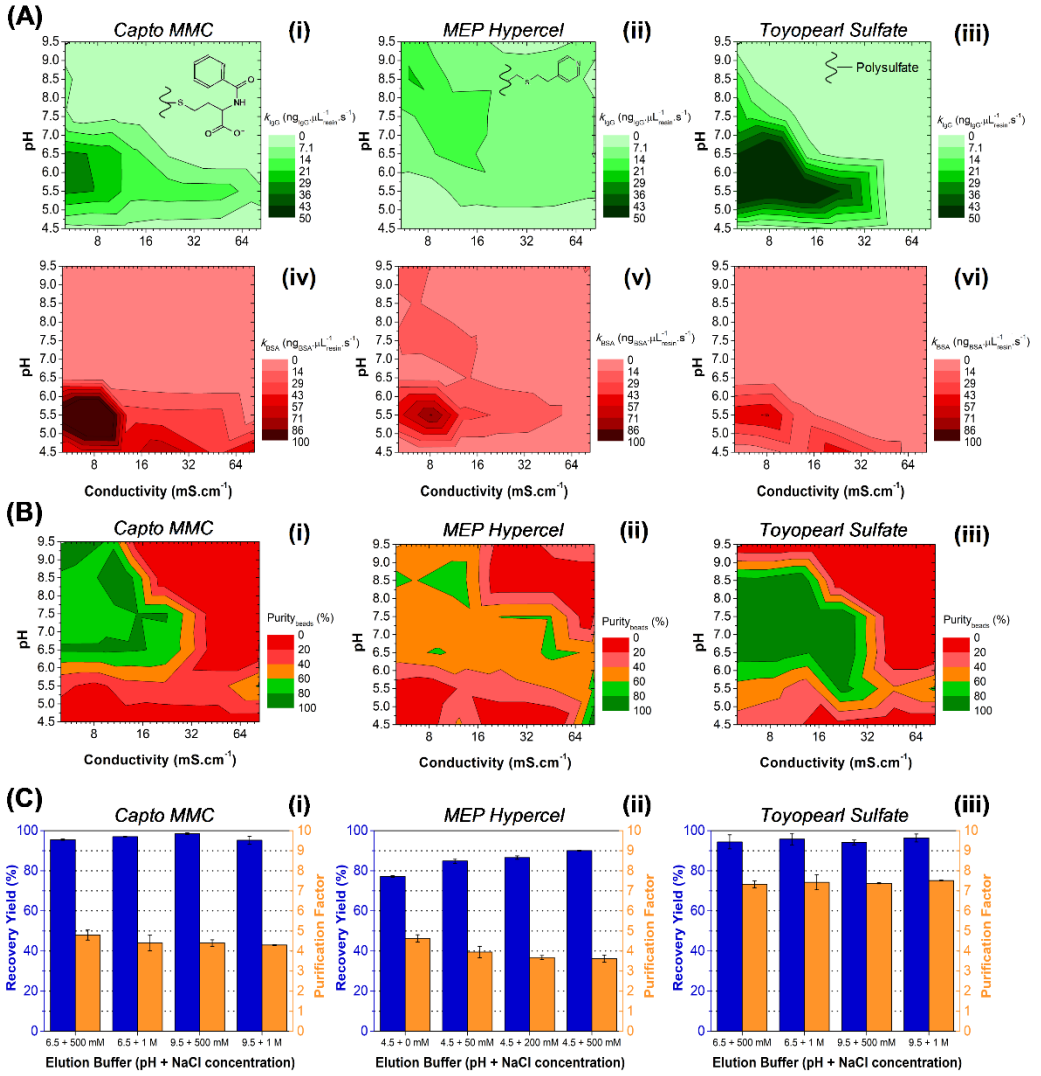

Figure 5.10 – Optimization of the capture step in terms of adsorption and elution of labeled IgG and BSA to the multimodal ligands Capto™ MMC, MEP Hypercel™ and Toyopearl Sulfate. **(A)** Contour plots of the adsorption of IgG **(i-iii)** and BSA **(iv-vi)** on Capto™ MMC, MEP Hypercel™ and Toyopearl Sulfate resins. **(B)** Contour plots of the purity in terms of IgG captured on **(i)** Capto™ MMC, **(ii)** MEP Hypercel™ and **(iii)** Toyopearl Sulfate. IgG purity at bead-level was calculated for each condition according to **Equation 5.4. (C)** Recovery yields and purification factors relative to the total mass adsorbed on the beads, after elution from **(i)** Capto™ MMC, **(ii)** MEP Hypercel™ and **(iii)** Toyopearl Sulfate at different operating conditions. Adsorption conditions were as follows: Capto™ MMC – 50 mM phosphate pH 6.5 + 0 mM NaCl; MEP Hypercel™ – 50 mM Tris pH 8.5 + 50 mM NaCl; Toyopearl Sulfate – 50 mM phosphate pH 6.5 + 50 mM NaCl.

The combination of the binding results for IgG and BSA allowed the calculation of the purity at bead-level for a given operating condition according to **Equation 5.4**, in order to obtain the contour plots shown in **Figure 5.10-B**.

$$Purity_{beads}\ (\%) = \frac{k_{Prot\,1}\left(ng_{Prot\,1}.\mu L_{resin}^{-1}.s^{-1}\right)}{k_{Prot\,1}\left(ng_{Prot\,1}.\mu L_{resin}^{-1}.s^{-1}\right) + k_{Prot\,2}\left(ng_{Prot\,2}.\mu L_{resin}^{-1}.s^{-1}\right)} \times 100 \qquad \textbf{Equation 5.4}$$

Toyopearl Sulfate showed the most promising results in terms of the selective capture of IgG, with values between 80 – 100% being achieved for a relatively broad range of operating conditions (pH 6.0 – 8.5, conductivity up to 32 $mS.cm^{-1}$). Although obtained with model solutions, these results anticipate the ability of this resin to efficiently capture IgG in cell culture supernatants at their native pH and conductivity conditions (pH 6.5-7.0; ~12 $mS.cm^{-1}$).

The purity contour plots combined with the binding kinetics measured for each molecule provided information on potentially efficient and selective elution conditions with which to proceed (*i.e.* minimum binding of IgG and maximum binding of BSA). Thus, for each multimodal resin, four different elution conditions (pH 6.5 and 9.0 with 0 or 500 mM NaCl) were tested under fixed adsorption conditions (Capto™ MMC: 50 mM phosphate pH 6.5 + 0 mM NaCl; MEP Hypercel™: 50 mM Tris pH 8.5 + 50 mM NaCl; Toyopearl Sulfate: 50 mM phosphate pH 6.5 + 50 mM NaCl). The results of the elution studies, relative to the total mass of IgG and BSA adsorbed on the beads, are shown in **Figure 5.10-C**. Overall, the results in terms of yields and purification factors were similar for all resins, which was expected considering that the elution conditions were selected from regions of low adsorption purity (*i.e.* low amount of IgG and high amount of BSA captured on the beads) combined with low binding of IgG. In all cases, it was possible to significantly improve the purity in comparison to the initial purity of the model mixture (~9%), with Toyopearl Sulfate showing the best performance with purification factors above 7. It is interesting to note that purification using multimodal resins normally results in a trade-off between yield and purity [102, 104], as the separation of molecules does not rely on highly specific affinity interactions. This effect was clearly observed using MEP Hypercel™ (**Figure 5.10-C ii**), where increasing recovery yields of the antibody resulted in a progressive reduction in the final purification factor.

5.5.2. Polishing studies

The multiplexed microfluidic device was also used for the optimization of the polishing step. In this case, Capto™ adhere, HEA Hypercel™ and Toyopearl NH_2 resins were packed in each chromatography chamber. Solutions of labeled IgG and BSA were prepared in the four elution buffers evaluated in the capture studies and loaded on the multi-chamber device. **Figure 5.11-A** shows the kinetic results for the binding of IgG and BSA to the three multimodal polishing resins using the elution conditions of the previous capture step for (**i**) Capto™ MMC, (**ii**) MEP Hypercel™ and (**iii**) Toyopearl Sulfate. The goal of this study was to evaluate whether the elution conditions from the capture step were suitable to maximize binding of BSA to the polishing resins, while allowing the IgG to flow through the packed bed. The data shown in **Figure 5.11-A** result from assays on solutions whose compositions of IgG and BSA were fixed in accordance to the respective yield and purity results from **Figure 5.10-C**. Thus, it is important to highlight that the results of the capture step will determine how challenging the subsequent polishing step will be. For example, the amount of BSA that reaches the polishing step after a capture step with Toyopearl Sulfate (**Figure 5.11-A iii**) is much lower than in the other cases, as purities after this capture were the highest obtained. On the other hand, the amount of IgG recovered after the capture on MEP Hypercel™ (**Figure 5.11-A ii**) was the lowest of all cases, since MEP Hypercel™ did not provide a significant binding of IgG in the first place (as clearly showed by the contour plot in **Figure 5.10-A ii**).

Overall, a high selectivity in the binding of the two proteins was rare amongst the conditions and resins evaluated, as most of the conditions studied promoted binding of IgG at an equal or even higher extent than BSA. This observation was particularly evident in the case of Capto™ adhere when performing the loading of the mixture at pH 6.5 and 9.5 with 500 mM or 1 M of NaCl. In these conditions, and considering that the global surface charge of IgG is either the same or opposite to that of the positively charged ligand, the results imply that binding was promoted significantly by hydrophobic interactions, since higher NaCl concentrations in the buffer resulted in higher binding kinetics. These observations are in accordance with previous reports of increasing NaCl concentrations promoting hydrophobic interactions between mAbs and Capto™ adhere [11]. Overall, Toyopearl NH_2 showed the best performance in terms of selectively, binding BSA regardless of the elution conditions in the preceding capture step.

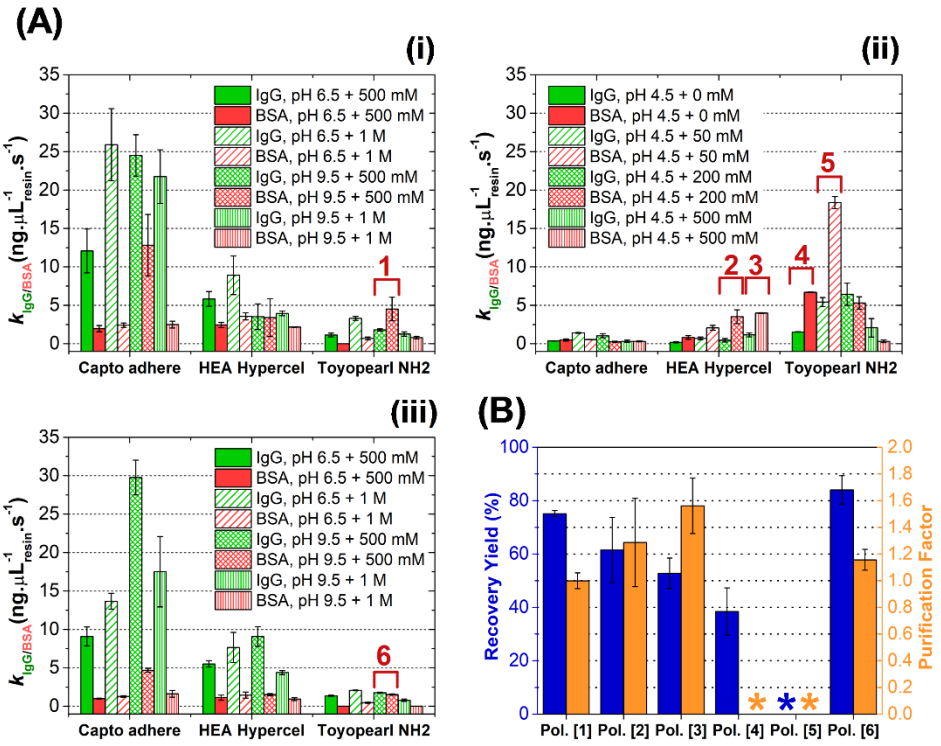

Figure 5.11 – Optimization studies of the polishing step by performing the loading of IgG and BSA solutions directly at the elution conditions used in the capture step. **(A)** Kinetic results for the binding of IgG and BSA to the three multimodal polishing resins at elution conditions after the capture being performed on **(i)** Capto™ MMC, **(ii)** MEP Hypercel™ and **(iii)** Toyopearl Sulfate. **(B)** Recovery yields and purification factors of the polishing step, obtained with selected polishing conditions (highlighted in **A**). Asterisks indicate that yield and purification factor could not be accurately determined due to the fluorescence signals (of IgG and/or BSA) being below the limit of detection of the analytical method.

According to the results obtained in **Figure 5.11-A**, only six conditions were considered promising for the polishing of IgG in flowthrough mode. These conditions (1-6 in **Figure 5.11-A**) were then individually evaluated in single-column microchannels to determine the corresponding yield and purification factor after this step (**Figure 5.11-B**). Compared to the results after the capture step (**Figure 5.10-C**), it is possible to observe that all the polishing conditions led to a decrease in the recovery yield and a slight increase in the purity in some cases, being the most promising result obtained for the polishing performed on Toyopearl NH_2 after capture on Toyopearl Sulfate.

In addition to evaluating the polishing by loading IgG and BSA solutions directly at the elution conditions used in the capture step, an extended study at a wide range of pH and conductivity conditions was also performed (**Figure 5.12-A**). The composition of IgG and BSA used in this study was fixed according to the previously optimized captured step based on Toyopearl Sulfate (Purity = (66.7 ± 1.5) %). The results confirmed that Capto™ adhere shows a high affinity for IgG under a wide range of conductivities, which is

gradually reduced as the pH decreases. HEA Hypercel™ showed very low binding kinetics towards BSA in all tested conditions, while Toyopearl NH_2 demonstrated potential for binding BSA at pH values from 4.5 to 6.5.

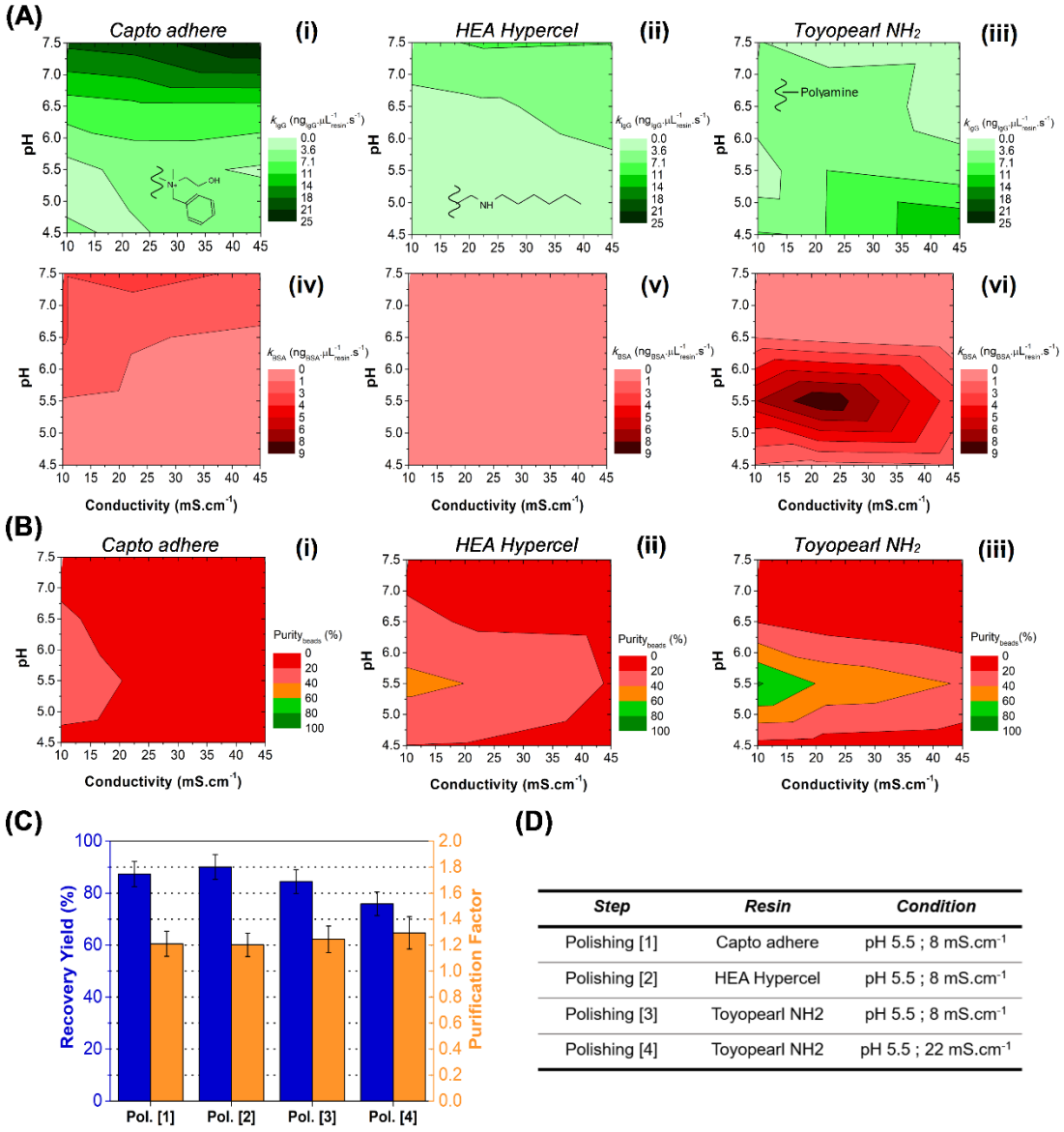

Step	Resin	Condition
Polishing [1]	Capto adhere	pH 5.5 ; 8 mS.cm^{-1}
Polishing [2]	HEA Hypercel	pH 5.5 ; 8 mS.cm^{-1}
Polishing [3]	Toyopearl NH2	pH 5.5 ; 8 mS.cm^{-1}
Polishing [4]	Toyopearl NH2	pH 5.5 ; 22 mS.cm^{-1}

Figure 5.12 – Optimization studies of the polishing step by performing the loading of IgG and BSA solutions after adjusting the elution conditions used in a previously optimized capture step. **(A)** Contour plots of the kinetic results for the binding of IgG **(i-iii)** and BSA **(iv-vi)** on Capto™ adhere, HEA Hypercel™ and Toyopearl NH_2 resins. **(B)** Contour plots of the purity in terms of BSA captured on **(i)** Capto™ adhere, **(ii)** HEA Hypercel™ and **(iii)** Toyopearl NH_2. BSA purity at bead-level was calculated for each condition according to **Equation 5.4**. **(C)** Recovery yields and purification factors obtained with selected polishing conditions, indicated in **(D)**. Purification factors were determined considering the average purity ((66.7 ± 1.5) %) obtained after performing the capture using Toyopearl Sulfate, according to **Figure 5.10-C, iii**.

The BSA purity at bead-level provided by each type of multimodal polishing resin (**Figure 5.12-B**) allowed the identification of potential operating windows to perform the polishing step at conditions that do not necessarily match the optimal elution conditions in the previous capture step. In a real purification scenario, this would require an additional unit operation to buffer exchange the eluate pools from the capture step.

This alternative approach to perform the polishing revealed promising results in terms of obtaining a purification scheme providing purities ranging from 80 – 86% while minimizing the decrease in the recovery yield (**Figure 5.12-C**). Optimal conditions to selectively remove BSA in the polishing step were consistently observed at a pH of 5.5 (**Figure 5.12-D**), significantly below the isoelectric point of the antibody, thus minimizing the amount of IgG that interacts with the positively charged multimodal resins via electrostatic interactions.

5.6. Evaluation of optimized conditions using 1 mL columns

The optimization studies performed in the miniaturized devices allowed to gather a considerable amount of information on promising purification sequences based on the model separation of IgG and BSA. Some of these purification sequences were replicated in conventional chromatography assays with pre-packed or *in-house* packed 1 mL columns using (i) model mixtures of IgG and BSA as performed in microfluidic studies or (ii) a serum-containing cell culture supernatant to validate the microfluidic screening process.

5.6.1. Assays with artificial model mixtures

The purification sequences evaluated using model mixtures and conventional chromatography assays (**Figure 5.13-A**) consisted of sequences in which the polishing was (i) directly performed at the elution conditions of the previous capture step (sequences [A] and [B]) or (ii) after adjusting the conditions following elution in the previous capture step (sequences [C] and [D]). **Figure 5.13-B** shows the recovery yields and purities determined for these purification sequences. The results obtained for the different capture steps were in very good agreement with the values obtained in the microfluidic experiments, namely Capto™ MMC performed the best in terms of recovery yield (macro: (95 ± 3)% *vs* micro: (98 ± 5)%) and the worst in terms of purity (macro: (15 ± 1)% *vs* micro: (40 ± 1)%). The capture performance of Toyopearl Sulfate was also

consistent with that observed in microfluidics, both in terms of trend and magnitude of the recovery yields (macro: (80 ± 1)% and (82 ± 5)% *vs* micro: (94 ± 1)% and (95 ± 2)% for [A] and [C], respectively) and purities (macro: (66 ± 0.3)% and (67 ± 4)% *vs* micro: (66 ± 0.2)% and (67 ± 2)% for [A] and [C], respectively). This consistency in the observed trends between macro and micro-scale had already been observed in the previous chapter, in which the performance of the capture of IgG studied in microfluidic devices was successfully validated in conventional chromatography assays.

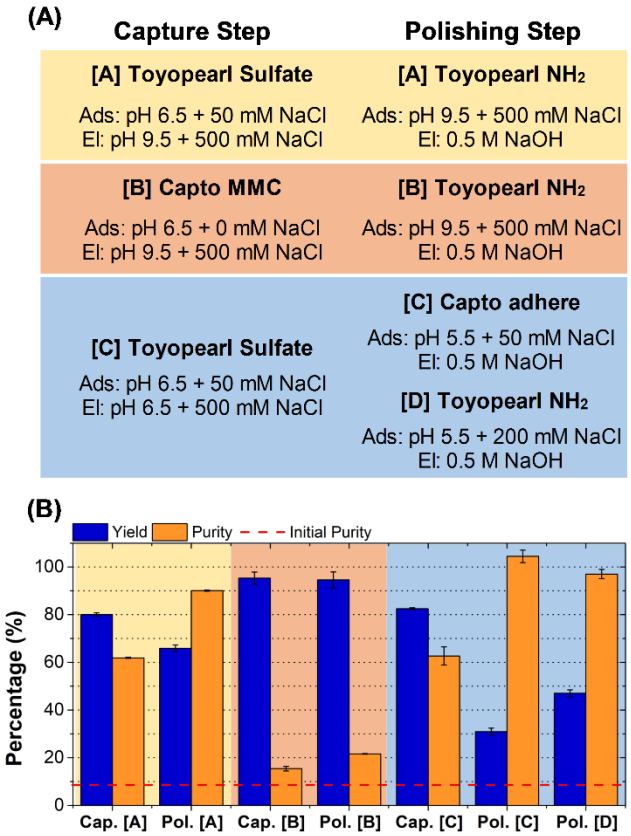

Figure 5.13 – Chromatography purification assays performed with artificial mixtures composed of IgG and BSA. **(A)** Capture + polishing sequences evaluated using standard column (1 mL) chromatography assays. **(B)** Recovery yield and purity parameters determined for each purification sequence.

Regarding the polishing experiments, the performance parameters obtained in macroscale showed significant deviations compared to those obtained in microfluidic experiments. Recovery yields were in general ~20-60% lower in comparison to the microfluidic assays, while purities were ~10-30% higher. This trend was consistent in all the sequences tested, except in sequence [B], which can be attributed to the differences in purity delivered by Capto™ MMC in the primary step. In fact, since Capto™ MMC provided lower purity in the assay performed at macroscale, this implied that a higher concentration (~3.5-fold) of BSA was loaded on the following polishing step, compared to the concentration of BSA

that was used in the corresponding microfluidic experiment. The presence of a higher concentration of BSA may justify the increased recovery yield relative to the microfluidic experiments due to a competitive interaction with the resin binding sites [171].

It is important to note that in the polishing studies the analyzed fraction is the one collected in the flowthrough, meaning a fraction containing molecules that did not interact with the resin, while in microfluidics all the analytical quantification is performed at bead-level. The significant differences identified in the polishing steps are likely related to differences in the residence time and linear velocity between the two approaches (macro: 1 min; ~2.5 $cm.min^{-1}$ *vs* micro: 0.048 s; ~50 $cm.min^{-1}$). As observed in the previous chapter, the optimization of the capture steps in bind-elute mode does not seem to be significantly affected by these differences, however the same may not happen when studying a process in flowthrough mode, where the retention time has a higher impact in the performance. For example, having a wider column and a lower linear velocity would allow IgG molecules to be retained to a larger extent by the resin even at unfavorable conditions for binding due to weaker secondary interactions, compared to the microfluidic assays, which have a significantly higher linear velocity and shear rate. This difference may explain the relative reduction of the recovery yields and relative increase of purities measured at macroscale. Thus, the potential application of this microfluidic screening approach to quantitatively predict the separation in flowthrough-based processes would require the optimization of the residence time using appropriate scaling models, without significantly compromising assay times.

Based on the results shown in **Figure 5.13-B**, it was possible to conclude that the purification sequence [A] based on Toyopearl Sulfate followed by Toyopearl NH_2 was the most promising, providing a purity of (90 ± 0.2) % after the two chromatographic steps. This sequence was then applied to a serum-containing cell culture supernatant.

5.6.2. Assays with a serum-containing cell culture supernatant

The chromatographic profiles shown in **Figure 5.14-A** and **Figure 5.14-B** correspond to the capture and polishing assays, respectively, performed using a serum-containing CHO cell culture supernatant directly at native conditions (no dilutions or adjustments to the pH or conductivity were performed) loaded on a 1 mL chromatographic column. It was possible to conclude that the yield of the capture was similar to the one obtained with the model mixture in the corresponding step, however the purity was, as expected, lower,

which is justified by the higher amount of uncharacterized protein impurities present in this feedstock. Regarding the polishing step, the analytical quantification of the flowthrough pool indicated that there were no significant losses of antibody in this step and, as observed for the capture step, the increase in purity was not as significant as the one obtained using the model mixture due to the high background of uncharacterized proteins.

The SDS-PAGE gel in **Figure 5.14-C** confirms that the cell culture supernatant (lane 1) is highly rich in proteins with a broad range of molecular weights, most of them derived from the serum used to supplement the cell growth. As expected, one of the most abundant impurities is BSA (MW ~ 66 kDa), justifying its selection as model impurity in the artificial mixture. Lanes 2 show that the capture step was effective in removing a high amount of impurities, particularly BSA, as can also be observed by the high flowthrough peak (2) in the corresponding chromatogram. While the gain in purity was not very prominent in the polishing step, some proteins with molecular weight between 50 – 25 kDa were successfully removed.

A final purity of 48% may fall short of the downstream purification standards for the purification of monoclonal antibodies, however the difference between lanes 1 and 4 in the gel is considerable in terms of the impurity clearance achieved in a two-step sequence entirely based on multimodal chromatography, using a highly challenging supernatant without any pretreatment step. As production processes are gradually shifting towards the use of serum-free media [30, 172], it is also expected that multimodal chromatography based sequences could provide enhanced performance when using less demanding feedstocks. Furthermore, complementary studies would be required to optimize the separation of other relevant contaminants, including other proteins or genomic DNA from the host cells. In all these cases, the use of versatile multiplexed microfluidic devices such as the one presented in this work holds great promise to rapidly address different needs in terms of purification processes, at reduced cost and low molecule consumption.

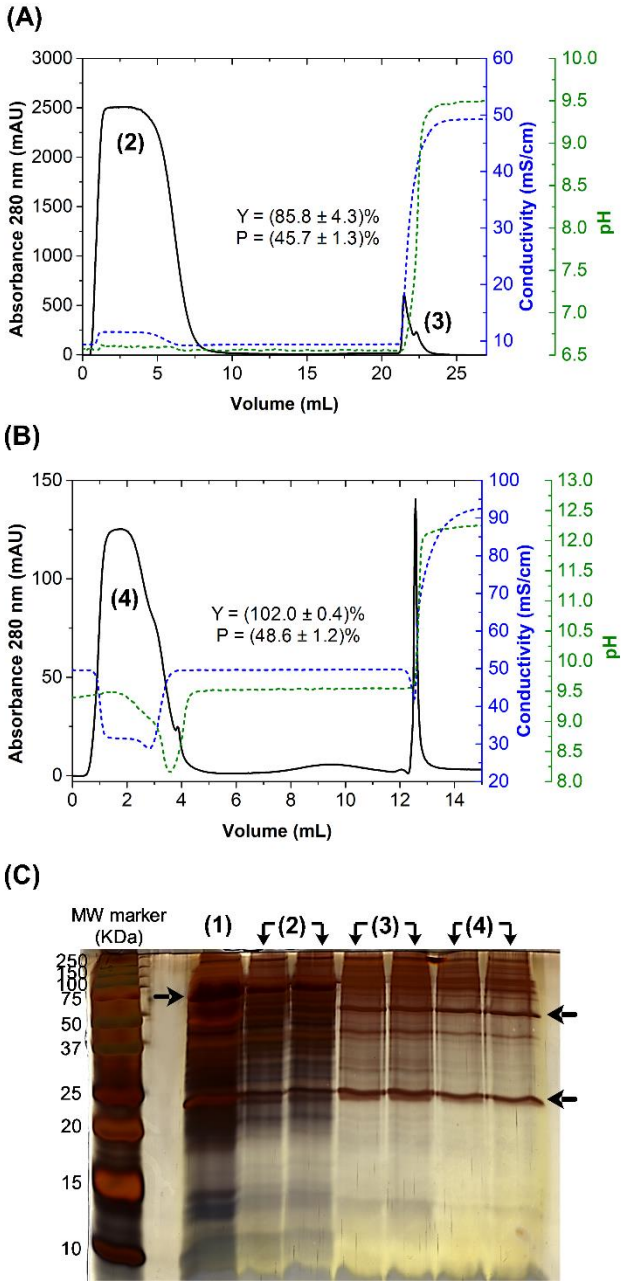

Figure 5.14 – Chromatography purification assays performed using a serum-containing cell culture supernatant. **(A)** Capture step performed with a Toyopearl Sulfate column. Adsorption: pH 6.5 + 50 mM NaCl; Elution: pH 9.5 + 500 mM NaCl. **(B)** Polishing step performed with a Toyopearl NH_2 column. Adsorption: pH 9.5 + 500 mM NaCl; Elution: 0.5 M NaOH. **(C)** Silver stained SDS-PAGE gel in reducing conditions. Lane 1: feedstock; lanes 2: flowthrough fraction collected in the capture; lanes 3: elution fraction collected in the capture; lanes 4: flowthrough fraction collected in the polishing. Duplicates from two independent purification sequences were included in the gel. Arrows indicate the position of BSA (→) and IgG (←) heavy and light chains.

5.7. Summary

This chapter demonstrates that microfluidics can be used as an analytical platform to perform a fast and cost-effective high-throughput screening of multiple chromatography

ligands, while providing quantitative information on capture/elution kinetics of different proteins in solution at low reagent and molecule consumption levels. The concept of multiplexing was introduced to increase the throughput of the screening methodology, compared to the strategy presented in chapter 4, and an analytical method was developed for the quantification of recovery yields and purities under different separation conditions.

The performance results of the microfluidic experiments were consistent with those obtained in conventional chromatography assays performed in bind-elute mode (capture studies). Validation of the polishing studies (flowthrough operation) relative to standard mL-scale column operation proved to be more challenging, as in this case an overestimation of recovery yields was observed, which was attributed to differences in retention time and linear velocity between the two approaches. A dedicated optimization of the flow rate conditions in both approaches would be required for separations in flowthrough mode. Nevertheless, the use of a microfluidic platform (or a standard microwell system) for optimization studies is not expected to exactly reproduce results in larger scales of operation [15, 173], but rather to rapidly provide information on the overall purification strategies that should be attempted and refined in standard chromatography formats.

"Somewhere, something incredible is waiting to be known."

Carl Sagan

Chapter 6

Sequential Liquid Insertion and On-chip Optical Transduction[†‡]

Current developments in the microfluidic technology allow the fabrication of the so-called self-contained systems [128, 174], which are able to perform multiple functions such as fluidic drive and control, sample preparation, purification of biomolecules and on-chip signal detection coupled to data processing. These extended functionalities contribute to the automation and nearly-user independent operation of microfluidic devices, making them particularly attractive for application in clinical or laboratory environments.

On-chip control of fluidic handling through the integration of microvalves and micropumps allows the design of systems that can perform more complex or multiplexed assays without increased user intervention by allowing automation and control. Microvalves and micropumps can be achieved with low Young's Moduli materials, such as polydimethylsiloxane (PDMS), via membrane-based pneumatic [175-177], thermopneumatic [178] or hydraulic actuators [179] fabricated by multilayer soft-lithography [112]. The working principle of these valves is based on the reversible deflection of a PDMS membrane by actuation of a "control channel" to interrupt the liquid flow in a "fluidic channel". These valves have been shown to be extremely effective and leak-proof when applied in fluidic channels with a round cross section [112]. Membrane-based valves can also withstand relatively high back pressures in the fluidic channels, are durable over repeated actuations and are amenable for parallelization.

This chapter contains sections reproduced from the following publications:

[†]I.F. Pinto, D.R. Santos, R.R.G. Soares, M.R. Aires-Barros, V. Chu, A.M. Azevedo, J.P. Conde 2018 "A regenerable microfluidic device with integrated valves and thin-film photodiodes for rapid optimization of chromatography conditions" *Sens Actuators B Chem* **255** 3636-3646.

[‡]I.F. Pinto, D.R. Santos, R.R.G. Soares, M.R. Aires-Barros, V. Chu, A.M. Azevedo, J.P. Conde 2016 "Integration of photosensors in a nano-liter scale chromatography column for the online monitoring of adsorption/desorption kinetics of a fluorophore-labeled monoclonal antibody" *Procedia Engineering* **168** 1426-1429.

In addition to fluidic control, integration of accurate and sensitive modules for signal acquisition and data analysis represents the ultimate step in the development of self-contained microfluidic systems. Optical detection is still the dominant choice over other methods, due to its robustness, high signal-to-noise ratio and high sensitivity [180]. In this context, the incorporation of LEDs and photodiodes, either commercially available [181, 182] or fabricated in-house [183], can be used for on-chip colorimetric [114] or photoluminescent [132, 133] assays. In particular, miniaturized hydrogenated amorphous silicon (a-Si:H) *p-i-n* photodiodes are attractive candidates for integrated optical-to-electrical signal transduction in microfluidic devices, due to their low dark current (~1×10^{-13} A), high sensitivity to visible light, wide range of linear photoresponse, and low temperature processing technology (< 250 °C) [184] that allow a more versatile selection of substrates such as glass or polymers.

The combination of chromatographic techniques with microfluidics has been reported for different purposes, including delivery of small quantities of pure proteins on demand [19], HPLC analysis of metabolites and oligomers [185, 186], proteomic investigations and detection of biomarkers [187], separation of nucleic acids and PCR amplification products [131] and rapid optimization of separation conditions for biopharmaceuticals [126].

In chapters 4 and 5, microfluidic-based approaches combined with fluorescence microscopy measurements were reported, aiming at optimizing multimodal chromatography operating conditions using target proteins (IgG and BSA) in plain buffer solutions. These approaches provided working conditions based on the use of high linear velocities and, consequently, low residence times (>200-fold difference from standard chromatography), in order to dramatically reduce mass transport limitations within the micro-columns and obtain a rapid output of results based on different kinetic profiles.

This chapter describes further improvements to the previous microfluidic devices, namely by integrating sequential liquid insertion and on-chip signal transduction towards a regenerable chromatography-on-chip device. Screening of chromatographic conditions were performed directly using a cell culture supernatant spiked with fluorophore-labeled antibody molecules. Sequential liquid flow was achieved by integrating pneumatically-actuated valves and chromatography cycles – comprising equilibration, adsorption, elution and regeneration – were repeatedly performed in the same device with high robustness and reproducibility. Furthermore, binding and elution kinetic profiles were

monitored in real-time by coupling the device with a-Si:H *p-i-n* photodiodes for on-chip signal acquisition, showing results comparable to detection using a microscope or conventional chromatography equipment.

6.1. Experimental section

6.1.1. Buffer solutions

Acetate buffer (50 mM) at pH 5.5 and 6.5 was prepared using sodium acetate from Merck (Darmstadt, Germany) and acetic acid 100% (AnalaR Normapur) from VWR BDH Prolabo (Radnor, PA, USA). Phosphate buffer (50 mM) at pH 7.5 was prepared using dipotassium phosphate and potassium dihydrogen phosphate from Panreac Quimica Sau (Barcelona, Spain). Tris buffer (50 mM) at pH 8.5 was prepared using Tris-(hydroxymethyl)aminomethane from Sigma-Aldrich (St. Louis, MO, USA). Carbonate buffer (50 mM) at pH 9.5 was prepared using sodium carbonate and sodium bicarbonate also from Sigma-Aldrich. All other chemicals used in buffer preparation were of analytical grade. Water used in all experiments was from a Milli-Q purification system (Millipore, Bedford, MA, USA).

6.1.2. Production and processing of monoclonal antibodies

Chinese hamster ovary cells (CHO DP-12 clone#1934, ATCC CRL-12445), containing a dihydrofolate reductase (DHFR) expression system, were grown in a serum-free medium, ProCHO™ 5 (Lonza Group Ltd Belgium) in order to produce anti-interleukin 8 (anti-IL8) monoclonal antibodies with an isoelectric point (pI) of 9 at a concentration of ~50 mg/L, according to the proceeding described in section 4.1.2.

Cell culture supernatants containing the target mAb were purified by protein A affinity chromatography using an ÄKTA™ Purifier system from GE Healthcare (Uppsala, Sweden). The supernatant depleted in antibody was collected in the flowthrough fractions, while the purified antibody was recovered in the elution fractions. The elution pool (volume 22.5 mL) was concentrated (90×) and diafiltered in PBS (Sigma-Aldrich) using Amicon Ultra-15 centrifugal filter units (MWCO of 50 kDa) from Merck Millipore, for 15 min at 5000 *g* in a fixed angle rotor centrifuge. The mAb solution was further concentrated (~5.7×) in 0.1 M sodium bicarbonate buffer, using Amicon Ultra-0.5 centrifugal filter units (MWCO of 10 kDa) also from Merck Millipore, for 7 min at

14000 *g*, to a final concentration of 15.5 mg/mL. The anti-IL8 mAbs were then conjugated to the amine-reactive dye Alexa Fluor® 430 (A430) – excitation 430 nm, emission 545 nm – NHS ester, obtained from Thermo Fisher Scientific. The fluorescent conjugate mAb-A430 was spiked in the mAb-depleted cell culture supernatant at a concentration of 50 μg/mL and used in the microfluidic experiments.

6.1.3. Liquid handling and valve manipulation

Agarose beads functionalized with a multimodal chromatography ligand (Capto™ MMC) were purchased from GE Healthcare as a slurry in 20% ethanol. The procedure for bead preparation and packing in the micro-columns is described in detail in chapter 3, section 3.4. Briefly, the beads were suspended in a polyethylene glycol 8000 (PEG) solution and flowed through the micro-column by applying a negative pressure at the outlet, using a syringe pump (NE-1002X, New Era Pump System, Inc., NY, USA). The entrance of the column was then sealed with a steel plug and the packed beads were washed by flowing equilibration buffer in the fluidic channels connected to the main column (fabrication process is described in detail in chapter 3, section 3.2). To perform the chromatography cycles, all solutions were flowed towards the micro-column by pulling the liquid from the outlet at 10 μL/min. The use of a negative pressure to continuously drive the liquid flow greatly simplifies the operation of the device in this case, since it is not necessary to have multiple tubing for the different solutions and replace them each time the solutions need to be changed. Instead, the liquids are handled using only ubiquitous and easily handled/discarded pipette tips.

Control channels were filled with DI water using capillary tubing (BTPE-90) from Instech Solomon (PA, USA) connected to compressed air lines and subjected to a pressure of 100 kPa. According to Fernandes *et al.* [188], the actuation of pneumatic channels previously filled with water prevents the generation and diffusion of air bubbles to the fluidic channels and, subsequently, to the micro-column packed with beads. The pneumatic valves were switched *on* or *off* via solenoid valves connected to compressed air that were controlled through a printed circuit board (PCB) supplied by a 24 V power source [188].

Adsorption and elution studies, in which different buffer conditions were sequentially screened by actuating the pneumatic valves, were performed as follows: (i) flow of the equilibration buffer for 40 s, (ii) flow of the pH-adjusted supernatant spiked with the

mAb-A430 at a concentration of 50 μg/mL for 100 s, (iii) flow of the elution buffer for 40 s, and (iv) flow of the regeneration solution (1 M NaOH) for 20 s. The regeneration of the chromatography column during this study was performed between 20-30 times in a single microfluidic device, without detriment to the results. In the adsorption cycles, the equilibration and adsorption conditions were varied (pH 5.5, 6.5 and 7.5), while the elution was systematically performed using pH 9.5 in the absence of NaCl. On the other hand, in the elution cycles the adsorption was systematically performed using pH 5.5, while different pH and conductivities were tested as elution buffers, namely pH 7.5, 8.5 and 9.5 in the absence and presence of NaCl (1 M).

The adsorption and elution experimental curves were fitted using a non-linear function based on a sigmoidal model (see **Equation 4.2** in section **4.3.2**), and the response parameters to evaluate the adsorption (K_{ads}) and elution (K_{el}) kinetics were calculated using **Equation 4.3**.

6.1.4. Fluorescence monitoring and analysis

Monitoring of the fluorescence emission from the beads during adsorption/elution assays was continuously performed using (i) an inverted fluorescence microscope and (ii) amorphous silicon *p-i-n* photodiodes.

Microscopy-based measurements were performed using an Olympus CKX41 inverted fluorescence microscope coupled to a CCD color camera (Olympus XC30) and equipped with a filter cube with a band-pass excitation of 460-490 nm and a long-pass emission of 520 nm. Fluorescence emission of the packed beads was recorded at a frame rate of 2 f/s, 5× gain and 100× total magnification during the different stages of the chromatographic cycles. Images were analyzed using ImageJ software (National Institutes of Health, USA) and fluorescence was quantified by averaging the entire end-section of the micro-column, as previously described in section 4.3.1. Microfluidic experiments comprising the adsorption chromatography cycles were performed in duplicate.

Optical acquisition using a-Si:H *p-i-n* photodiodes was performed using low noise coaxial and triaxial connections to a Keithley 237 picoammeter and a computer graphical user interface for real-time monitoring of the current generated by the photosensor. The photodiodes were addressed at 0 V bias and experimental data points were acquired with an interval of 1.25 s. The measurements were performed initially in the dark, to monitor the dark current of the photosensor, and then under illumination for the fluorescence

detection of Alexa Fluor® 430. A semiconductor 405 nm laser was used as excitation light source, impinging on the micro-column with a spot size of approximately 1 mm in diameter and a photon flux of 1.08×10^{15} $cm^{-2}.s^{-1}$. The laser light reached the photosensor at normal incidence after passing through a 2.0 neutral density filter for 100-fold attenuation of light intensity.

6.1.5. Standard column chromatography assays

Column chromatography assays were performed using a pre-packed (1 mL) HiTrap Capto™ MMC column (GE Healthcare) in an ÄKTA™ Purifier System. The cell culture supernatant containing the target mAb was loaded at a flow rate of 1 mL/min using a 5 mL injection loop. Equilibration was performed with 50 mM acetate buffer pH 5.5 and elution was performed with 50 mM carbonate buffer pH 9.5 with 0 M or 1 M NaCl addition. UV absorbance at 280 nm, conductivity and pH of the outlet stream were continuously monitored. Flowthrough and eluate fractions were collected and further analyzed with respect to antibody concentration.

6.1.6. Post-chromatography antibody and total protein quantification

The concentration of IgG in the flowthrough and elution fractions collected during the standard chromatography (non-microfluidic) experiments was determined by analytical protein A chromatography using a POROS PA ImmunoDetection sensor-cartridge (Applied Biosystems) [155]. Recovery yields were then calculated by dividing the mass of IgG in the elution fractions by the mass of IgG in the initial cell culture supernatant feedstock and the trends were compared with the microfluidic results.

Total protein content in the collected fractions was determined by the Bradford method using a Coomassie assay reagent and bovine gamma globulin (BGG) standard ampules (2 mg/mL) from Pierce (Rockford, IL, USA). Samples were diluted five times in phosphate buffer and analyzed in a 96-well plate by measuring the absorbance at 595 nm using a microplate reader from Molecular Devices (Sunnyvale, CA, USA). The absorbance signal for each sample was corrected considering the contribution of blank samples containing the same buffer composition. Purity was calculated by the ratio between the IgG concentration determined by analytical protein A chromatography and the total protein concentration derived from the Bradford method.

6.1.7. Protein gel electrophoresis

Sodium dodecyl sulfate-polyacrylamide gel electrophoresis (SDS-PAGE) was performed using a 12% acrylamide gel, prepared from a 40% acrylamide/bisacrylamide stock solution (29:1) from Bio-Rad (Hercules, CA, USA), and ran at 90 mV using a running buffer containing 192 mM glycine, 25 mM Tris-HCl and 0.1% SDS at pH 8.3. Before being loaded in the gel, protein samples were diluted in a buffer containing 62.5 mM Tris-HCl, pH 6.2, 2% SDS, 0.01% bromophenol blue and 10% glycerol, and denatured in reducing conditions (100 mM dithiothreitol from Sigma-Aldrich) at 100°C for 5 minutes. Gels were stained with silver nitrate according to the protocol described in [165] and imaged using a GS-800 calibrated densitometer from Bio-Rad.

6.2. Sequential liquid flow in the microfluidic device

The microfluidic structures were designed to allow an integrated and automated screening of operating conditions for chromatographic processes. The devices included a micro-column for packing of beads and four individually-addressable fluidic channels connected to the main column (**Figure 6.1-A**). In order to have a sequential liquid flow of different solutions in an automated setup, pneumatically-actuated valves were integrated in the PDMS device, fabricated beneath the fluidic channels each at single intersection regions of 500 × 700 μm.

Chromatography beads (average size 75 μm) functionalized with a multimodal ligand (Capto™ MMC, GE Healthcare) were packed in the micro-column and efficient trapping was achieved by the difference in height of the two channels composing the micro-column. Similarly to the fabrication strategy described in chapter 3, a taller channel (100 μm) arrested the beads in place creating a packed bed, while a shallower channel (30 μm) prevented the movement of the beads downstream during the chromatographic assay. After the packing step, the entrance of the micro-column was closed with a steel plug and the flow of different solutions towards the micro-column was initiated by actuation of the pneumatic valves. The working principle of the pneumatic valves is based on the deflection of a PDMS membrane beneath the fluidic channels, caused by the injection of compressed air in water-filled control channels. It is important to highlight that the fluidic channels need to be fabricated with a round cross-section, in order to ensure their complete closure by the valves. **Figure 6.1-B** shows the selective flow of a

single solution contained inside a pipette tip towards the micro-column, achieved by applying a constant negative pressure at the outlet of the micro-column, while the valves of the other three channels remained closed. It is clear from **Figure 6.1-B** that while the valves are closed the fluidic channels are fully interrupted and there is no mixing of the different solutions in the micro-column. Furthermore, the response times of the pneumatic valves are virtually instantaneous (<0.5 s), which allows a high degree of control of flow times and volumes during the process.

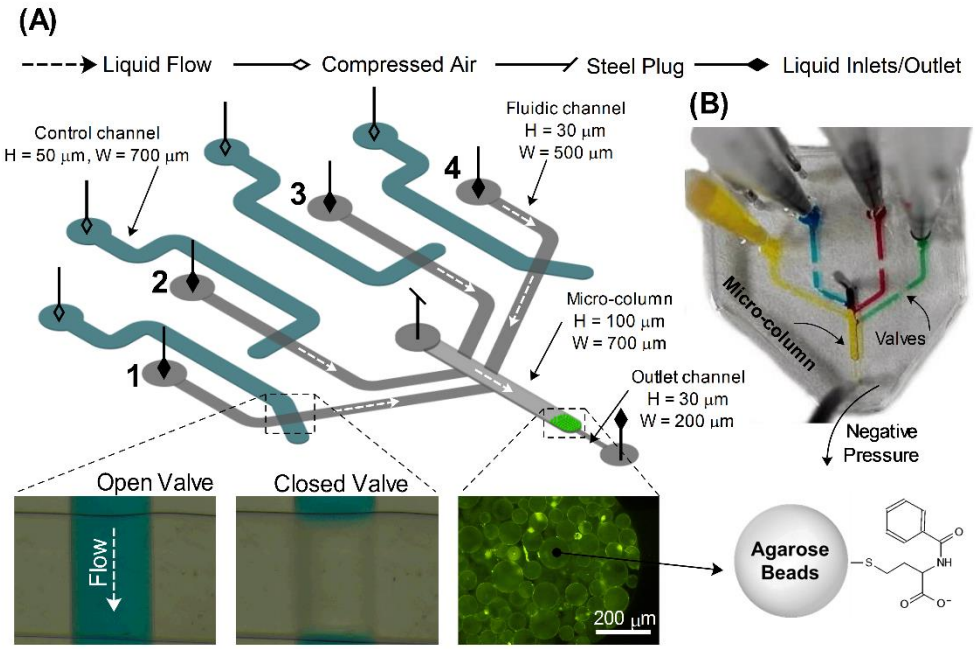

Figure 6.1 - Regenerable microfluidic structure comprising a main channel for bead packing and four fluidic channels for sequential liquid insertion controlled by integrated pneumatic valves. **(A)** Agarose beads functionalized with a chromatography multimodal ligand (Capto™ MMC) were packed in a micro-column and evaluated in their ability to capture a target mAb labeled with Alexa 430 from a cell culture supernatant. Different solutions were flowed sequentially in an automatic manner by actuating the pneumatic valves. **(B)** PDMS structure showing the selective flow of four different colored solutions towards the micro-column. Liquid was flowed using pipette tips in the inlets and by applying a negative pressure at the outlet.

This approach allowed to significantly speed up the screening of chromatography operating conditions through the miniaturization of a conventional mL-scale chromatographic cycle. The sequence at which the different solution were flowed comprised (1) equilibration of the beads with an appropriate buffer; (2) flow of a cell culture supernatant spiked with a fluorophore-labeled mAb; (3) flow of the elution buffer; and, finally, (4) regeneration of the beads with a 1 M NaOH solution. The complete regeneration of the micro-column represents a very important step in this process, as it allowed the reuse of the same microfluidic device, with the same packing bed, over

repeated cycles. In fact, the integration of a regeneration step greatly reduces assay variability, particularly in comparison to experiments performed using different micro-columns each time with variable packings. Moreover, having a regenerable microfluidic device is an added value in terms of cost-effectiveness, versatility and, especially, when considering process scalability and assay parallelization.

6.3. Fluorescence detection using a-Si:H *p-i-n* photodiodes

The next step towards the development of a stand-alone and automated microfluidic device for rapid screening of chromatography conditions was the integration of an optical signal transduction module to perform the fluorescence measurements. The use of a-Si:H thin-film *p-i-n* photodiodes (**Figure 6.2-A**) for this application was motivated by their high efficiency in the visible spectrum, thus providing high sensitivity for fluorescence measurements. In addition, the photocurrent at low intensity light levels is extremely stable over time (coefficient of variation = 0.97%). Furthermore, the photodiodes can be operated at zero bias voltage, which is an advantage in terms of simplifying future discrete electronics designs to address the device.

Considering that the average diameter of the chromatography beads is around 75 μm, the size of a single photodiode (200 × 200 μm) was adequate to provide an average signal to monitor the increase/decrease of fluorescence at different stages of the chromatography cycles. The validity of this approach is supported by the homogeneous distribution of fluorescence along the micro-column, as previously demonstrated in chapter 4 (**Figure 4.4**), resulting in the current generated by the photosensor being proportional to the fluorescence emitted by the beads.

The photographs in **Figure 6.2-B** show the alignment of the microfluidic structure with the packed beads on top of the photodiodes and the spot of the laser impinging on the end-part of the micro-column. In order to accurately measure the emitted light, the a-SiC:H absorption filter was integrated between the micro-column and the photodiodes in order to prevent the 405 nm excitation light from generating a considerable background of non-specific photocurrent.

The plot in **Figure 6.2-B** shows the transmission spectra of the thin-film a-SiC:H high-pass absorption filter, deposited on a glass substrate, measured in four different regions separated by 0.5 mm. The superimposition of the curves obtained in the different measurements suggests that the filter absorption properties are homogeneous over the

entire area covering the photodiode. The transmission of the filter was measured using a spectrophotometer (PerkinElmer Lambda 950) in the wavelength range of 300-800 nm. Observing **Figure 6.2-B** it is possible to conclude that the a-SiC:H filter is capable of suppressing the excitation light (λ_{ex} = 405 nm) by at least five orders of magnitude relative to the emission light emitted by the Alexa 430 label (λ_{em} = 539 nm).

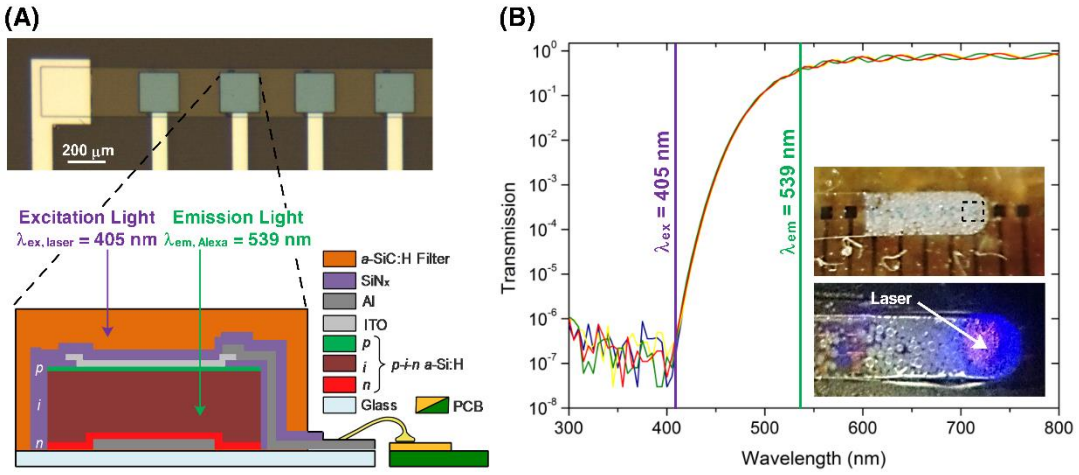

Figure 6.2 – Fluorescence detection using photodiodes. **(A)** Micrograph and cross-sectional schematic view of the a-Si:H *p-i-n* photodiodes used in fluorescence measurements. The excitation light is filtered by an a-SiC:H thin-film (1.6 µm thick) deposited on top of the SiN_x passivation layer. The emission light enters the photodiode through an Indium Tin Oxide (ITO) transparent contact. **(B)** Transmission spectral characteristics of the a-SiC:H filter deposited on a glass substrate and alignment of the micro-column with packed beads on top of the photodiode array. The active photodiode used for data acquisition is highlighted. The different curves correspond to transmission measurements performed in different parts of the absorption filter.

6.4. Antibody capture from cell culture supernatants using single-channel microfluidic columns

The capture of monoclonal antibodies directly from CHO cell culture supernatants was firstly evaluated using single-channel microfluidic columns comprising a single inlet and outlet. In chapter 4, it was shown that a microfluidic approach based on real-time fluorescence measurements at bead-level could be successfully used for analyzing adsorption and elution kinetics of mAb-ligand interactions in plain buffer solutions. However, to be useful for real applications, this microfluidic approach needs to be able to work also in complex matrices (*e.g.* real cell culture supernatants), which include high titers of different biomolecules such as proteins, lipids and nucleic acids.

Figure 6.3 shows the kinetic profiles and the response parameters for adsorption **(A)** and elution **(B)** studies performed using a pH-adjusted serum-free cell culture supernatant

spiked with the fluorescent conjugate anti-IL8-Alexa 430 at a concentration of 50 μg/mL. Similarly to what was previously observed in buffer solutions, binding of the antibody to the multimodal beads increases as the pH decreases to 5.5. Interestingly, at pH 4.5 this tendency was inverted as binding of the mAb became less effective than at pH 5.5, which suggests that binding capacity reaches an optimum at around pH 5.5 and then decreases when the pH is further decreased. A similar observation has been reported by Kaleas *et al.* [97] when using different non-purified feedstocks containing basic monoclonal antibodies and the same multimodal chromatography resin. This decrease in biding efficiency for more acidic pH values is probably related to the increased protonation of the carboxylic acid group of the ligand (pKa of aliphatic and aromatic carboxylic acids falls in the range between 4 and 5) [189] and, consequently, to the decreased number of charged groups. Another possible explanation for this behavior is the fact that as the pH of the supernatant decreases below 5.5, the host cell proteins contained in the feedstock (mostly acidic [190]) become positively charged and compete with the mAb for binding sites. Alternatively, the operation at low pH values may affect the integrity of the antibody molecules, by inducing aggregation/precipitation or by altering their native conformation, thus negatively impacting binding to the beads [191]. Considering these results, elution studies were subsequently performed after accomplishing adsorption at pH 5.5.

The elution screening strategy (**Figure 6.3-B**) was based on the successive increase in the pH at constant conductivity, based on previous evidence that binding of mAbs to Capto™ MMC occurs primarily through electrostatic interactions [97, 192]. The results showed very similar behaviors obtained at pH 7.5, 8.5 and 9.5, although a more efficient elution is clearly observed at pH 9.5, which is above the antibody isoelectric point. Comparing these results with those obtained using plain buffer solutions (chapter 4), the major difference that can be identified is related to the velocity at which the fluorescence decreases and a plateau is reached. In fact, the elution kinetics were considerably slower when a cell culture supernatant was used, taking approximately 20 seconds for the fluorescence values to stabilize in all the conditions, while in model buffer solutions, a plateau was reached 5 seconds after the beginning of the elution. The flow of a complex feedstock can make the elution of mAbs more challenging, due to the presence of adsorbed impurities that can create a buffering effect, thus hindering the increase in pH and consequently reducing the elution kinetics of the antibody. Another aspect to take into account when using complex feedstocks is the possibility of non-specific binding of

the antibody due to electrostatic interaction with non-eluted impurities, which can preclude a fast and effective elution of the target mAb in the absence of salt.

Although the kinetic response parameters for the elution at pH 7.5, 8.5 and 9.5 are fairly similar, it is still possible to differentiate the performance of the elution at these conditions by considering the antibody recovery yield after 40 s. While a complete recovery of antibody is achieved at pH 9.5, a yield of 85% and 83% was obtained for elution at pH 7.5 and 8.5, respectively. The similar recovery yields obtained for both pH 7.5 and 8.5 may be due to the lower conductivity of Tris buffer at pH 8.5 relative to phosphate buffer at pH 7.5, since it was expected that higher recoveries can be achieved by increasing the pH value. This observation further reinforces the necessity of using high ionic strengths in the elution when cell culture supernatants are used, as reported in the literature [97] for the operation with this multimodal ligand. This subject will be further addressed ahead in this chapter.

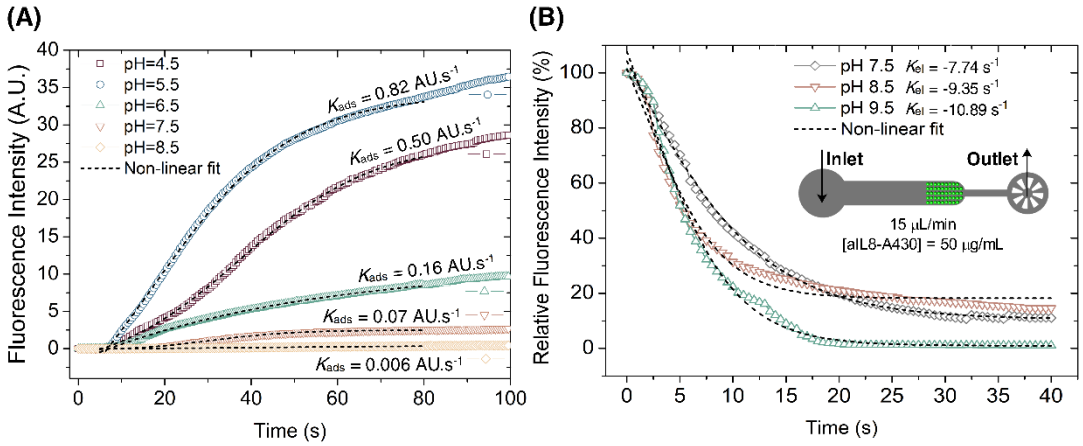

Figure 6.3 – Experiments using single-channel microfluidic columns. **(A)** Adsorption kinetic curves obtained by continuously monitoring the fluorescence emission of packed beads upon flowing a cell culture supernatant with a fluorophore labeled antibody (50 µg/mL of anti-IL8-Alexa430; pI = 9) at different pH values. **(B)** Elution kinetic curves obtained by flowing elution buffers at different pH values after adsorption at pH 5.5. The fluorescence intensity was normalized to the maximum fluorescence value (t = 0) for each pH condition. Curves were fitted using a non-linear function based on a sigmoidal model in order to derive kinetic response parameters (K_{ads} and K_{el}). Experiments were performed using a single-channel microfluidic column and fluorescence was monitored using a microscope. A flow rate of 15 µL/min was used.

6.5. Chromatography cycles monitored using fluorescence microscopy

The signal acquisition of the chromatography cycles using the structure with integrated pneumatic valves was first performed by fluorescence microscopy. The studies were divided into (i) adsorption studies, in which the elution was fixed and only the equilibration and adsorption solutions were changed, and (ii) elution studies, in which equilibration and adsorption conditions were fixed and only the elution solution was changed.

Figure 6.4-A shows adsorption cycles performed at three different conditions, namely pH 5.5, 6.5 and 7.5. Elution was performed with a fixed pH of 9.5. The difference observed in the extent of elution is related to the different maximum fluorescence intensities achieved for different adsorption conditions. It is possible to see that regeneration of the beads is successfully accomplished in a few seconds by flowing a concentrated NaOH solution (1 M). The residual fluorescence is completely removed from the beads in the end of each cycle, which ensures that the subsequent cycles are always initiated from the same baseline. Thus, regeneration of the micro-column revealed to be effective in ensuring reproducible results for each condition under analysis. In addition, the adsorption kinetic profiles obtained using this regenerable device were in good agreement with those discussed in section 6.4, showing decreased binding of the mAb-Alexa 430 conjugate as the pH increased.

In the elution studies (**Figure 6.4-B**) the impact of increasing pH (7.5, 8.5 and 9.5) and salt concentration (1 M NaCl) was evaluated in terms of the recovery yield of antibody, after performing the adsorption at pH 5.5. As expected, according to the results obtained using single-channel microfluidic columns, the elution of the antibody is more effective as the pH increases and crosses the isoelectric point of the mAb, with all the obtained yields being above 85%. Interestingly, the addition of NaCl in the elution buffer allowed the increase of the recovery yields to more than 96%, regardless of the pH value. In particular, it was possible to recover 99.5% of the captured antibody using an elution buffer at pH 9.5 containing 1 M NaCl. This result is in line with several references that report the elution from Capto™ MMC as a multimodal procedure [67, 68], typically requiring an increase in both pH and conductivity to promote antibody detachment from the beads.

Although a different flow rate was used in the experiments using single-channel microfluidic columns (15 µL/min) and the valve-integrated device (10 µL/min), the overall trend for the performance of the elution was maintained in both approaches. The use of a lower flow rate to operate the structure with pneumatic valves allowed the prevention of spontaneous air bubble formation in the micro-column, more prone to occur upon application of a higher negative pressure to drive the liquid flow in this design configuration.

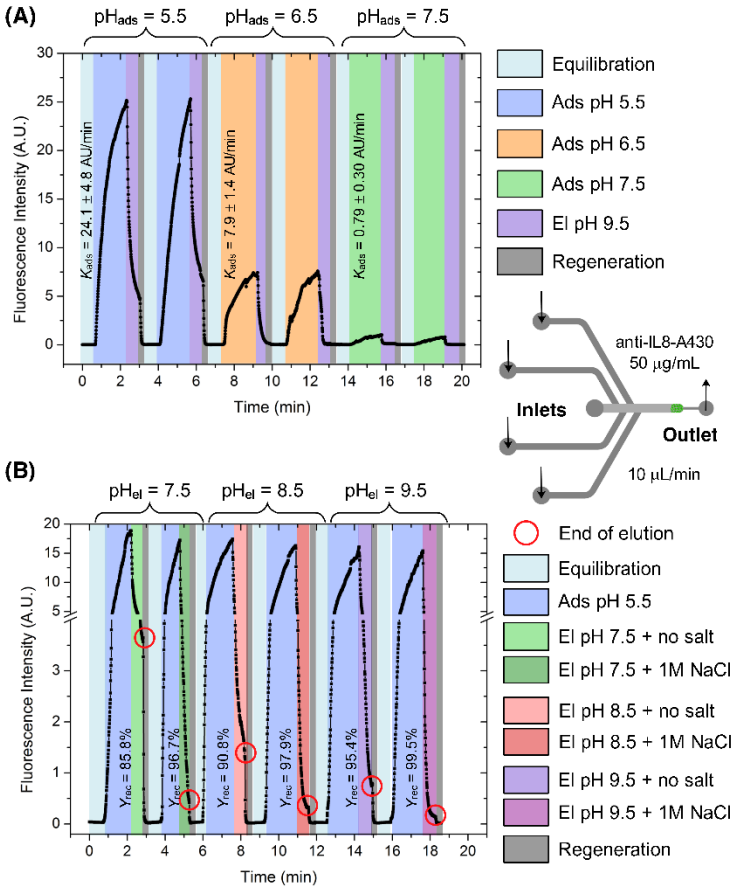

Figure 6.4 – Chromatographic cycles obtained using a microfluidic structure with integrated pneumatic valves. A pH-adjusted cell culture supernatant (50 µg/mL of anti-IL8-Alexa430) was flowed to evaluate the mAb-ligand interaction over different adsorption **(A)** and elution conditions **(B)**. Fluorescence of packed beads was continuously monitored using a microscope. In the end of each cycle, regeneration of beads was accomplished by flowing a solution of 1 M NaOH. The red circles highlight the end of the elution and beginning of the regeneration. A flow rate of 10 µL/min was used in all runs.

6.6. Chromatography cycles monitored using a-Si:H photodiodes

After validating the operation of the microfluidic structure with integrated micro-valves using a fluorescence microscope, additional integration of a signal acquisition module for on-chip monitoring of fluorescence was addressed. **Figure 6.5-A** shows a characteristic

curve of a chromatographic cycle measured using an amorphous silicon *p-i-n* photodiode. Initially, the dark current of the photosensor was measured without applied bias (0 V). Then, the background signal, defined as the response of the photodiode under laser illumination at $\lambda_{ex,\ laser}$ = 405 nm and in the absence of liquid flowing through the microfluidic device, was measured. It is possible to observe that the photoresponse of the device at the excitation wavelength is higher than the dark current, indicating that the a-SiC:H filter did not cut off 100% of the excitation light at the conditions the excitation was performed. However, in this case, this does not affect the fluorescence measurements since the maximum fluorescence signal emitted by the beads was still approximately 70× higher than three times the standard deviation (3σ) of the laser illumination background. Thus, the high signal-to-noise ratio in the measurements allowed clearly differentiating and quantifying adsorption/elution kinetics at different conditions with high reproducibility and sensitivity. It is important to highlight that during the regeneration of the beads the photoresponse of the device drops almost instantaneously to the background levels, thus confirming the effectiveness of the regeneration step. In addition, after turning off the laser the signal rapidly returns to the dark response and remains stable thereafter, confirming that the photodiode response does not drift with time.

Chromatography cycles at different adsorption and elution conditions were then performed using a-Si:H photodiodes for fluorescence detection (**Figure 6.5-B**) and the kinetic profiles were in excellent agreement with those obtained using fluorescence microscopy for the same evaluated conditions. Considering the particular case of the antibody adsorption at pH 7.5, an important remark is the increased sensitivity that was obtained with the photosensors in comparison to the microscope experiments. While **Figure 6.4-A** suggests that antibody adsorption at pH 7.5 is almost negligible, the results in **Figure 6.5-B** show that there is still a small but significant amount of antibody molecules that bind to the beads at this condition. Regarding the results of the elution assays, the measurements with the photosensors also allowed to discern minor differences in antibody recovery yields at pH 9.5, with and without NaCl addition, providing results consistent with the ones previously calculated after image processing of data acquisition by fluorescence microscopy.

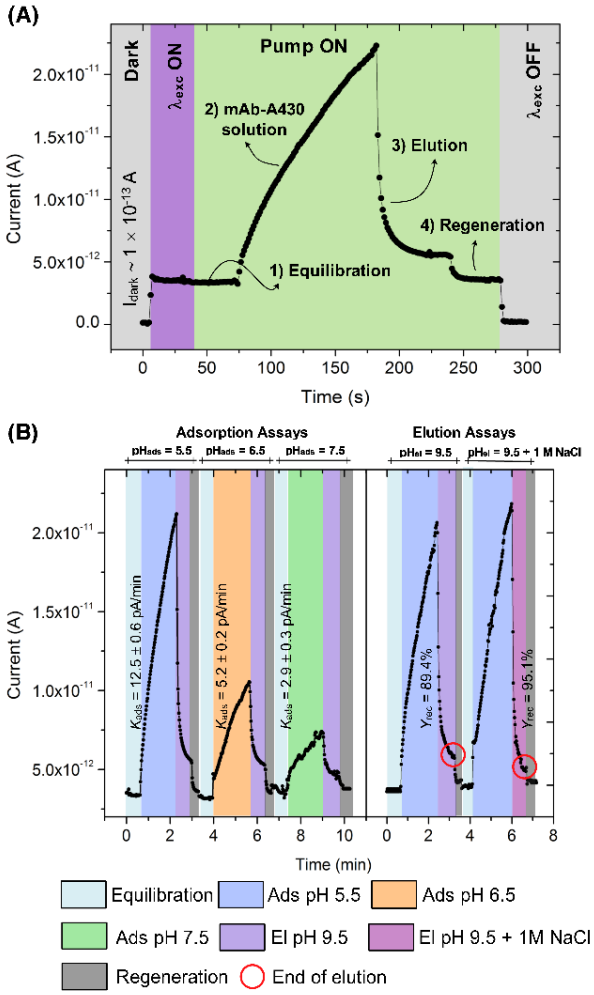

Figure 6.5 – Fluorescence monitoring using photosensors. **(A)** Curve obtained by measuring the current generated by the *p-i-n* photodiodes at 0 V bias at different stages of the fluorescence assay. Dark current acquisition was performed in the absence of excitation light. The baseline for the fluorescence measurements is the current generated by the excitation light. During the interval for liquid flow (Pump ON), four solutions were flowed in sequence by actuating the pneumatic valves in order to perform complete chromatographic cycles. **(B)** Photoresponse of the a-Si:H *p-i-n* photodiode during the adsorption and elution assays. A flow rate of 10 µL/min was used in all runs.

6.7. Assays in 1-mL chromatography columns

According to the work previously presented in chapter 4, results obtained using a similar microfluidics-based approach for the evaluation of different chromatographic operating conditions show a very good correlation with results from standard chromatography assays, despite differences in residence time, detection and quantification methodologies. For this reason, an elution pH of 9.5, which was observed to provide the highest antibody recovery, was further analyzed on a standard 1 mL pre-packed chromatography column using salt concentrations of 0 or 1 M NaCl.

Figure 6.6-A shows the chromatographic profiles that were obtained by loading 5 mL of cell culture supernatant previously adjusted to pH 5.5 to match the adsorption buffer pH. It is possible to observe differences in the antibody elution peaks, both in terms of area and retention time. The presence of a high salt concentration promoted a rapid and complete antibody elution, considering that the recovery yield was determined to be approximately 100%, thus matching the trend observed using the microfluidic device. It is important to highlight that the presence of NaCl in the elution buffer when using a real cell culture supernatant as feedstock gave an opposite trend in terms of recovery yield compared to that obtained when plain buffer solutions were used. This observation suggests the occurrence of ionic interactions between the antibody and other impurities retained in the column, which required the addition of a neutral salt in solution, in order to promote an effective elution of the antibody.

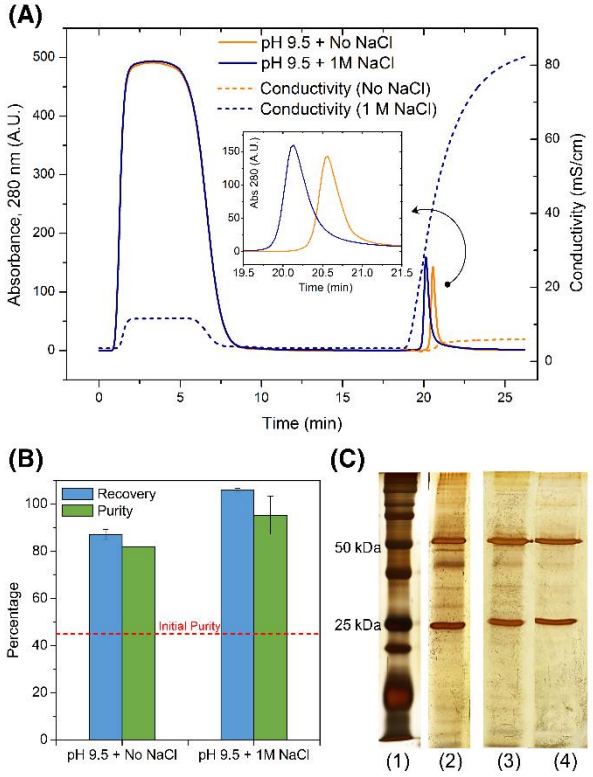

Figure 6.6 – Standard column chromatography assays. **(A)** Chromatographic profiles obtained by loading 5 mL of cell culture supernatant onto a pre-packed Capto™ MMC 1 mL-column. Adsorption was performed at pH 5.5 and elution was accomplished at pH 9.5 with 0 M or 1 M NaCl. Absorbance at 280 nm (full lines) and conductivity (dashed lines) of the outlet stream were continuously monitored. **(B)** Performance parameters (recovery yield and purity) of the mAb chromatographic purification from the cell culture supernatant. **(C)** Silver stained SDS-PAGE analysis of collected elution fractions. Lanes ID – 1: Precision Plus Protein™ Dual Color Standards; 2: Feed sample of serum-free cell culture supernatant; 3: Elution fraction collected using pH 9.5 + 0 M NaCl; 4: Elution fraction collected using pH 9.5 + 1 M NaCl. Position of IgG heavy chain (50 kDa) and light chain (25 kDa) is indicated on the molecular weight ladder.

The purity of the eluted fractions was also quantitatively (**Figure 6.6-B**) and qualitatively (**Figure 6.6-C**) evaluated. The protein composition of the cell culture supernatant is displayed in lane 2 from **Figure 6.6-C**, where the most noticeable bands correspond to the heavy and light chains of the antibody. This was already expected, considering that the initial purity of the antibody in the serum-free cell culture supernatant was determined to be higher than 40%. The purification procedure using pH 9.5 with 0 and 1 M NaCl as elution buffers allowed to improve the final purity to (81.98 ± 0.58)% and (95.33 ± 8.03)%, respectively. This improvement is also illustrated in **Figure 6.6-C**, lanes 3 and 4, where it is possible to see a great clearance in the impurity bands comparing to the feedstock lane. As is desirable, the elution condition giving the highest recovery yield was also the one that provided the best impurity clearance, thus reinforcing the importance of adding NaCl to the elution buffer when performing the antibody separation from complex cell culture media.

6.8. Summary

In this chapter the integration of valves and photosensors in a microfluidic platform for optimization of chromatography conditions was presented. Pneumatic valves allowed the performance of chromatography cycles by sequentially flowing equilibration, adsorption, elution and regeneration solutions in a controlled and automated manner. The coupling of the device with amorphous silicon photodiodes enabled continuous on-chip monitoring of adsorption and elution kinetics without the need of complex instrumentation and external software for data analysis. It is important to highlight that the photosensors could be reused with several PDMS structures, since they were not placed in direct contact with the flowing solution when performing the measurements.

The possibility to completely regenerate and reuse the microfluidic device provided enormous advantages allowing for a series of experiments to be performed sequentially in the same micro-column, which not only reduced the time needed for optimization but also resulted in more reliable and robust results. The architecture of the device is amenable to parallelization of assays, which would further increase the output of results that can be achieved within a short time frame.

This analytical approach was compatible with the use of a complex matrix without any pre-treatment. In fact, the performance of the adsorption and elution obtained in the microfluidic experiments was successfully validated in conventional chromatography

assays, even though intrinsic differences, such as the method of sample injection and the detection, can be found in micro and macro-scale approaches.

Fluorescence-based measurements proved to be effective for quantification of adsorption and elution kinetics, however this may not always be the preferable procedure when addressing a purification challenge since it relies on previous modification of the target molecule with a fluorophore. To overcome this potential limitation, future efforts may be focused on the integration of other types of sensors, such as pH, conductivity, UV or refractive index transducers.

"The good thing about science is that it's true whether or not you believe in it"

Neil deGrasse Tyson

Chapter 7
Label-free Monitoring of Chromatography in Microfluidics[§]

Previously mentioned approaches to screen molecular binding kinetics at bead-level relied strictly on a labeling process with an adequate fluorophore. While this strategy proved robust and provided minimal interference under a wide range of conditions, three main disadvantages can be highlighted, namely (i) a relatively time-consuming labeling step of the target molecule/impurity is required, preceded by an appropriate purification procedure or commercial acquisition of the pure molecule; (ii) the signal transduction step is only sensitive to each labeled molecule, meaning that it is not possible to determine, for example, the total concentration of protein bound to the resin and; (iii) while in this thesis the tested fluorophores were not observed to significantly affect molecular binding relative to the native protein for IgG and BSA, possible interference effects cannot be discarded without a previous investigation and may be particularly significant for target molecules with molecular weights comparable to those of the fluorophores. Therefore, this chapter aims at establishing a proof-of-concept for the integration of a label-free detection module in a nL-scale chromatography column, similarly to the standard detection employed in bench-scale chromatographers. This label-free detection was achieved both at bead-level and downstream of the microcolumn by aligning a-Si:H photodiodes below the microfluidic device. The signal transduction strategy was similar to that used in chapter 6 with two major differences: (i) the photodiodes did not contain an integrated a-SiC:H filter and were optimized to maximize the photoresponse in the UV region and (ii) the incident light had a wavelength of 280 nm in order to monitor total protein concentration by variations in absorptivity.

This chapter contains experimental results obtained within a collaborative work that is currently submitted to *Sensors and Actuators A: Physical.* My contribution to this work was on planning the chromatography assays as well as discussing the results obtained and revising the manuscript. The text and figures presented in this chapter were not reproduced from the submitted manuscript.

[§]D.R. Santos, R.R.G. Soares, I.F. Pinto, C.R.F. Caneira, R.M.R. Pinto, V. Chu, J.P. Conde, "Label-free detection of biomolecules in bead-based microfluidics using on-chip UV and impedance sensors" (*submitted*).

7.1. Experimental section

7.1.1. Fabrication of thin-film a-Si:H photodiodes optimized for UV detection

The photodiodes were fabricated using the same process described in detail in section 3.3 with a couple of differences in fabrication, optimized for UV detection. Namely, the ITO top contact thickness was reduced from 1000 Å to 500 Å and the a-SiC:H absorption filter was not deposited on top of the devices. The reduced ITO thickness allowed a reasonable UV transmission of 45% at λ=280 nm. For the measurements performed in this chapter, all PDMS devices aligned on top of the sensors had a thickness of 5.17 ± 0.15 mm to minimize UV absorption while still providing a tight sealing against the fluidic connectors.

7.1.2. UV transmission measurements on the microcolumns

For UV measurements, the light from a deuterium UV lamp (30 W High Irradiance, Ozone Free, Model 70621, Newport), coupled to a monochromator (Oriel Instruments 77250) for wavelength selection, was focused on the photosensors at normal incidence. The photon flux at λ = 280 nm was approximately 2.6×10^{13} $cm^{-2}.s^{-1}$, calibrated with a crystalline silicon photosensor with known responsivity R(λ) (Hamamatsu c-Si S1226-5BQ). The external quantum efficiency (EQE) at this wavelength was 16.6%. The photocurrent was acquired with a Keithley 237 picoammeter. The measurements from the picoammeter were then acquired through General Purpose Interface Bus (GPIB) by a computer software programmed in Python and PyQT4, allowing to read and process the data. Unless stated otherwise, all experiments were performed by diluting the target proteins (BSA and IgG) in 100-fold diluted PBS, *i.e.* 0.1 mM phosphate and 1.4 mM NaCl at pH 7.28 with a conductivity of 189 $\mu S.cm^{-1}$, hereafter referred as $PBS_{0.01}$. For the calibrations performed with a microcolumn without beads, the 700 μm wide microfluidic device was first aligned on top of the 200 μm square photodiode. Then, two syringe pumps (NE-1000, New Era Pump System, Inc.) connected to a "Y"-shaped connector were used to alternate between the solution containing the protein of interest and the $PBS_{0.01}$ buffer solution without stopping the photocurrent acquisition. The flow rate was kept at 1.5 μL/min in all experiments and all the measurements were started with the microchannels filled with $PBS_{0.01}$. Each protein concentration was tested in a different microchannel. For the chromatography experiments, the photocurrent was acquired both at bead-level and at the outlet of the column. These measurements were performed in two

different steps after regenerating the column in between. For the first measurement, the proteins at a specific concentration were flowed inside the microchannel and the sensor located under the microbeads was addressed (microcolumn sensor). After each measurement, the column was regenerated by flowing, in sequence, a 1 M NaOH solution for 1 min at 10 µL/min, DI water for 1 min at 20 µL/min and finally PBS for 2 min at 10 µL/min. For the second measurement, the photosensor was aligned to the outlet of the column and the same concentration of proteins was flowed. BSA was purchased from Sigma-Aldrich and a mixture of human antibodies (Gammanorm®) was acquired from Octapharma. According to the product information sheet, Gammanorm® is composed of IgGs in the following mass fractions: 59% of IgG1 (pI = 8.6 ± 0.4), 36% of IgG2 (pI = 7.4 ± 0.6), 4.9% of IgG3 (pI = 8.3 ± 0.7) and 0.5% of IgG4 (pI = 7.2 ± 0.8). The isoelectric points of the different IgGs were obtained from the literature [193, 194]. Spherical agarose beads (average size ~90 µm) functionalized with a carboxymethyl group (CM Sepharose Fast Flow) or a quaternary amine (Q Sepharose Fast Flow) were purchased from GE Healthcare.

7.2. Proof-of-concept of UV absorbance measurements performed at bead-level

The first model experiment to access the feasibility of performing UV absorbance measurements directly at bead-level was based on flowing unlabeled BSA through a microcolumn packed with anion exchange (Q Sepharose) beads. The microcolumn structure was the same as that reported in chapter 4 and the BSA solution was flowed at a concentration typically found in serum containing cell culture supernatants (250 µg/mL), prepared in a neutral (pH ~7.5), low conductivity buffer (189 $\mu S.cm^{-1}$) to promote binding. The raw current measurements of the photodiode aligned below the packed microcolumn are shown in **Figure 7.1-A**. It could be observed that the agarose beads alone are sufficiently transparent to UV light to provide a current signal approximately 30-fold above the dark current value. Then, while flowing the BSA solution at 15 µL/min, the current value was observed to steadily decrease for approximately 4 min, until a new baseline was reached. By computing two of these replicate experiments in terms of absorbance over time, as shown in **Figure 7.1-B**, the kinetic adsorption profiles are comparable to those obtained using labeled molecules in the previous chapters 4 to 6.

These results showed significant promise for the integration of UV sensing in miniaturized chromatography as an alternative or complementary technique to fluorescence monitoring. On the other hand, neither all bead materials are sufficiently optically transparent (*e.g.* Toyopearl polyacrylate beads) nor all functionalized ligands are non-absorbing in the UV range (*e.g.* protein A). Therefore, the subsequent step was to explore the versatility of the label-free UV absorbance detection by not only performing the detection at bead-level, but also downstream of the packed column, as is the standard in bench scale chromatographers.

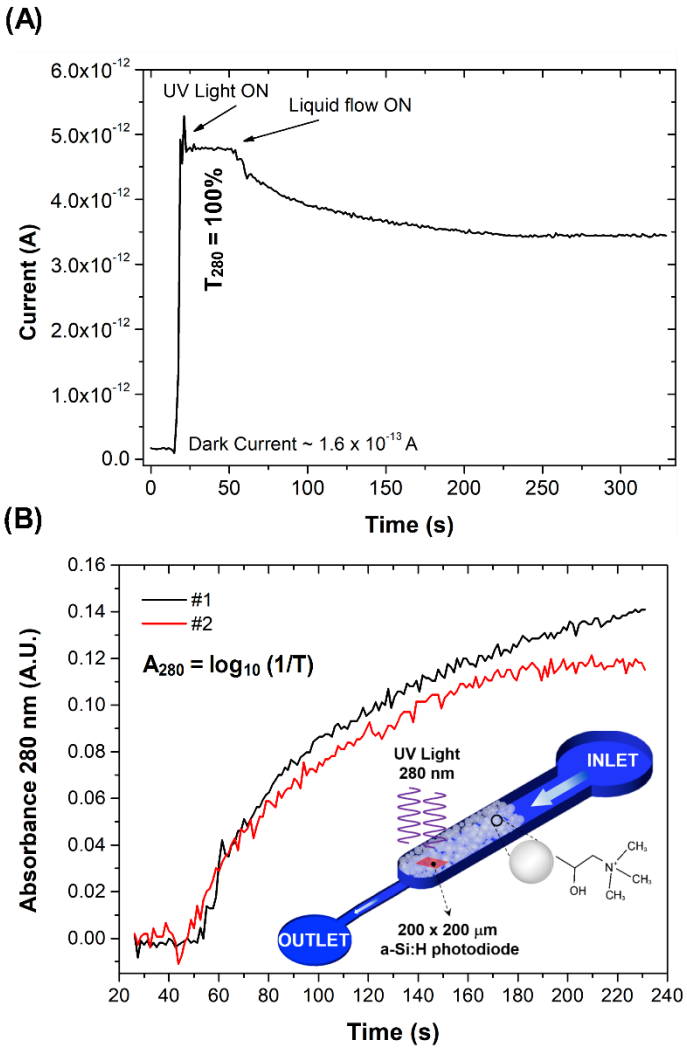

Figure 7.1 – Real-time monitoring of BSA adsorption on Q Sepharose beads by measuring UV absorbance directly at bead-level. **(A)** Raw current measurements before and after impinging UV light (280 nm) on top of the photodiode aligned below the packed beads. The current value was observed to steadily decrease while flowing a BSA solution. To calculate transmittance or absorbance values, the current corresponding to 100% transmission (beads only) is the value measured before flowing the protein solution. **(B)** Two replicate (#1, #2) continuous absorbance measurements performed in two separate chromatography columns. In all experiments the BSA solution had a concentration of 250 µg/mL, prepared in low conductivity phosphate buffer at pH 7.5 and flowed through the column at 15 µL/min.

7.3. UV absorbance measurements at bead-level and downstream of the packed beads

The first step towards the integration of UV absorbance monitoring at bead-level and downstream of the packed microcolumn was to redesign the microfluidic device to include a taller microchannel with H = 100 µm at the outlet. This device and respective regions to align each of the photodiodes is schematized in **Figure 7.2**. The main purpose of measuring the absorbance in a 100 µm tall microchannel, instead of in the thinner 20 µm bead barrier, was to increase the sensitivity of the measurement 5-fold due to the longer optical path.

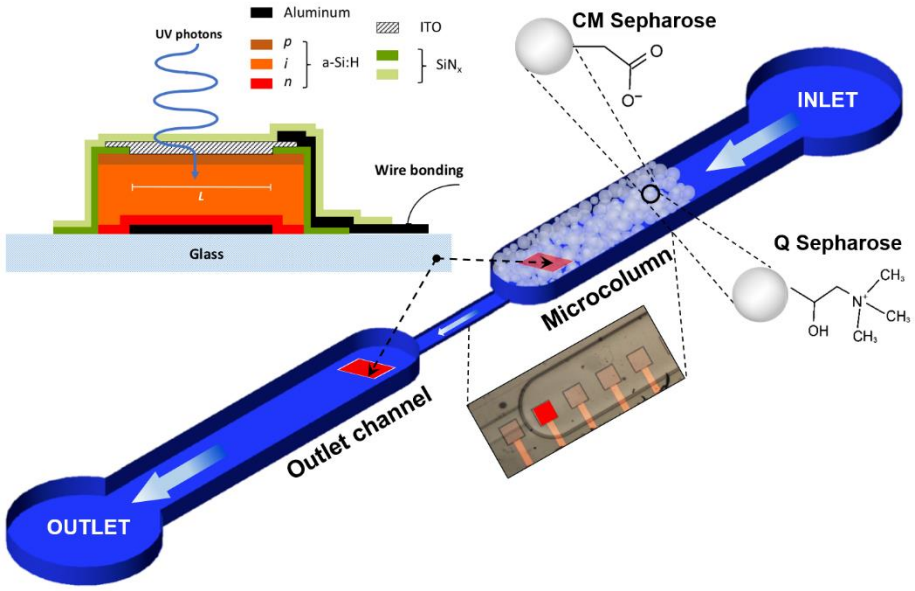

Figure 7.2 – Schematics of the microcolumn device used to perform UV transmission measurements at bead-level and downstream of the packed column. The a-Si:H photodiodes schematized on the top were aligned with the device regions highlighted in red. For a proof-of-concept, the structure was packed with either cation exchange (CM Sepharose) or anion exchange (Q Sepharose) beads.

Considering that only the molecules in solution are being measured downstream of the column, *i.e.* there are no beads to provide a molecular concentration effect, it was first necessary to calibrate the measured absorbance at increasing protein concentrations to validate the method at the target concentrations of interest. BSA and IgG were selected as model proteins and were flowed through microcolumns without packed beads. The results are shown in **Figure 7.3**. The curves of UV transmission *vs* time (**Figure 7.3-A**) show one measurement cycle of each protein at a specific concentration. The pump transitions (between $PBS_{0.01}$ and protein solutions and vice-versa) are visible in the figure

as short noise bursts at ~60 and ~660 s. **Figure 7.3-B** shows the UV photocurrent signal for all measured concentrations of IgG and BSA.

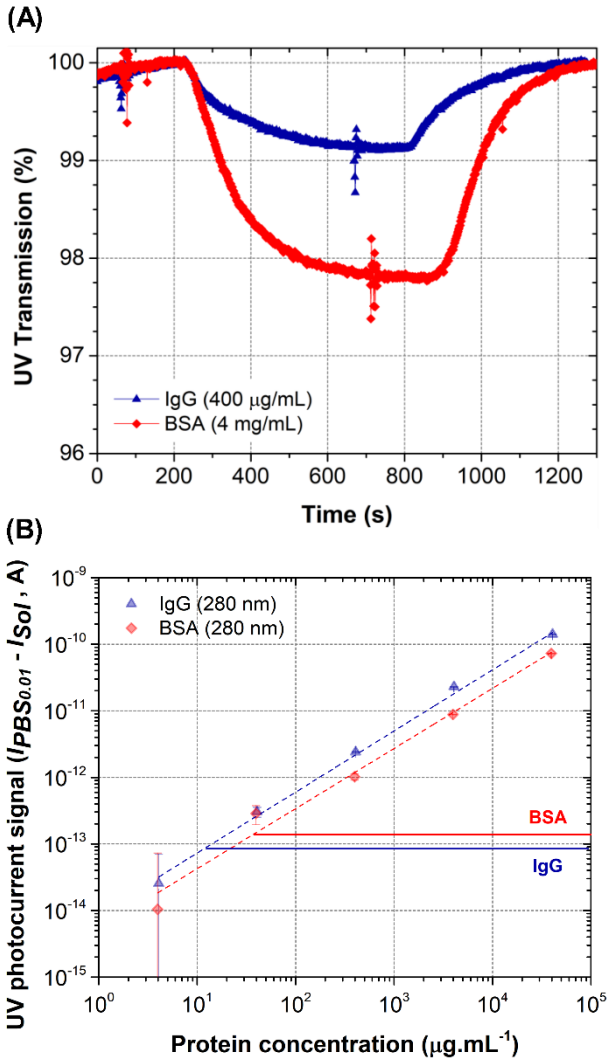

Figure 7.3 – Calibration of transmission measurements at increasing BSA or IgG concentrations flowed through a microcolumn without chromatography beads. **(A)** Transmission measurements over time while flowing 400 µg/mL IgG or 4 mg/mL BSA solutions in $PBS_{0.01}$ at 1.5 µL/min. The protein solutions were flowed at a t ≈ 200 s, followed by $PBS_{0.01}$ only at t ≈ 700 s. **(B)** UV photocurrent signal, *i.e.* difference of current measured without ($PBS_{0.01}$ only) and with ($PBS_{0.01}$ plus target protein) BSA or IgG molecules inside the microcolumn. The horizontal lines indicate the limit of detection for each protein (38.0 µg/mL for BSA and 11.8 µg/mL for IgG), meaning the protein concentration that results in a signal equal to 3.29 times the standard deviation of the background signal. The error bars are the standard deviation of two independent measurements performed on the same microcolumn.

Each experimental point of **Figure 7.3-B** was calculated as the difference between the average stable photocurrent (after waiting at least 20 s from the start of flow) corresponding to the minimum of UV transmission (maximum absorption) and the photocurrent plateau resulting from the maximum transmission of the $PBS_{0.01}$ ($I_{PBS0.01}$ - I_{SOL}, where $I_{PBS0.01}$ is the photocurrent measured when flowing $PBS_{0.01}$ and I_{SOL} is the

photocurrent measured when flowing the solution with the protein of interest). A linear correlation could be observed between the absorbed UV light and the concentration for both proteins. As the protein concentration decreases to the tens of µg/mL, the optical signal is limited by noise intrinsic to the electronics, material and photodetection. The limits of detection (LoDs) were calculated as 3.29σ (shown as horizontal lines in **Figure 7.3-B**), where σ represents the noise amplitude of the transmitted photocurrent of the $PBS_{0.01}$ buffer.

The LoDs for each protein (38 µg/mL for BSA and 11.8 µg/mL for IgG) were below the typical concentrations of interest for the optimization of IgG capture from cell culture supernatants. Nevertheless, to accurately characterize the breakthrough of the column down to trace amounts of proteins, the device would need to be further optimized to provide a longer optical path. This could be achieved either using a taller outlet channel or a planar waveguide configuration as previously reported [195, 196].

To make a proof-of-concept without the possible sensitivity limitations discussed above, relatively high concentrations of IgG (400 µg/mL) and BSA (4 mg/mL) were flowed through columns packed either with cation (CM Sepharose) or anion (Q Sepharose) exchange beads. In this case, a 10-fold lower flow rate was also used relative to the previous chapters, since the goal was to monitor the time-dependent retention and breakthrough of the proteins. The results of UV transmission monitored over time while continuously flowing IgG or BSA in $PBS_{0.01}$ at 1.5 µL/min through each type of beads are compiled in **Figure 7.4**. Focusing on the results provided by the photodiode aligned below the microcolumn for the IgG mixture, whose fractions have isoelectric points mostly above the working pH (7.28), the molecules were strongly adsorbed on the CM Sepharose beads, resulting in a decrease in transmission of almost 70% after 50 min (**Figure 7.4-A**). On the other hand, the Q Sepharose beads also captured a fraction of IgG molecules, resulting in a decrease in transmission of 5% after ~4 min (**Figure 7.4-B**). This is due to a fraction of the IgG mixture, namely 36% of IgG2 (pI = 7.4 ± 0.6) and 0.5% of IgG4 (pI = 7.2 ± 0.8) having a pI very close (~0.1 units above or below, respectively) to the buffer pH, meaning that there are still some molecules with a net negative charge. Regarding the results from the photodiode aligned with the outlet of the column, these can be evaluated in terms of break-point time (t_{b10}) that was defined as the time when the measured transmission (T_{UV}) in the outlet microchannel decreases by an amount equal to 10% × ($T_{UV\text{-}PBS0.01}$ - $T_{UV\text{-}SOL}$). In the case of IgG, the t_{b10} was 54 s for CM

Sepharose and 52 s for Q Sepharose. Again, this minimal difference in t_{b10} is due to the simultaneous presence of IgG molecules with both charges at the working pH, resulting in a sub-optimal molecular capture using each type of beads.

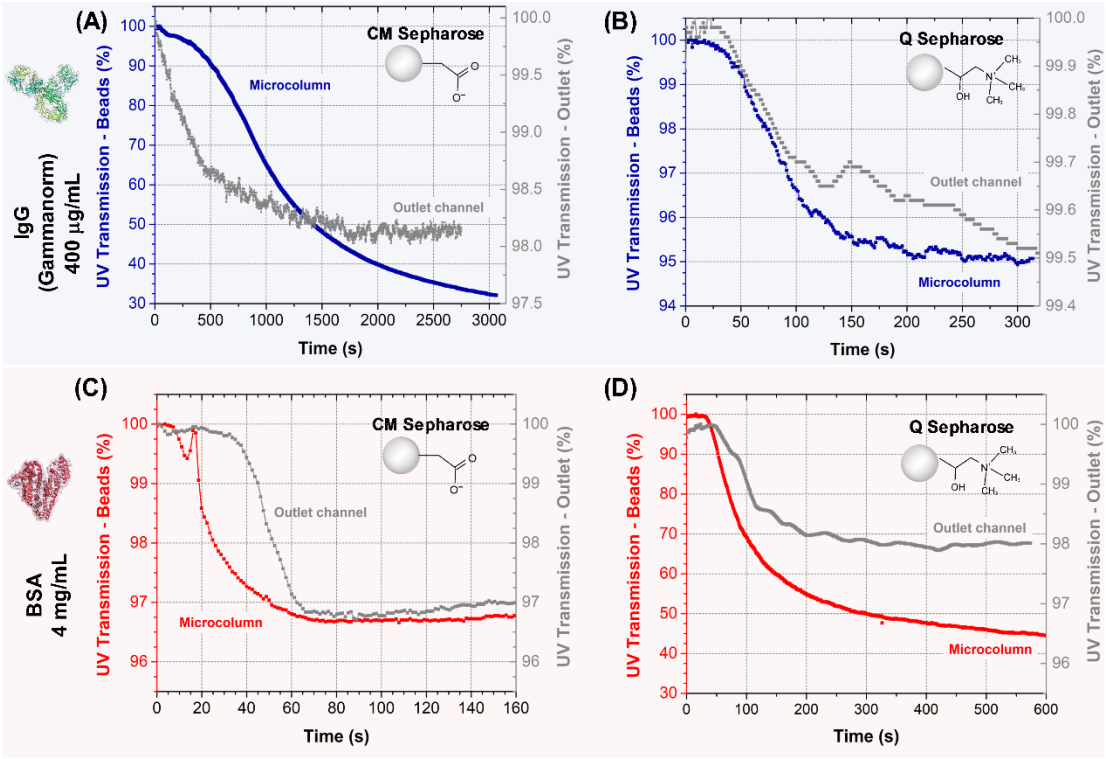

Figure 7.4 – UV transmission measurements over time performed at bead-level (microcolumn) and downstream of the beads (outlet channel) while flowing IgG **(A and B)** or BSA **(C and D)** through cation **(A and C)** or anion **(B and D)** exchange beads. The IgG and Gammanorm solutions were prepared in 100-fold diluted PBS ($PBS_{0.01}$) with a conductivity of 189 µS.cm^{-1} and a pH of 7.28 and were flowed through the microcolumn at 1.5 µL/min.

The results obtained for BSA, both at bead-level and downstream of the column, were significantly more expressive when comparing the cation and anion exchangers. In the case of CM Sepharose, no detectable interaction of BSA with the beads occurred, due to the pI of BSA (4.6) being significantly below the pH of the solution. Therefore, the lag in the decrease of the UV transmission between the microcolumn and outlet channels shown in **Figure 7.4-C** is simply due to the linear velocity of the solution combined with longitudinal diffusion effects. Differently, a considerable degree of BSA capture by the Q Sepharose beads was observed, resulting in a 55% decrease in transmission after only 12 min of flowing the solution. Such rapid decrease in transmission relative to IgG is due to the 10-fold higher concentration of BSA, inducing a proportionally faster molecular binding rate [119]. Finally, in this case the calculated t_{b10} for BSA was 60 s for Q Sepharose, significantly longer than that measured for the CM Sepharose (t_{b10} = 37 s).

7.4. Summary

In this chapter the optical signal transduction strategies combined with miniaturized chromatography were extended to label-free UV absorption measurements. In particular, a proof-of-concept for the measurement of IgG and BSA both at bead-level and downstream of the column was established. While the measurements at bead-level were performed using agarose beads and ligands that do not absorb light in the UV region, it is reasonable to assume that, by appropriately optimizing the incident light intensity to provide a measurable signal above the dark current background, such measurements may also be feasible in mildly absorbing beads and ligands. Otherwise, focusing on the UV measurement at the outlet of the column is an adequate alternative.

Overall, the integration of an effective UV monitoring module in the microfluidic high-throughput screening approach explored in this thesis is of critical importance to extract information regarding total protein binding and overall purity, without relying on fluorophore labels. Nevertheless, it is possible to envision the simultaneous integration of a fluorescence and UV detection in the microcolumn, to simultaneously measure the adsorption of the labeled target protein in a complex mixture (as discussed in chapter 6) and total protein as a means of easily extracting information about protein purity.

"Not everything that counts can be counted, and not everything that can be counted counts"
Albert Einstein

Chapter 8
Conclusions

This thesis described the development of a microfluidic-based strategy envisioning a high-throughput optimization of chromatographic separations. In particular, the purification of monoclonal antibodies (mAbs) from cell culture supernatants using multimodal chromatographic ligands was addressed. The project required a multidisciplinary approach combining knowledge in (i) biochemistry and engineering of chromatographic processes, (ii) microfabrication technologies and (iii) electronics and signal acquisition.

The first microfluidic structure developed to miniaturize the chromatographic operation allowed to successfully predict the binding of a mAb to a multimodal ligand in model buffer solutions. The amount of resin and mass of mAb used per assay was decreased by a factor of 10^4 and 10, respectively, compared to the operation using conventional 1 mL chromatography columns. Although the microfluidic optimization was based on fluorescence measurements at bead-level, the results in terms of recovery yield of the target mAb were successfully validated in conventional chromatography assays, in which the unlabeled analyte is detected in the outlet stream of the column by a UV sensor.

The throughput of the miniaturized assay was improved by introducing multiple chromatography chambers in series within a single device. In addition, the performance of the separation was simultaneously evaluated in terms of recovery yield and purity, using an artificial mixture of a mAb and BSA. The main challenge was to develop an appropriate analytical method that allowed to discriminate the fluorescence signal of the two proteins in solution and calibrate the fluorescence signal with respect to the mass of protein bound to the beads. In this part of the work, the chromatographic operation in *flowthrough* mode was also evaluated. In such conditions, the antibody is expected not to interact with the stationary phase while the BSA is captured by the beads. This study allowed to understand that the high linear velocity and low residence time of the liquid in

the microfluidic experiments may preclude an optimal correlation with results at macroscale, which was not observed when a *bind-elute* mode was employed.

Ultimately, the concept of chromatography-on-a-chip was demonstrated by integrating pneumatic valves in the device and coupling miniaturized photosensors for the fluorescence measurements of the target molecule. The integrated device showed promise in providing a scalable, parallelizable, rapid (3 min for a complete chromatographic cycle) and potentially low-cost high-throughput screening strategy. Compared with a conventional methodology based on 96-well plates operated in automated liquid handling stations, this microfluidic device allowed a reduction in resin consumption of ~700-fold [197] and a reduction in the mass of monoclonal antibody of ~100-fold [16, 197]. Also dramatic was the reduction in the assay time, since in 96-well plates the settling times of the resin are normally very lengthy [16], ranging from several minutes to hours, and during the process there are multiple incubation times that take as long as 30 minutes each [14].

It is important to highlight that a critical and innovative advantage of the microfluidic devices here presented is the possibility of extracting information about the association/dissociation kinetics from the adsorption/elution events at bead-level, which is impracticable in conventional batch experiments performed in 96-well plates and other batch adsorption microfluidic devices published in the literature [21, 126].

Future inroads are expected to focus on complementing the microfluidic studies with model-based approaches, to provide further insights on the structural basis of protein interactions with the multimodal ligands. A more profound understanding of the predominant molecular regions involved in protein binding and the identification of synergic interactions would be of critical importance to demonstrate the competitiveness of multimodal chromatography over conventional techniques. Furthermore, the generality of the developed technique, beyond the scope of multimodal chromatography ligands and monoclonal antibodies in particular, may contribute to the fields of separation sciences and analytical chemistry and inspire new developments within the downstream processing of biopharmaceuticals or other molecules.

Future work: Towards fully integrated and miniaturized high-throughput screening platforms to optimize chromatographic conditions

The microfluidic strategy developed in this thesis paves the way for further developments and implementations envisioning an autonomous high-throughput screening tool for applications beyond the optimization of multimodal chromatography. An outlook for potential future projects is presented below:

1) Considering that buffer preparation for testing multiple pH and conductivity conditions is a time-consuming task, the operation of the microfluidic system would greatly benefit from the integration of an on-chip buffer generator to feed the microcolumn. The successful implementation of a buffer generator is not straightforward, as mixing in microfluidics is difficult to achieve due to the laminar flow inside microchannels. Thus, the integration of microvalves for precise control of fluid flow, metering and mixing of solutions (as discussed in chapter 6) would be necessary to generate stable gradients of different buffer compositions. There are some reports in the literature of chemical [116], conductivity [198] and pH [199] gradient generators, which involve progressively branched channels to generate the desired composition by manipulating the volume ratio of two initial solutions.

2) In line with the fluorescence detection performed using a-Si:H photodiodes, reported in chapter 6, it would be interesting to couple an array of photodiodes in which each sensor would be specific for detecting a single type of molecule in solution (multiplexed detection). This would require that the molecules of interest were previously labeled with different fluorophores and that each sensor would be fabricated with an appropriate absorption filter, to match the excitation/emission wavelength fingerprints of the selected fluorophores. The fabrication of absorbing hydrogenated silicon-carbon alloy filters (a-SiC:H) with different carbon compositions has been reported [134], providing a broad selection of filtering characteristics to obtain the optimal sensitivity of the fluorescence detection system.

3) Alternative or complementary to the previous point is the development of label-free sensors, to monitor the chromatographic separation at bead-level and/or downstream of the column. A proof-of-concept integration of UV sensors has been presented in chapter 7, highlighting the potential of continuously monitoring total protein titers at bead-level and downstream of the packed column. On the other hand, impedimetric

and electrokinetic detection, based on the electrical properties of the molecules in solution, would also be amenable for miniaturization and coupling with the microfluidic device. The optical label-free detection appears to be preferable over charge-based methods, as in the latter it is still not clear how to deconvolute the measured signal in terms of the contribution of (i) charged molecules in solution, (ii) conductive buffer solutions, and (iii) chromatography beads functionalized with charged ligands. In addition, optical detection does not require the sensors to be in direct contact with the solution, avoiding regeneration or the disposal of the sensor after each measurement. Overall, a significant potential and low-risk is envisioned for a research project aiming at combining integrated fluorescence and UV optical detection to monitor the binding of the labeled target molecule, while simultaneously estimating protein purity for a range of operating conditions.

4) In an attempt to mimic the setup of a conventional chromatographic operation and perform a systematic optimization of buffer conditions, the real-time measurement of different operating parameters in the outlet of the microcolumn holds great promise. The integration of a multifunctional sensor to measure pH, conductivity and UV in an outlet channel, with appropriate dimensions to ensure an adequate optical pathlength, could be used not only to follow the chromatographic separation, but also to combine with a gradient generator module (mentioned in point 1), for iterative adjustments of the flow rate of the initial buffer solutions until the desired buffer composition is obtained and directed to the microcolumn.

5) Finally, towards the full automation of such microfluidic devices and aiming at capturing the interest and funding from the pharma industry, another critical step would be the combination of the microcolumns with widely established liquid handling platforms. This concept has been demonstrated by Waldbaur *et al.* [200] through the fabrication of a microfluidic chip format for interfacing of a microfluidic structure to a standard liquid handling station (LHS). This implementation would overcome some of the limitations of 96-well plates (as discussed in section 2.4.1) in the context of high-throughput screening of chromatographic conditions and would facilitate the migration of microfluidic devices from academia to an industry environment.

Bibliography

[1] A.T. Hanke, M. Ottens, Purifying biopharmaceuticals: knowledge-based chromatographic process development, Trends Biotechnol, 32(2014) 210-20.

[2] Hardman&co, Global Pharmaceuticals, 2016 industry statistics, 2017.

[3] IMS Institute for Healthcare Informatics, Global Oncology Trend Report: A review of 2015 and outlook to 2020, 2016.

[4] H.F. Liu, J. Ma, C. Winter, R. Bayer, Recovery and purification process development for monoclonal antibody production, mAbs, 2(2010) 480-99.

[5] S. Ghose, B. Hubbard, S.M. Cramer, Evaluation and comparison of alternatives to protein A chromatography: mimetic and hydrophobic charge induction chromatographic stationary phases, J Chromatogr A, 1122(2006) 144-52.

[6] J. Wang, J. Zhou, Y.K. Gowtham, S.W. Harcum, S.M. Husson, Antibody purification from CHO cell supernatant using new multimodal membranes, Biotechnol Progr, 33(2017) 658-65.

[7] A.R. Mazzer, X. Perraud, J. Halley, J. O'Hara, D.G. Bracewell, Protein A chromatography increases monoclonal antibody aggregation rate during subsequent low pH virus inactivation hold, J Chromatogr A, 1415(2015) 83-90.

[8] H.S. Karkov, B.O. Krogh, J. Woo, S. Parimal, H. Ahmadian, S.M. Cramer, Investigation of protein selectivity in multimodal chromatography using in silico designed Fab fragment variants, Biotechnol Bioeng, (2015).

[9] L. Sejergaard, H.S. Karkov, J.K. Krarup, A.B.B. Hagel, S.M. Cramer, Model-based process development for the purification of a modified human growth hormone using multimodal chromatography, Biotechnol Progr, 30(2014) 1057-64.

[10] W.-N. Chu, Q.-C. Wu, S.-J. Yao, D.-Q. Lin, High-throughput screening and optimization of mixed-mode resins for human serum albumin separation with microtiter filter plate, Biochem Eng J, 131(2018) 47-57.

[11] J. Pezzini, G. Joucla, R. Gantier, M. Toueille, A.M. Lomenech, C. Le Senechal, et al., Antibody capture by mixed-mode chromatography: a comprehensive study from determination of optimal purification conditions to identification of contaminating host cell proteins, J Chromatogr A, 1218(2011) 8197-208.

[12] J.L. Coffman, J.F. Kramarczyk, B.D. Kelley, High-throughput screening of chromatographic separations: I. Method development and column modeling, Biotechnol Bioeng, 100(2008) 605-18.

[13] J.F. Kramarczyk, B.D. Kelley, J.L. Coffman, High-throughput screening of chromatographic separations: II. Hydrophobic interaction, Biotechnol Bioeng, 100(2008) 707-20.

[14] B.K. Nfor, M. Noverraz, S. Chilamkurthi, P.D.E.M. Verhaert, L.A.M. van der Wielen, M. Ottens, High-throughput isotherm determination and thermodynamic modeling of protein adsorption on mixed mode adsorbents, J Chromatogr A, 1217(2010) 6829-50.

[15] J. Feliciano, A. Berrill, M. Ahnfelt, E. Brekkan, B. Evans, Z. Fung, et al., Evaluating high-throughput scale-down chromatography platforms for increased process understanding, Eng Life Sci, 16(2016) 169-78.

[16] J.P. Welsh, H. Bao, K. Barlow, J.M. Pollard, E. Brekkan, K.M. Lacki, et al., High-throughput techniques to evaluate the effect of ligand density for impurity separations with multimodal cation exchange resins, Eng Life Sci, 16(2015) 160-8.

[17] V.B. Brochier, A. Schapman, P. Santambien, L. Britsch, Fast purification process optimization using mixed-mode chromatography sorbents in pre-packed mini-columns, J Chromatogr A, 1177(2008) 226-33.

[18] S. Chhatre, D.G. Bracewell, N.J. Titchener-Hooker, A microscale approach for predicting the performance of chromatography columns used to recover therapeutic polyclonal antibodies, J Chromatogr A, 1216(2009) 7806-15.

[19] L.J. Millet, J.D. Lucheon, R.F. Standaert, S.T. Retterer, M.J. Doktycz, Modular microfluidics for point-of-care protein purifications, Lab on a Chip, 15(2015) 1799-811.

[20] M.S. Shapiro, S.J. Haswell, G.J. Lye, D.G. Bracewell, Design and characterization of a microfluidic packed bed system for protein breakthrough and dynamic binding capacity determination, Biotechnol Progr, 25(2009) 277-85.

[21] H.S. Rho, A.T. Hanke, M. Ottens, H. Gardeniers, A microfluidic device for the batch adsorption of a protein on adsorbent particles, Analyst, 142(2017) 3656-65.

[22] A. Nascimento, I.F. Pinto, V. Chu, M.R. Aires-Barros, J.P. Conde, A.M. Azevedo, Studies on the purification of antibody fragments, Sep Purif Technol, 195(2018) 388-97.

[23] A. Harada, N. Sekido, T. Akahoshi, T. Wada, N. Mukaida, K. Matsushima, Essential involvement of interleukin-8 (IL-8) in acute inflammation, J Leukoc Biol, 56(1994) 559-64.

[24] S. Vlahopoulos, I. Boldogh, A. Casola, A.R. Brasier, Nuclear factor-kappaB-dependent induction of interleukin-8 gene expression by tumor necrosis factor alpha: evidence for an antioxidant sensitive activating pathway distinct from nuclear translocation, Blood, 94(1999) 1878-89.

[25] E.J. Cohn, L.E. Strong, W.L. Hughes, D.J. Mulford, J.N. Ashworth, M. Melin, et al., Preparation and properties of serum and plasma proteins. IV. A system for the separation into fractions of the protein and lipoprotein components of biological tissues and fluids, J Am Chem Soc, 68(1946) 459-75.

[26] P.A. Marichal-Gallardo, M.M. Álvarez, State-of-the-art in downstream processing of monoclonal antibodies: process trends in design and validation, Biotechnol Progr, 28(2012) 899-916.

[27] B. Kelley, G. Blank, A. Lee, Downstream processing of monoclonal antibodies: current practices and future opportunities., in: U. Gottschalk (Ed.) Process Scale Purification of Antibodies, John Wiley & Sons, Inc2009, pp. 1–23.

[28] M. Butler, A. Meneses-Acosta, Recent advances in technology supporting biopharmaceutical production from mammalian cells, Appl Microbiol Biotechnol, 96(2012) 885-94.

[29] M. Matasci, D.L. Hacker, L. Baldi, F.M. Wurm, Recombinant therapeutic protein production in cultivated mammalian cells: current status and future prospects, Drug Discov Today Technol, 5(2008) e37-e42.

[30] A.R. Costa, M.E. Rodrigues, M. Henriques, J. Azeredo, R. Oliveira, Guidelines to cell engineering for monoclonal antibody production, Eur J Pharm Biopharm, 74(2010) 127-38.

[31] K. Sang Jick, P. Youngwoo, H. Hyo Jeong, Antibody engineering for the development of therapeutic antibodies, Mol Cells, 20(2005) 17-29.

[32] S. Hober, K. Nord, M. Linhult, Protein A chromatography for antibody purification, J Chromatogr B, 848(2007) 40-7.

[33] T.M. Pabst, R. Palmgren, A. Forss, J. Vasic, M. Fonseca, C. Thompson, et al., Engineering of novel Staphylococcal protein A ligands to enable milder elution pH and high dynamic binding capacity, J Chromatogr A, 1362(2014) 180-5.

[34] S. Ghose, B. Hubbard, S.M. Cramer, Binding capacity differences for antibodies and Fc-fusion proteins on protein A chromatographic materials, Biotechnol Bioeng, 96(2007) 768-79.

[35] J. Curling, The development of antibody purification technologies, in: U. Gottschalk (Ed.) Process Scale Purification of Antibodies, John Wiley & Sons2009, pp. 25-8.

[36] M.D. Costioli, C. Guillemot-Potelle, C. Mitchell-Logean, H. Broly, Cost of goods modeling and quality by design for developing cost-effective processes, BioPharm Int, 23(2010).

[37] A.A. Shukla, B. Hubbard, T. Tressel, S. Guhan, D. Low, Downstream processing of monoclonal antibodies - Application of platform approaches, J Chromatogr B, 848(2007) 28-39.

[38] S. Vunnum, G. Vedantham, B. Hubbard, Protein A-based affinity chromatography, in: U. Gottschalk (Ed.) Process Scale Purification of Antibodies, John Wiley & Sons, Inc.2009, pp. 79-89.

[39] E.O. Saphire, P.W. Parren, R. Pantophlet, M.B. Zwick, G.M. Morris, P.M. Rudd, et al., Crystal structure of a neutralizing human IGG against HIV-1: a template for vaccine design, Science, 293(2001) 1155-9.

[40] J. Deisenhofer, Crystallographic refinement and atomic models of a human Fc fragment and its complex with fragment B of protein A from Staphylococcus aureus at 2.9- and 2.8-A resolution, Biochemistry, 20(1981) 2361-70.

[41] H.M. Berman, J. Westbrook, Z. Feng, G. Gilliland, T.N. Bhat, H. Weissig, et al., The Protein Data Bank, Nucleic Acids Res, 28(2000) 235-42.

[42] E. Jain, A. Kumar, Upstream processes in antibody production: evaluation of critical parameters, Biotechnol Adv, 26(2008) 46-72.

[43] X. Wang, A.K. Hunter, N.M. Mozier, Host cell proteins in biologics development: identification, quantitation and risk assessment, Biotechnol Bioeng, 103(2009) 446-58.

[44] J.A. Asenjo, B.A. Andrews, Protein purification using chromatography: selection of type, modelling and optimization of operating conditions, J Mol Recognit, 22(2009) 65-76.

[45] S.M. Cramer, M.A. Holstein, Downstream bioprocessing: recent advances and future promise, Curr Opin Chem Eng, 1(2011) 27-37.

[46] P. Gagnon, Technology trends in antibody purification, J Chromatogr A, 1221(2012) 57-70.

[47] P. Gagnon, Purification of monoclonal antibodies by mixed-mode chromatography, in: U. Gottschalk (Ed.) Process Scale Purification of Antibodies, John Wiley & Sons, Inc.2009, p. 126.

[48] M. Toueille, A. Uzel, J.F. Depoisier, R. Gantier, Designing new monoclonal antibody purification processes using mixed-mode chromatography sorbents, J Chromatogr B, 879(2011) 836-43.

[49] A. Forss, G. Rodrigo, J. Liderfelt, K. Torstensson, K. Eriksson, Optimization, robustness, and scale-up of mAb purification, Bioprocess Int, 9(2011) 64-8.

[50] B.-L. Johansson, M. Belew, S. Eriksson, G. Glad, O. Lind, J.-L. Maloisel, et al., Preparation and characterization of prototypes for multi-modal separation aimed for capture of positively charged biomolecules at high-salt conditions, J Chromatogr A, 1016(2003) 35-49.

[51] G. Zhao, X.Y. Dong, Y. Sun, Ligands for mixed-mode protein chromatography: Principles, characteristics and design, J Biotechnol, 144(2009) 3-11.

[52] G. Carta, A. Jungbauer, Chromatography Media, Protein Chromatography: Process Development and Scale-up, Wiley-VCH Verlag GmbH & Co. KGaA2010, pp. 85-124.

[53] G.E. Hamilton, F. Luechau, S.C. Burton, A. Lyddiatt, Development of a mixed mode adsorption process for the direct product sequestration of an extracellular protease from microbial batch cultures, J Biotechnol, 79(2000) 103-15.

[54] V.B. Brochier, H. Chabre, A. Lautrette, V. Ravault, M.N. Couret, A. Didierlaurent, et al., High throughput screening of mixed-mode sorbents and optimisation using pre-packed lab-scale columns for the purification of the recombinant allergen rBet v 1a, J Chromatogr B, 877(2009) 2420-7.

[55] D. Gao, D.Q. Lin, S.J. Yao, Mechanistic analysis on the effects of salt concentration and pH on protein adsorption onto a mixed-mode adsorbent with cation ligand, J Chromatogr B, 859(2007) 16-23.

[56] T. Yang, G. Malmquist, B.-L. Johansson, J.-L. Maloisel, S. Cramer, Evaluation of multi-modal high salt binding ion exchange materials, J Chromatogr A, 1157(2007) 171-7.

[57] R.Z. Wang, D.Q. Lin, H.F. Tong, H.L. Lu, S.J. Yao, Evaluation of mixed-mode chromatographic resins for separating IgG from serum albumin containing feedstock, J Chromatogr B, 936(2013) 33-41.

[58] E. Boschetti, The use of thiophilic chromatography for antibody purification: a review, J Biochem Bioph Methods, 49(2001) 361-89.

[59] S. Oscarsson, J. Porath, Protein chromatography with pyridine- and alkylthioether-based agarose adsorbents, J Chromatogr A, 499(1990) 235-47.

[60] S.C. Burton, N.W. Haggarty, D.R.K. Harding, One step purification of chymosin by mixed mode chromatography, Biotechnol Bioeng, 56(1997) 45-55.

[61] P. Gagnon, C.-W. Cheung, E.J. Lepin, A.M. Wu, M.A. Sherman, A.A. Raubitschek, et al., Minibodies and multimodal chromatography methods: a convergence of challenge and opportunity, Bioprocess Int, 8(2010) 26-35.

[62] S.C. Burton, D.R.K. Harding, Hydrophobic charge induction chromatography: salt independent protein adsorption and facile elution with aqueous buffers, J Chromatogr A, 814(1998) 71-81.

[63] B.-L. Johansson, M. Belew, S. Eriksson, G. Glad, O. Lind, J.-L. Maloisel, et al., Preparation and characterization of prototypes for multi-modal separation media aimed for capture of negatively charged biomolecules at high salt conditions, J Chromatogr A, 1016(2003) 21-33.

[64] F. Oehme, J. Peters, Mixed-mode chromatography in downstream process development, BioPharm Int, (2010) 12-9.

[65] S.J. Mountford, E.M. Campi, A.J. Robinson, M.T. Hearn, Synthesis of N-heterocyclic ligands for use in affinity and mixed mode chromatography, Tetrahedron, 67(2011) 471-85.

[66] M.A. Holstein, A.A. Nikfetrat, M. Gage, A.G. Hirsh, S.M. Cramer, Improving selectivity in multimodal chromatography using controlled pH gradient elution, J Chromatogr A, 1233(2012) 152-5.

[67] A. Hirano, T. Arakawa, T. Kameda, Interaction of arginine with Capto MMC in multimodal chromatography, J Chromatogr A, 1338(2014) 58-66.

[68] L.S. Wolfe, C.P. Barringer, S.S. Mostafa, A.A. Shukla, Multimodal chromatography: characterization of protein binding and selectivity enhancement through mobile phase modulators, J Chromatogr A, 1340(2014) 151-6.

[69] H.S. Karkov, L. Sejergaard, S.M. Cramer, Methods development in multimodal chromatography with mobile phase modifiers using the steric mass action model, J Chromatogr A, 1318(2013) 149-55.

[70] M.A. Holstein, S. Parimal, S.A. McCallum, S.M. Cramer, Mobile phase modifier effects in multimodal cation exchange chromatography, Biotechnol Bioeng, 109(2012) 176-86.

[71] Y. Hou, S.M. Cramer, Evaluation of selectivity in multimodal anion exchange systems: A priori prediction of protein retention and examination of mobile phase modifier effects, J Chromatogr A, 1218(2011) 7813-20.

[72] S.J. Mountford, R. Daly, A.J. Robinson, M.T. Hearn, Design, synthesis and evaluation of pyridine-based chromatographic adsorbents for antibody purification, J Chromatogr A, 1355(2014) 15-25.

[73] J. Chen, J. Tetrault, A. Ley, Comparison of standard and new generation hydrophobic interaction chromatography resins in the monoclonal antibody purification process, J Chromatogr A, 1177(2008) 272-81.

[74] E. Boschetti, Antibody separation by hydrophobic charge induction chromatography, Trends Biotechnol, 20(2002) 333-7.

[75] T. Arakawa, M. Futatsumori-Sugai, K. Tsumoto, Y. Kita, H. Sato, D. Ejima, MEP HyperCel chromatography II: binding, washing and elution, Protein Expr Purif, 71(2010) 168-73.

[76] T. Arakawa, Y. Kita, H. Sato, D. Ejima, MEP chromatography of antibody and Fc-fusion protein using aqueous arginine solution, Protein Expr Purif, 63(2009) 158-63.

[77] R. Bischoff, L.W. McLaughlin, Chemically synthesized hydrophobic anion-exchange high-performance liquid chromatography supports used for oligonucleotide resolution by mixed mode chromatography, J Chromatogr A, 270(1983) 117-26.

[78] A. Zimmermann, R. Greco, I. Walker, J. Horak, A. Cavazzini, M. Lämmerhofer, Synthetic oligonucleotide separations by mixed-mode reversed-phase/weak anion-exchange liquid chromatography, J Chromatogr A, 1354(2014) 43-55.

[79] R. Bischoff, L.W. McLaughlin, Nucleic acid resolution by mixed-mode chromatography, J Chromatogr A, 296(1984) 329-37.

[80] T. Matos, J.A. Queiroz, L. Bülow, Plasmid DNA purification using a multimodal chromatography resin, J Mol Recognit, 27(2014) 184-9.

[81] D.C.A. Neville, R.A. Dwek, T.D. Butters, Development of a single column method for the separation of lipid- and protein-derived oligosaccharides, J Proteome Res, 8(2008) 681-7.

[82] M. Gilar, Y.-Q. Yu, J. Ahn, J. Fournier, J.C. Gebler, Mixed-mode chromatography for fractionation of peptides, phosphopeptides, and sialylated glycopeptides, J Chromatogr A, 1191(2008) 162-70.

[83] R.J. Carvalho, J. Woo, M.R. Aires-Barros, S.M. Cramer, A.M. Azevedo, Phenylboronate chromatography selectively separates glycoproteins through the manipulation of electrostatic, charge transfer, and cis-diol interactions, Biotechnol J, 9(2014) 1250-8.

[84] K.A. Kaleas, C.H. Schmelzer, S.A. Pizarro, Industrial case study: evaluation of a mixed-mode resin for selective capture of a human growth factor recombinantly expressed in E. coli, J Chromatogr A, 1217(2010) 235-42.

[85] A.M. Azevedo, A.G. Gomes, L. Borlido, I.F. Santos, D.M. Prazeres, M.R. Aires-Barros, Capture of human monoclonal antibodies from a clarified cell culture supernatant by phenyl boronate chromatography, J Mol Recognit, 23(2010) 569-76.

[86] R. dos Santos, S.A. Rosa, M.R. Aires-Barros, A. Tover, A.M. Azevedo, Phenylboronic acid as a multi-modal ligand for the capture of monoclonal antibodies: Development and optimization of a washing step, J Chromatogr A, 1355(2014) 115-24.

[87] W. Schwartz, D. Judd, M. Wysocki, L. Guerrier, E. Birck-Wilson, E. Boschetti, Comparison of hydrophobic charge induction chromatography with affinity chromatography on protein A for harvest and purification of antibodies, J Chromatogr A, 908(2001) 251-63.

[88] L. Guerrier, P. Girot, W. Schwartz, E. Boschetti, New method for the selective capture of antibodies under physiological conditions, Bioseparation, 9(2000) 211-21.

[89] L. Guerrier, I. Flayeux, E. Boschetti, A dual-mode approach to the selective separation of antibodies and their fragments, J Chromatogr B, 755(2001) 37-46.

[90] J. Vlasak, R. Ionescu, Fragmentation of monoclonal antibodies, mAbs, 3(2011) 253-63.

[91] S.S. Ranjini, D. Bimal, A.P. Dhivya, M.A. Vijayalakshmi, Study of the mechanism of interaction of antibody (IgG) on two mixed mode sorbents, J Chromatogr B, 878(2010) 1031-7.

[92] V. Brenac, V. Ravault, P. Santambien, E. Boschetti, Capture of a monoclonal antibody and prediction of separation conditions using a synthetic multimodal ligand attached on chips and beads, J Chromatogr B, 818(2005) 61-6.

[93] P. Girot, E. Averty, I. Flayeux, E. Boschetti, 2-Mercapto-5-benzimidazolesulfonic acid: an effective multimodal ligand for the separation of antibodies, J Chromatogr B, 808(2004) 25-33.

[94] M.D. Wenger, M. Woodling, US 2012/0208986 A1, 2011.

[95] R. Falkenstein, T. Lemm, M. Strasser, H. Yamada, WO 2012/059495 A1, 2012.

[96] G. Joucla, C. Le Senechal, M. Begorre, B. Garbay, X. Santarelli, C. Cabanne, Cation exchange versus multimodal cation exchange resins for antibody capture from CHO supernatants: identification of contaminating host cell proteins by mass spectrometry, J Chromatogr B, 942-943(2013) 126-33.

[97] K.A. Kaleas, M. Tripodi, S. Revelli, V. Sharma, S.A. Pizarro, Evaluation of a multimodal resin for selective capture of CHO-derived monoclonal antibodies directly from harvested cell culture fluid, J Chromatogr B, 969(2014) 256-63.

[98] D. Gao, S.-J. Yao, D.-Q. Lin, Preparation and adsorption behavior of a cellulose-based, mixed-mode adsorbent with a benzylamine ligand for expanded bed applications, J Appl Polym Sci, 107(2008) 674-82.

[99] D. Gao, L.L. Wang, D.Q. Lin, S.J. Yao, Evaluating antibody monomer separation from associated aggregates using mixed-mode chromatography, J Chromatogr A, 1294(2013) 70-5.

[100] R.A. Chmielowski, S. Meissner, D. Roush, T.O. Linden, E. Glowacki, J. Konietzko, et al., Resolution of heterogeneous charged antibody aggregates via multimodal chromatography: a comparison to conventional approaches, Biotechnol Progr, 30(2014) 636-45.

[101] J. Chen, J. Tetrault, Y. Zhang, A. Wasserman, G. Conley, M. Dileo, et al., The distinctive separation attributes of mixed-mode resins and their application in monoclonal antibody downstream purification process, J Chromatogr A, 1217(2010) 216-24.

[102] K. Eriksson, A. Ljunglöf, G. Rodrigo, E. Brekkan, Mab contaminant removal with a multimodal anion exchanger: a platform step to follow protein A, Bioprocess Int, 7(2009) 52-6.

[103] A. Voitl, T. Muller-Spath, M. Morbidelli, Application of mixed mode resins for the purification of antibodies, J Chromatogr A, 1217(2010) 5753-60.

[104] T. Müller-Späth, L. Aumann, G. Ströhlein, H. Kornmann, P. Valax, L. Delegrange, et al., Two step capture and purification of IgG2 using multicolumn countercurrent solvent gradient purification (MCSGP), Biotechnol Bioeng, 107(2010) 974-84.

[105] Datamonitor, Maximizing R&D Productivity - Getting more bang for your R&D Buck, Research and Markets, New York, 2001.

[106] C.B. Mazza, K. Rege, C.M. Breneman, N. Sukumar, J.S. Dordick, S.M. Cramer, High-throughput screening and quantitative structure-efficacy relationship models of potential displacer molecules for ion-exchange systems, Biotechnol Bioeng, 80(2002) 60-72.

[107] J.P. Welsh, M.A. Rauscher, H. Bao, S. Meissner, I. Han, T.O. Linden, et al., Domain antibody downstream process optimization: High-throughput strategy and analytical methods, Eng Life Sci, 16(2015) 133-42.

[108] M.D. Wenger, P. Dephillips, C.E. Price, D.G. Bracewell, An automated microscale chromatographic purification of virus-like particles as a strategy for process development, Biotechnol Appl Biochem, 47(2007) 131-9.

[109] M. Wiendahl, P. Schulze Wierling, J. Nielsen, D. Fomsgaard Christensen, J. Krarup, A. Staby, et al., High Throughput Screening for the Design and Optimization of Chromatographic Processes – Miniaturization, Automation and Parallelization of Breakthrough and Elution Studies, Chem Eng Technol, 31(2008) 893-903.

[110] A. Kecskemeti, A. Gaspar, Particle-based liquid chromatographic separations in microfluidic devices - A review, Anal Chim Acta, 1021(2018) 1-19.

[111] X. Younan, W.G. M., Soft Lithography, Angew Chem Int Ed, 37(1998) 550-75.

[112] M.A. Unger, H.-P. Chou, T. Thorsen, A. Scherer, S.R. Quake, Monolithic microfabricated valves and pumps by multilayer soft lithography, Science, 288(2000) 113-6.

[113] D. Caputo, G.d. Cesare, A. Nascetti, R. Negri, R. Scipinotti, Amorphous silicon sensors for single and multicolor detection of biomolecules, IEEE Sens J, 7(2007) 1274-80.

[114] P. Novo, D.M. Franca Prazeres, V. Chu, J.P. Conde, Microspot-based ELISA in microfluidics: chemiluminescence and colorimetry detection using integrated thin-film hydrogenated amorphous silicon photodiodes, Lab Chip, 11(2011) 4063-71.

[115] C.-Y. Lee, C.-L. Chang, Y.-N. Wang, L.-M. Fu, Microfluidic Mixing: A Review, International Journal of Molecular Sciences, 12(2011) 3263-87.

[116] J.T.S. Fernandes, S. Tenreiro, A. Gameiro, V. Chu, T.F. Outeiro, J.P. Conde, Modulation of alpha-synuclein toxicity in yeast using a novel microfluidic-based gradient generator, Lab Chip, 14(2014) 3949-57.

[117] S. Gerontas, M.S. Shapiro, D.G. Bracewell, Chromatography modelling to describe protein adsorption at bead level, J Chromatogr A, 1284(2013) 44-52.

[118] N. Madaboosi, R.R.G. Soares, V. Chu, J.P. Conde, A microfluidic immunoassay platform for the detection of free prostate specific antigen: a systematic and quantitative approach., Analyst, 140(2015) 4423-33.

[119] T.M. Squires, R.J. Messinger, S.R. Manalis, Making it stick: convection, reaction and diffusion in surface-based biosensors, Nat Biotech, 26(2008) 417-26.

[120] F. Batista-Viera, J.-C. Janson, J. Carlsson, Affinity Chromatography, Protein Purification, John Wiley & Sons, Inc.2011, p. 231.

[121] J. Chou, A. Lennart, J. Wong, M.F. Ali, P.N. Floriano, N. Christodoulides, et al., Modeling analyte transport and capture in porous bead sensors., Anal Chem, 84(2012) 2569-75.

[122] J.A. Thompson, H.H. Bau, Porous bead-based microfluidic assay: theory and confocal microscope imaging., Microfluid Nanofluid, 12(2011) 625-37.

[123] N.V. Lavrik, L.T. Taylor, M.J. Sepaniak, Nanotechnology and chip level systems for pressure driven liquid chromatography and emerging analytical separation techniques: A review, Anal Chim Acta, 694(2011) 6-20.

[124] M.C. Nweke, R.G. McCartney, D.G. Bracewell, Mechanical characterisation of agarose-based chromatography resins for biopharmaceutical manufacture, J Chromatogr A, 1530(2017) 129-37.

[125] C. Harinarayan, J. Mueller, A. Ljunglof, R. Fahrner, J. Van Alstine, R. van Reis, An exclusion mechanism in ion exchange chromatography, Biotechnol Bioeng, 95(2006) 775-87.

[126] M.S. Shapiro, S.J. Haswell, G.J. Lye, D.G. Bracewell, Microfluidic chromatography for early stage evaluation of biopharmaceutical binding and separation conditions., Sep Sci Technol, 46(2010) 185-94.

[127] M. Niimi, T. Masuda, K. Kaihatsu, N. Kato, S. Nakamura, T. Nakaya, et al., Virus purification and enrichment by hydroxyapatite chromatography on a chip, Sensors Actuators B: Chem, 201(2014) 185-90.

[128] M. Boyd-Moss, S. Baratchi, M. Di Venere, K. Khoshmanesh, Self-contained microfluidic systems: a review, Lab Chip, 16(2016) 3177-92.

[129] H.S. Rho, Y. Yang, A.T. Hanke, M. Ottens, L.W.M.M. Terstappen, H. Gardeniers, Programmable v-type valve for cell and particle manipulation in microfluidic devices, Lab Chip, 16(2016) 305-11.

[130] J. Huft, C.A. Haynes, C.L. Hansen, Fabrication of High-Quality Microfluidic Solid-Phase Chromatography Columns, Anal Chem, 85(2013) 1797-802.

[131] J. Huft, C.A. Haynes, C.L. Hansen, Microfluidic integration of parallel solid-phase liquid chromatography, Anal Chem, 85(2013) 2999-3005.

[132] F. Fixe, V. Chu, D.M.F. Prazeres, J.P. Conde, An on-chip thin film photodetector for the quantification of DNA probes and targets in microarrays, Nucleic Acids Res, 32(2004) e70.

[133] A.C. Pimentel, D.M.F. Prazeres, V. Chu, J.P. Conde, Fluorescence detection of DNA using an amorphous silicon p-i-n photodiode, J Appl Phys, 104(2008) 054913.

[134] B. Lipovšek, A. Jóskowiak, J. Krč, M. Topič, D.M.F. Prazeres, V. Chu, et al., Characterisation of hydrogenated silicon–carbon alloy filters with different carbon composition for on-chip fluorescence detection of biomolecules, Sensors and Actuators A: Physical, 163(2010) 96-100.

[135] B. Susan, H.V. H., R.R. E., Fluorescent Dyes Modify Properties of Proteins Used in Microvascular Research, Microcirculation, 10(2003) 221-31.

[136] J. Romanowska, D.B. Kokh, R.C. Wade, When the Label Matters: Adsorption of Labeled and Unlabeled Proteins on Charged Surfaces, Nano Lett, 15(2015) 7508-13.

[137] M. Krejc˛í, K. S˛lais, K. Tesar˛ík, Electrokinetic detection in liquid chromatography: Measurement of the streaming current generated on analytical and capillary columns, J Chromatogr A, 149(1978) 645-52.

[138] S. Terabe, K. Yamamoto, T. Ando, Streaming current detector for reversed-phase liquid chromatography, Can J Chem, 59(1981) 1531-7.

[139] J.K.-K. Ng, H. Feng, W.-T. Liu, Rapid discrimination of single-nucleotide mismatches using a microfluidic device with monolayered beads., Anal Chim Acta, 582(2007) 295-303.

[140] K. Sato, M. Tokeshi, H. Kimura, T. Kitamori, Determination of carcinoembryonic antigen in human sera by integrated bead-bed immunoasay in a microchip for cancer diagnosis., Anal Chem, 73(2001) 1213-8.

[141] H. Andersson, W. van der Wijngaart, G. Stemme, Micromachined filter-chamber array with passive valves for biochemical assays on beads., Electrophoresis, 22(2001) 249-57.

[142] J.C. McDonald, D.C. Duffy, J.R. Anderson, D.T. Chiu, H. Wu, O.J.A. Schueller, et al., Fabrication of microfluidic systems in poly(dimethylsiloxane). Electrophoresis, 21(2000) 27-40.

[143] A.d. Campo, C. Greiner, SU-8: A photoresist for high-aspect-ratio and 3D submicron lithography., J Micromech Microeng, 17(2007) R81.

[144] H. Zhang, X. Hu, X. Fu, Aptamer-based microfluidic beads array sensor for simultaneous detection of multiple analytes employing multienzyme-linked nanoparticle amplification and quantum dots labels., Biosens Bioelectron, 57(2014) 22-9.

[145] D.N. Kim, Y. Lee, W.-G. Koh, Fabrication of microfluidic devices incorporating bead-based reaction and microarray-based detection system for enzymatic assay., Sens Actuators, B, 137(2009) 305-12.

[146] H. Zhang, L. Liu, X. Fu, Z. Zhu, Microfluidic beads-based immunosensor for sensitive detection of cancer biomarker proteins using multienzyme-nanoparticle amplification and quantum dots labels., Biosens Bioelectron, 42(2013) 23-30.

[147] K. Treier, S. Hansen, C. Richter, P. Diederich, J. Hubbuch, P. Lester, High-throughput methods for miniaturization and automation of monoclonal antibody purification processes, Biotechnol Progr, 28(2012) 723-32.

[148] J. Kim, J. Heo, R.M. Crooks, Hybridization of DNA to bead-immobilized probes confined within a microfluidic channel, Langmuir, 22(2006) 10130-4.

[149] G.H. Seong, R.M. Crooks, Efficient mixing and reactions within microfluidic channels using microbead-supported catalysts., J Am Chem Soc, 124(2002) 13360-1.

[150] N. Buffi, D. Merulla, J. Beutier, F. Barbaud, S. Beggah, H. van Lintel, et al., Development of a microfluidics biosensor for agarose-bead immobilized Escherichia coli bioreporter cells for arsenite detection in aqueous samples, Lab Chip, 11(2011) 2369-77.

[151] S. Maria, G. Joucla, B. Garbay, W. Dieryck, A.-M. Lomenech, X. Santarelli, et al., Purification process of recombinant monoclonal antibodies with mixed mode chromatography, J Chromatogr A, 1393(2015) 57-64.

[152] S. Parimal, S. Garde, S.M. Cramer, Interactions of Multimodal Ligands with Proteins: Insights into Selectivity Using Molecular Dynamics Simulations, Langmuir, 31(2015) 7512-23.

[153] J.A. Woo, H. Chen, M.A. Snyder, Y. Chai, R.G. Frost, S.M. Cramer, Defining the property space for chromatographic ligands from a homologous series of mixed-mode ligands, J Chromatogr A, 1407(2015) 58-68.

[154] K. Srinivasan, S. Parimal, M.M. Lopez, S.A. McCallum, S.M. Cramer, Investigation into the molecular and thermodynamic basis of protein interactions in multimodal chromatography using functionalized nanoparticles, Langmuir, 30(2014) 13205-16.

[155] A.M. Azevedo, P.A.J. Rosa, I.F. Ferreira, M.R. Aires-Barros, Integrated process for the purification of antibodies combining aqueous two-phase extraction, hydrophobic interaction chromatography and size-exclusion chromatography, J Chromatogr A, 1213(2008) 154-61.

[156] T. Linden, A. Ljunglöf, L. Hagel, M.-R. Kula, J. Thömmes, Visualizing patterns of protein uptake to porous media using confocal scanning laser microscopy, Sep Sci Technol, 37(2002) 1-32.

[157] N. Cohen, P. Sabhachandani, A. Golberg, T. Konry, Approaching near real-time biosensing: Microfluidic microsphere based biosensor for real-time analyte detection, Biosens Bioelectron, 66(2015) 454-60.

[158] J.-W. Choi, D.-K. Kang, H. Park, A.J. deMello, S.-I. Chang, High-Throughput analysis of protein–protein interactions in picoliter-volume droplets using fluorescence polarization, Anal Chem, 84(2012) 3849-54.

[159] L.F. Cheow, R. Viswanathan, C.-S. Chin, N. Jennifer, R.C. Jones, E. Guccione, et al., Multiplexed Analysis of Protein–Ligand Interactions by Fluorescence Anisotropy in a Microfluidic Platform, Anal Chem, 86(2014) 9901-8.

[160] P. Baumann, K. Baumgartner, J. Hubbuch, Influence of binding pH and protein solubility on the dynamic binding capacity in hydrophobic interaction chromatography, J Chromatogr A, 1396(2015) 77-85.

[161] P.A. Levkin, S. Eeltink, T.R. Stratton, R. Brennen, K. Robotti, H. Yin, et al., Monolithic porous polymer stationary phases in polyimide chips for the fast high-performance liquid chromatography separation of proteins and peptides, J Chromatogr A, 1200(2008) 55-61.

[162] Y. Ladner, A. Bruchet, G. Cretier, V. Dugas, J. Randon, K. Faure, New "one-step" method for the simultaneous synthesis and anchoring of organic monolith inside COC microchip channels, Lab on a Chip, 12(2012) 1680-5.

[163] A. Ishida, T. Yoshikawa, M. Natsume, T. Kamidate, Reversed-phase liquid chromatography on a microchip with sample injector and monolithic silica column, J Chromatogr A, 1132(2006) 90-8.

[164] S. Wouters, J. De Vos, J.L. Dores-Sousa, B. Wouters, G. Desmet, S. Eeltink, Prototyping of thermoplastic microfluidic chips and their application in high-performance liquid chromatography separations of small molecules, J Chromatogr A, 1523(2017) 224-33.

[165] I.F. Pinto, S.A.S.L. Rosa, M.R. Aires-Barros, A.M. Azevedo, Exploring the use of heparin as a first capture step in the purification of monoclonal antibodies from cell culture supernatants, Biochem Eng J, 104(2015) 27-33.

[166] I. Olsson, U.-B. Axiö-Fredriksson, M. Degerman, B. Olsson, Fast horizontal electrophoresis. I. Isoelectric focusing and polyacrylamide gel electrophoresis using PhastSystem™, Electrophoresis, 9(1988) 16-22.

[167] A. Staby, I.H. Jensen, I. Mollerup, Comparison of chromatographic ion-exchange resins: I. Strong anion-exchange resins, J Chromatogr A, 897(2000) 99-111.

[168] R. Necina, K. Amatschek, A. Jungbauer, Capture of human monoclonal antibodies from cell culture supernatant by ion exchange media exhibiting high charge density, Biotechnol Bioeng, 60(1998) 689-98.

[169] A. Hirano, T. Maruyama, K. Shiraki, T. Arakawa, T. Kameda, A study of the small-molecule system used to investigate the effect of arginine on antibody elution in hydrophobic charge-induction chromatography, Protein Expr Purif, 129(2017) 44-52.

[170] X.M. Yuan, D.Q. Lin, Q.L. Zhang, D. Gao, S.J. Yao, A microcalorimetric study of molecular interactions between immunoglobulin G and hydrophobic charge-induction ligand, J Chromatogr A, 1443(2016) 145-51.

[171] Q. Zhang, F. Schimpf, H.-L. Lu, D.-Q. Lin, S.-J. Yao, Binary adsorption processes of albumin and immunoglobulin on hydrophobic charge-induction resins, J Chem Eng Data, 61(2016) 1353-60.

[172] F. Li, N. Vijayasankaran, A. Shen, R. Kiss, A. Amanullah, Cell culture processes for monoclonal antibody production, mAbs, 2(2010) 466-77.

[173] M. Micheletti, G.J. Lye, Microscale bioprocess optimisation, Curr Opin Biotechnol, 17(2006) 611-8.

[174] L. Zhang, S.M. Rafei, L. Xie, M.B.-R. Chew, H.M. Ji, Y. Chen, et al., A self-contained disposable cartridge microsystem for dengue viral ribonucleic acid extraction, Sens Actuator B-Chem, 160(2011) 1557-64.

[175] B. Li, L. Li, A. Guan, Q. Dong, K. Ruan, R. Hu, et al., A smartphone controlled handheld microfluidic liquid handling system, Lab Chip, 14(2014) 4085-92.

[176] K.A. Addae-Mensah, Y.K. Cheung, V. Fekete, M.S. Rendely, S.K. Sia, Actuation of elastomeric microvalves in point-of-care settings using handheld, battery-powered instrumentation, Lab Chip, 10(2010) 1618-22.

[177] I.E. Araci, S.R. Quake, Microfluidic very large scale integration (mVLSI) with integrated micromechanical valves, Lab Chip, 12(2012) 2803-6.

[178] A. Zahra, R. Scipinotti, D. Caputo, A. Nascetti, G. de Cesare, Design and fabrication of microfluidics system integrated with temperature actuated microvalve, Sens Actuator A-Phys, 236(2015) 206-13.

[179] W. Gu, H. Chen, Y.-C. Tung, J.-C. Meiners, S. Takayama, Multiplexed hydraulic valve actuation using ionic liquid filled soft channels and Braille displays, Appl Phys Lett, 90(2007) 033505.

[180] L. Novak, P. Neuzil, J. Pipper, Y. Zhang, S. Lee, An integrated fluorescence detection system for lab-on-a-chip applications, Lab Chip, 7(2007) 27-9.

[181] R.R.G. Soares, D. Ramadas, V. Chu, M.R. Aires-Barros, J.P. Conde, A.S. Viana, et al., An ultrarapid and regenerable microfluidic immunoassay coupled with integrated photosensors for point-of-use detection of ochratoxin A, Sens Actuator B-Chem, 235(2016) 554-62.

[182] G. Ryu, J. Huang, O. Hofmann, C.A. Walshe, J.Y.Y. Sze, G.D. McClean, et al., Highly sensitive fluorescence detection system for microfluidic lab-on-a-chip, Lab Chip, 11(2011) 1664-70.

[183] P. Novo, G. Moulas, D.M. França Prazeres, V. Chu, J.P. Conde, Detection of ochratoxin A in wine and beer by chemiluminescence-based ELISA in microfluidics with integrated photodiodes, Sens Actuators B Chem, 176(2013) 232-40.

[184] P. Alpuim, V. Chu, J.P. Conde, Amorphous and microcrystalline silicon films grown at low temperatures by radio-frequency and hot-wire chemical vapor deposition, J Appl Phys, 86(1999) 3812-21.

[185] P. Sajonz, W. Schafer, X. Gong, S. Shultz, T. Rosner, C.J. Welch, Multiparallel microfluidic high-performance liquid chromatography for high-throughput normal-phase chiral analysis, J Chromatogr A, 1145(2007) 149-54.

[186] J. Xie, Y. Miao, J. Shih, Y.-C. Tai, T.D. Lee, Microfluidic platform for liquid chromatography − tandem mass spectrometry analyses of complex peptide mixtures, Anal Chem, 77(2005) 6947-53.

[187] I.M. Lazar, P. Trisiripisal, H.A. Sarvaiya, Microfluidic liquid chromatography system for proteomic applications and biomarker screening, Anal Chem, 78(2006) 5513-24.

[188] J.T.S. Fernandes, O. Chutna, V. Chu, J.P. Conde, T.F. Outeiro, A novel microfluidic cell co-culture platform for the study of the molecular mechanisms of Parkinson's disease and other synucleinopathies, Front Neurosci, 10(2016).

[189] F.A. Bettelheim, W.H. Brown, M.K. Campbell, S.O. Farrell, O. Torres, Introduction to General, Organic and Biochemistry: Cengage Learning; 2015.

[190] M. Jin, N. Szapiel, J. Zhang, J. Hickey, S. Ghose, Profiling of host cell proteins by two-dimensional difference gel electrophoresis (2D-DIGE): Implications for downstream process development, Biotechnol Bioeng, 105(2010) 306-16.

[191] M.E.M. Cromwell, E. Hilario, F. Jacobson, Protein aggregation and bioprocessing, The AAPS Journal, 8(2006) E572-E9.

[192] J. Woo, S. Parimal, M.R. Brown, R. Heden, S.M. Cramer, The effect of geometrical presentation of multimodal cation-exchange ligands on selective recognition of hydrophobic regions on protein surfaces, J Chromatogr A, 1412(2015) 33-42.

[193] I.V. Nikolayenko, O.Y. Galkin, N.I. Grabchenko, M.Y. Spivak, Preparation of highly purified human IgG, IgM, and IgA for immunization and immunoanalysis, 2(2005) 3-11.

[194] Agrisera, Molecular weight and isoelectric point of various animal immunoglobulins, https://www.agrisera.com/cgi-bin/ibutik/AIR_ibutik.pl?funk=Webbsida&ID=10020, accessed on 2018/07/11.

[195] J.S. Kee, D.P. Poenar, P. Neuzil, L. Yobas, Poly(dimethylsiloxane) Waveguides Integrated with Microfluidics for Absorbance Measurement, 2008 IEEE PhotonicsGlobal@Singapore2008, pp. 1-4.

[196] S.M. Azmayesh-Fard, E. Flaim, J.N. McMullin, PDMS biochips with integrated waveguides, Journal of Micromechanics and Microengineering, 20(2010) 087002.

[197] B. D. Kelley, S.A. Tobler, P. Brown, J.L. Coffman, R. Godavarti, T. Iskra, et al., Weak partitioning chromatography for anion exchange purification of monoclonal antibodies, Biotechnol Bioeng, 101(2008) 553-66.

[198] S. Höving, D. Janasek, P. Novo, Flow rate independent gradient generator and application in microfluidic free-flow electrophoresis, Anal Chim Acta, (2018).

[199] H.S. Rho, A.T. Hanke, M. Ottens, H.J.G.E. Gardeniers, A microfluidic chip with a staircase pH gradient generator, a packed column and a fraction collector for chromatofocusing of proteins, Electrophoresis, 39(2018) 1031-9.

[200] A. Waldbaur, J. Kittelmann, C.P. Radtke, J. Hubbuch, B.E. Rapp, Microfluidics on liquid handling stations ([small mu]F-on-LHS): an industry compatible chip interface between microfluidics and automated liquid handling stations, Lab on a Chip, 13(2013) 2337-43.

Appendix A

Conductivity and pH conditions tested in Chapter 4

Table A2 – Conductivity and pH conditions tested in the adsorption and elution assays performed in microfluidics using Capto™ MMC beads. The concentration of NaCl corresponding to the conductivity values is also indicated. The response parameters for the adsorption ($k_{1/2}$) and elution (Y_r) represent the experimental values used to obtain the contour plot analysis.

Capto™ MMC – Adsorption				**Capto™ MMC – Elution**			
pH	**[NaCl] (mM)**	**Conductivity ($mS.cm^{-1}$)**	**$k_{1/2}$ ($AU.s^{-1}$)**	**pH**	**[NaCl] (M)**	**Conductivity ($mS.cm^{-1}$)**	**Y_r (%)**
5.5	0	0.9	0.731	**7.5**	0	7.2	68.0
	12.5	2.2	0.625		0.5	47.3	40.0
	25	3.6	0.531		1	84.3	72.2
	50	6.1	0.749		1.5	117.4	63.3
	100	11.1	0.455		2	145.7	66.5
	200	20.2	0.693		-	-	-
6.5	0	1.5	0.66	**8.0**	0	7.6	81.8
	12.5	2.7	0.457		0.5	45.5	73.4
	25	3.9	0.551		1	83.5	71.6
	50	6.5	0.468		1.5	115.8	73.8
	100	11.3	0.276		2	143.9	72.4
	200	20.7	0.13		-	-	-
7.5	0	2.1	0.66	**8.5**	0	6.1	82.3
	12.5	3.2	0.113		0.5	49.1	74.7
	25	4.6	0.03		1	84.3	72.7
	50	7.2	0.015		1.5	116.1	61.5
	100	12.2	0.027		2	144.2	74.1
	200	21.2	0.004		-	-	-
8.5	0	0.7	0.032	**9.0**	0	6.5	89.9
	12.5	1.7	0.004		0.5	48.4	86.2
	25	3.0	0.001		1	83.7	78.6
	50	5.6	0.015		1.5	117.4	67.0
	100	10.5	0.044		2	145.9	65.4
	200	19.7	0.073		-	-	-
9.5	0	1.5	0.002	**9.5**	0	6.5	95.3
	12.5	2.4	0.006		0.5	49.9	91.2
	25	3.7	0.011		1	86.2	83.3
	50	6.2	0.003		1.5	119.1	80.7
	100	11.1	0.004		2	147.2	74.2
	200	20.2	0.008		-	-	-

Table A3 – Conductivity and pH conditions tested in the adsorption and elution assays performed in microfluidics using CM Sepharose™ beads. The concentration of NaCl corresponding to the conductivity values is also indicated. The response parameters for the adsorption ($k_{1/2}$) and elution (Y_r) represent the experimental values used to obtain the contour plot analysis.

CM Sepharose™ - Adsorption				**CM Sepharose™ - Elution**			
pH	**[NaCl] (mM)**	**Conductivity ($mS.cm^{-1}$)**	**$k_{1/2}$ ($AU.s^{-1}$)**	**pH**	**[NaCl] (M)**	**Conductivity ($mS.cm^{-1}$)**	**Y_r (%)**
5.5	0	0.9	0.909	**7.5**	0	7.2	40.5
	12.5	2.2	0.649		0.5	47.3	73.4
	25	3.6	0.726		1	84.3	67.9
	50	6.1	0.193		1.5	117.4	72.6
	100	11.1	0.030		2	145.7	64.5
	200	20.2	0.020		-	-	-
6.5	0	1.5	0.542	**8.0**	0	7.6	28.5
	12.5	2.7	0.183		0.5	45.5	71.7
	25	3.9	0.168		1	83.5	72.3
	50	6.5	0.039		1.5	115.8	71.7
	100	11.3	0.008		2	143.9	62.4
	200	20.7	0.018		-	-	-
7.5	0	2.1	0.025	**8.5**	0	6.1	48.5
	12.5	3.2	0.001		0.5	49.1	84.8
	25	4.6	0.001		1	84.3	82.9
	50	7.2	0.003		1.5	116.1	82.1
	100	12.2	0.004		2	144.2	74.7
	200	21.2	0.003		-	-	-
8.5	0	0.7	0.002	**9.0**	0	6.5	81.6
	12.5	1.7	0.008		0.5	48.4	83.8
	25	3.0	0.007		1	83.7	87.4
	50	5.6	0.003		1.5	117.4	87.0
	100	10.5	0.002		2	145.9	66.1
	200	19.7	0.002		-	-	-
9.5	0	1.5	0.033	**9.5**	0	6.5	95.7
	12.5	2.4	0.049		0.5	49.9	89.5
	25	3.7	0.004		1	86.2	89.6
	50	6.2	0.008		1.5	119.1	84.3
	100	11.1	0.002		2	147.2	78.0
	200	20.2	0.003		-	-	-

Table A4 – Conductivity and pH conditions tested in the adsorption and elution assays performed in microfluidics using Phenyl Sepharose™ beads. The concentration of NaCl corresponding to the conductivity values is also indicated. The response parameters for the adsorption ($k_{1/2}$) and elution (Y_r) represent the experimental values used to obtain the contour plot analysis.

Phenyl Sepharose™ - Adsorption				***Phenyl Sepharose™ - Elution***			
pH	**[NaCl] (mM)**	**Conductivity ($mS.cm^{-1}$)**	**$k_{1/2}$ ($AU.s^{-1}$)**	**pH**	**[NaCl] (M)**	**Conductivity ($mS.cm^{-1}$)**	**Y_r (%)**
5.5	0	0.9	0.092	**7.5**	0	7.2	72.8
	12.5	2.2	0.084		0.5	47.3	74.2
	25	3.6	0.105		1	84.3	46.4
	50	6.1	0.109		1.5	117.4	12.5
	100	11.1	0.090		2	145.7	12
	200	20.2	0.070		-	-	-
6.5	0	1.5	0.087	**8.0**	0	7.6	79.3
	12.5	2.7	0.061		0.5	45.5	51.7
	25	3.9	0.076		1	83.5	40.4
	50	6.5	0.081		1.5	115.8	17.2
	100	11.3	0.057		2	143.9	17.2
	200	20.7	0.068		-	-	-
7.5	0	2.1	0.041	**8.5**	0	6.1	85
	12.5	3.2	0.008		0.5	49.1	50.2
	25	4.6	0.011		1	84.3	20.8
	50	7.2	0.046		1.5	116.1	15.8
	100	12.2	0.015		2	144.2	13.8
	200	21.2	0.033		-	-	-
8.5	0	0.7	6.00E-04	**9.0**	0	6.5	81.1
	12.5	1.7	1.60E-03		0.5	48.4	67.7
	25	3.0	1.70E-03		1	83.7	26.5
	50	5.6	3.80E-03		1.5	117.4	39.5
	100	10.5	4.60E-03		2	145.9	12.7
	200	19.7	3.30E-02		-	-	-
9.5	0	1.5	1.25E-03	**9.5**	0	6.5	98.1
	12.5	2.4	2.11E-03		0.5	49.9	66.4
	25	3.7	1.00E-03		1	86.2	59.9
	50	6.2	1.20E-03		1.5	119.1	20.1
	100	11.1	1.30E-03		2	147.2	28.8
	200	20.2	2.40E-02		-	-	-

Curriculum vitae

Inês Fernandes Pinto

Nationality: Portuguese
Date of birth: 1990/08/24

+351 962482183

ines.f.pinto@tecnico.ulisboa.pt

https://pt.linkedin.com/in/inês-pinto-4632b94b

https://goo.gl/UhChJS

https://www.researchgate.net/profile/Ines_Pinto7

Education

February 2014 - present

PhD in Biotechnology and Biosciences
Instituto Superior Técnico - Universidade de Lisboa, Portugal

September 2011 - November 2013

Master of Science (MSc) degree in Biological Engineering (18/20), ECTS Grade A
Instituto Superior Técnico - Universidade de Lisboa, Portugal

September 2008 - July 2011

Bachelor of Science (BSc) degree in Biological Engineering (16/20), ECTS Grade A
Instituto Superior Técnico - Universidade de Lisboa, Portugal

Presentations in Scientific Meetings

1. **Poster Presentation**, *"Quantitative analysis of optical transduction in microfluidic biosensing platforms: nanoporous microbeads coupled with thin-film photodiodes"*, **31st IEEE International Conference on Micro Electro Mechanical Systems** (**MEMS2018**), Belfast, Northern Ireland, January 2018.
2. **Oral Presentation,** *"Miniaturization of chromatography for rapid screening of operating conditions: a microfluidic approach for multiplexed optimization of different ligands and target molecules"*, **ABC² - Anything But Conventional Chromatography**, Lisbon, Portugal, November 2017.
3. **Oral Presentation,** *"A microfluidic approach for rapid screening of chromatography operating conditions: multiplexed optimization of different target molecules"*, **HTPD - High-throughput Process Development**, Toledo, Spain, October 2017.
4. **Oral Presentation**, *"Rapid optimization of chromatography operating conditions using a nano-liter scale column on a microfluidic chip with integrated pneumatic valves and optical sensors"*, **ECI - Separations Technology IX: New Frontiers in Media, Techniques, and Technologies**, Albufeira, Portugal, March 2017.
5. **Oral Presentation**, *"Miniaturization of chromatography for rapid optimization of antibody separations: multiplexed screening of different ligands and target molecules",* **Hydrophobic Bioprocessing Conference (HIC-RPC)**, Scottsdale, Arizona, USA, February 2017.

6. **Poster Presentation**, *"On-chip chromatography for rapid screening of multimodal ligand-target interactions"*, **International Symposium on the Separation of Proteins, Peptides and Polynucleotides (ISPPP),** Salzburg, Austria, November 2016.

7. **Poster Presentation**, *"Development of a microfluidic device with integrated pneumatic valves and a-Si:H photodiodes for rapid optimization of chromatographic separations using a fluorophore-labeled monoclonal antibody",* **20th International Conference on Miniaturized Systems for Chemistry and Life Sciences (MicroTAS)**, Dublin, Ireland, October 2016.

8. **Poster Presentation**, *"Integration of photosensors in a nano-liter scale chromatography column for the online monitoring of adsorption/desorption kinetics of a fluorophore-labeled monoclonal antibody",* **Eurosensors XXX**, Budapest, Hungary, September 2016.

9. **Oral Presentation**, ***"****Multimodal chromatography for the purification of monoclonal antibodies: towards a high-throughput optimization using micro-columns on a chip"*, **XVICOLACRO & 9ENC**, Lisboa, Portugal, January 2016.

10. **Poster Presentation**, *"A microfluidic approach for high-throughput screening of chromatography operating conditions for the purification of monoclonal antibodies"*, **Congress of Microbiology and Biotechnology (MicroBiotec)**, Évora, Portugal, December 2015.

11. **Oral Presentation**, *"Novel strategies for capturing monoclonal antibodies using alternative multimodal and electrostatic ligands",* **Biopartitioning & Purification Conference (BPP)**, Vienna, Austria, June 2015.

12. **Poster Presentation**, *"A multimodal alternative for antibody capture from cell culture supernatants"*, **International Symposium on the Separation of Proteins, Peptides and Polynucleotides (ISPPP)**, Würzburg, Germany, November 2014.

13. **Poster Presentation**, *"Exploring the use of heparin as a first capture step in the purification of monoclonal antibodies from cell culture supernatants"*, **12th International Chemical and Biological Engineering Conference (ChemPor2014)**, Porto, Portugal, September 2014.

Publications in international peer-reviewed journals

1. Pinto, I.F., Soares, R.R.G., Aires-Barros, M.R., Chu, V., Conde, J.P., Azevedo, A.M., *"Optimizing the performance of chromatographic separations using microfluidics: multiplexed and quantitative screening of ligands and target molecules"* (submitted).

2. Santos, D.R., Soares, R.R.G., Pinto, I.F., Caneira, C.R.F., Pinto, R.M.R., Chu, V., Conde, J.P., *"Label-free detection of biomolecules in bead-based microfluidics using on-chip UV and impedimetric sensors"* (submitted).

3. Pinto, I.F., Santos, D.R., Caneira, C.R.F., Soares, R.R.G., Chu, V., Conde, J.P., *"Quantitative analysis of optical transduction in microfluidic biosensing platforms: nanoporous microbeads coupled with thin-film photodiodes",* **2018 IEEE Micro Electro Mechanical Systems (MEMS)**, Belfast (2018), 278-281.

4. Soares, R.R.G., Santos, D.R., Pinto, I.F., Azevedo, A.M., Aires-Barros, M.R., Chu, V., Conde, J.P., *"Multiplexed microfluidic platform coupled with photodetector array for point-of-need and sub-minute detection of food contaminants",* **2018 IEEE Micro Electro Mechanical Systems (MEMS)**, Belfast (2018), 6-9.

5. Soares, R.R.G., Santos, D.R., Pinto, I.F., Azevedo, A.M., Aires-Barros, M.R., Chu, V., Conde, J.P., *"Point-of-need and sub-minute detection of food contaminants: A multiplexed microfluidic fluorescence immunoassay addressed by a photodetector array"*, **Lab-on-a-chip** (2018) 18, 1569-1580.

6. Pinto, I.F., Santos, D.R., Caneira, C.R.F., Soares, R.R.G., Azevedo, A.M., Chu, V., Conde, J.P., *"Optical biosensing in microfluidics using nanoporous microbeads and amorphous silicon thin-film photodiodes: quantitative analysis of molecular recognition and signal transduction"*, **Journal of Micromechanics and Microengineering** (2018) 28, 094004 (15pp).

7. Epifania, R., Soares, R.R.G., Pinto, I.F., Chu, V., Conde, J.P., *"Capillary-driven microfluidic device with integrated nanoporous microbeads for ultrarapid and single-step biosensing assays",* **Sensors and Actuators B: Chemical** (2018) 265, 452-458.

8. Pinto, I.F., Santos, D.R., Soares, R.R.G., Aires-Barros, M.R., Chu, V., Azevedo, A.M., Conde, J.P., *"A regenerable microfluidic device with integrated valves and thin-film photodiodes for rapid optimization of chromatography conditions"*, **Sensors and Actuators B: Chemical** (2018) 255, 3636-3646.

9. Nascimento, A., Pinto, I.F., Chu, V., Aires-Barros, M.R., Conde, J.P., Azevedo, A.M., *"Studies on the purification of antibody fragments"*, **Separation and Purification Technology** (2018) 195, 388-397.

10. Pinto, I.F., Santos, D.R., Soares, R.R.G., Aires-Barros, M.R., Chu, V., Azevedo, A.M., Conde, J.P., *"Integration of photosensors in a nano-liter scale chromatography column for the online monitoring of adsorption/desorption kinetics of a fluorophore-labeled monoclonal antibody",* **Procedia Engineering** (2016) 168, 1426-1429.

11. Soares, R.R.G., Santos, D.R., Pinto, I.F., Azevedo, A.M., Chu, V., Aires-Barros, M.R., Conde, J.P., *"Point-of-use ultrafast single-step detection of food contaminants: a novel microfluidic fluorescence-based immunoassay with integrated photodetection",* **Procedia Engineering** (2016) 168, 329-332.

12. Pinto, I.F., Caneira, C.R.F., Soares, R.R.G., Madaboosi N., Aires-Barros, M.R., Conde, J.P., Azevedo, A.M., Chu, V., *"The application of microbeads to microfluidic systems for enhanced detection and purification of biomolecules",* **Methods** (2016) 116(1), 112–124.

13. Pinto, I.F., Soares, R.R.G., Rosa, S.A.S.L., Aires-Barros, M.R., Chu, V., Conde, J.P., Azevedo, A.M., *"High-throughput nanoliter-scale analysis and optimization of multimodal chromatography for the capture of monoclonal antibodies",* **Analytical Chemistry** (2016) 88(16), 7959-7967.

14. Pinto, I.F., Aires-Barros, M.R., Azevedo, A.M., *"Multimodal chromatography: debottlenecking the downstream processing of monoclonal antibodies",* **Pharmaceutical Bioprocessing** (2015) 3(3), 263-279.

15. Pinto, I.F., Rosa, S.A.S.L., Aires-Barros, M.R., Azevedo, A.M., *"Exploring the use of heparin as a first capture step in the purification of monoclonal antibodies from cell culture supernatants",* **Biochemical Engineering Journal** (2015) 104, 27-33.

16. Taipa, M.A, Azevedo, A.M., Grilo, A.L., Couto, P.T., Ferreira, F.A.G., Fortuna, A.R.M., Pinto, I.F., Santos, R.M., Santos, S.B., *"Student collaboration in a series of integrated experiments to study enzyme reactor modeling with immobilized cell-based invertase",* **Journal of Chemical Education** (2015) 92, 1238-1243.

Experience in orientation

- **Co-supervision** of summer intern student **Carlos Lopes** in INESC-MN Laboratory, **July - September 2017**; Project title: *"Streaming current measurements as a label-free method for monitoring adsorption/elution of biomolecules on chromatography beads inside a microchannel"*.

- **Co-supervision** of MSc student **Catarina Bombaça** in INESC-MN Laboratory, **September 2016 - September 2017**; Project title: *"Grape-chip: a microfluidic device for monitoring metabolites during grape maturation".*

- **Supervision** of summer intern student **Inês Peixoto** in INESC-MN Laboratory, **July – September 2016**; Project title: *"Optimization of BSA adsorption conditions on Capto adhere beads in microfluidic chromatography channels".*

- **Co-supervision** of MSc student **Yün Zhai** (ERASMUS student from Karlsruhe Institute of Technology, Germany) in the Bioseparations Laboratory at Institute for Bioengineering and Biosciences (IBB), Instituto Superior Técnico, **February - August 2015**; Project title: *"Multimodal chromatography for the capture of monoclonal antibodies"*.

- **Co-supervision** of summer intern student **Carolina Fernandes** in the Bioseparations Laboratory at Institute for Bioengineering and Biosciences (IBB), Instituto Superior Técnico, **June - September 2013**; Project title: *"Assessment of 2-benzamido-4-mercaptobutanoic acid as a multimodal ligand for the capture of monoclonal antibodies"*.

- **Orientation** of several MSc students and summer intern students in experimental activities involving (i) operation of ÄKTA chromatography equipment; (ii) protein gel electrophoresis; (iii) microfabrication of microfluidic structures, in particular SU-8 mold fabrication and polydimethylsiloxane (PDMS) soft-lithography; and (iv) fluorescence microscopy.

Participation in other scientific activities

- **Peer-review** of manuscripts submitted to the following journals: Separation and Purification Technology, Elsevier (#6); Journal of Chemical Technology & Biotechnology, Wiley Online Library (#1). Publons profile URL: https://publons.com/a/1213906/

- **Innovate, Connect, Transform (ICT), MAGNETRODES Exhibition Stand (October 2015)**: participation in an exhibition within the MAGNETRODES EU FP7 project, aiming at presenting the research fields and services provided at INESC Microsystems and Nanotechnologies to the general public and potential clients/collaborators.

- **NANODEM Workshop on Fluorescence for Biosensing (September 2015)**: attendance of the NANODEM (NANOphotonic DEvice for Multiple therapeutic drug monitoring) EU FP7 project workshop held in the Complutense University of Madrid, Spain. The workshop was aimed at providing insights on different fluorescence spectroscopy methods and probes for biosensing applications.

Honors & Awards

1. **Poster Presentation Award - First Prize**, awarded by the International Symposium on the Separation of Proteins, Peptides and Polynucleotides - **ISPPP**, November 2016.

2. **CHEMINAS Young Researcher Poster Award**, awarded by the 20th International Conference on Miniaturized Systems for Chemistry and Life Sciences - **MicroTAS**, October 2016.

3. **Student Travel Grant** awarded by the Chemical and Biological Microsystems Society (CBMS) to MicroTAS 2016 presenting authors, October 2016.

4. **Best Poster Award**, awarded by the **Eurosensors XXX**, September 2016.

5. **Honorable Mention** Poster Communication, awarded by the 12th International Chemical and Biological Engineering Conference - **ChemPor**, September 2014.

6. Individual **PhD Student Fellowship Grant**, Fundação para a Ciência e Tecnologia (September 2014). PhD Fellowship awarded to the top 14% (18/128) of candidates in the field of Biotechnology and Bioengineering. The evaluation was based on (1) academic merit of the candidate, (2) impact, feasibility and novelty of the project, and (3) merit of the supervisors and institutions hosting the candidate.

7. **Academic Merit Diploma**, Instituto Superior Técnico (2009/2010). Awarded to students with an average ECTS grade A in the corresponding year.

Competences & Skills

Column chromatography	●●●●●	Thin film photodetectors	●●○○○
ÄKTA purification systems	●●●●●	Fluorescence microscopy	●●●●○
Monoclonal antibodies	●●●●○	Bioanalytical assays	●●●●○
Microfabrication	●●●●○	Molecular biology	●●○○○

Languages

Portuguese (Native)		**English**		**French**	
Writing	●●●●●	Writing	●●●●●	Writing	●○○○○
Reading	●●●●●	Reading	●●●●●	Reading	●●○○○
Oral	●●●●●	Oral	●●●●●	Oral	●○○○○